Geoscience Canada - Active well into Middle Age

Oblique Convergence East of Superior - A New Angle on an Old Problem

Attributes of Appinites and Ascending Asthenosphere

Ten Thousand Holes in British Columbia?

A journal published quarterly by the Geological Association of Canada, incorporating the Proceedings.
Une revue trimestrielle publiée par l'Association géologique du Canada et qui en diffuse les actes.

Subscriptions: Receiving four issues of Geoscience Canada per year for $50 is one of the benefits of being a GAC member. To obtain institutional subscriptions, please contact Érudit: www.erudit.org

Abonnement: Recevoir quatre numéros par année pour 50,00 $ du magazine Geoscience est l'un des avantages réservés aux membres de l'AGC. Pour les abonnements institutionnels, s'il vous plaît contacter Érudit: www.erudit.org

Photocopying: The Geological Association of Canada grants permission to individual scientists to make photocopies of one or more items from this journal for non-commercial purposes advancing science or education, including classroom use. Other individuals wishing to copy items from this journal must obtain a copying licence from Access Copyright (Canadian Copyright Licensing Agency), 1 Yonge Street, Suite 1900, Toronto, Ontario M5E 1E5, phone (416) 868-1620. This permission does not extend to other kinds of copying such as copying for general distribution, for advertising or promotional purposes, for creating new collective works, or for resale. Send permission requests to *Geoscience Canada*, at the Geological Association of Canada (address above).

La photocopie: L'Association géologique du Canada permet à tout scientifique, de reprographier une ou des parties du présent périodique, pour ses besoins, à condition que ce soit dans un but non-commercial, pour l'avancement de la science ou pour des buts éducatifs, y compris l'usage en classe. Toute autre personne désirant utiliser des reproductions du présent périodique doit préalablement obtenir une licence à cet effet d'Access Copyright (Canadian Copyright Licensing Agency), 1 Yonge Street, suite 1900, Toronto, Ontario M5E 1E5, Tél.: (416) 868-1620. L'autorisation susmentionnée exclut toute autre reproduction, telle la reproduction pour fins de distribution générale, de publicité ou de promotion, pour la création de nouveaux travaux collectifs ou pour la revente. Faites parvenir vos demandes d'autorisation à *Geoscience Canada*, au soin de l'Association géologique du Canada (voir l'adresse indiquée ci-dessus).

Those wishing to submit material for publication in Geoscience Canada should refer to the Instructions to Authors on the journal's website, www.geosciencecanada.ca

AUTHORS PLEASE NOTE:
Please use the web address http://journals.hil.unb.ca/index.php/GC/index for submissions; please do not submit articles directly to the editor.

The Mission of the Geological Association of Canada is to facilitate the scientific well-being and professional development of its members, the learned discussion of geoscience in Canada, and the advancement, dissemination and wise use of geosciences in public, professional and academic life. Articles in Geoscience Canada are freely available one year after their publication date, unless authors have arranged for immediate open access. Opinions expressed and interpretations presented are those of the authors and do not necessarily reflect those of the editors, publishers and other contributors. Your comments are welcome.

Cover Image: Dry karst stream and canyon in limestone of the Quatsino Formation, Tahsish River, Vancouver Island, British Columbia, Canada. Photo credit: Paul Griffiths.

EDITORIAL

GEOSCIENCE CANADA – FORTY-FIVE YEARS YOUNG

Andrew Kerr

Scientific Editor
Department of Earth Sciences, Memorial University
St. John's, Newfoundland and Labrador, A1B 3X5, CANADA
E-mail: akerr@mun.ca

PREAMBLE

In my four years working as an editor for this journal, I have tried to provide an editorial for each volume, to touch on issues and concerns that publishers and authors alike might need to consider. But it is equally important that I take the time to formally thank many others who share the effort involved in producing *Geoscience Canada* for you each year. To say that the journal would not exist without their efforts is an understatement. First and foremost on that list is our Managing Editor Cindy Murphy, whose role is actually far more demanding than mine. Cindy carefully tracks each article through the publication process and communicates with authors as revisions and layout proceed, and the quality of final products reflects her energy, organizational skills and her keen eye for detail. I simply could not do my job without her massive contribution, not to mention her numerous timely reminders. I also sincerely thank several 'Section Editors' who look after contributions in our thematic series papers. Jarda Dostal (Igneous Rock Associations), Brendan Murphy (Andrew Hynes tectonic series) and Dave Lentz (Economic Geology Models) deserve special mention for working on some interesting papers in 2018. We depend on hard-working and dedicated volunteers to assist with the sometimes tedious copy-editing of manuscripts, and I acknowledge the diligent work of Rob Raeside, Stephen Amor and Lawson Dickson. Jean-Alfred Renaud, who has assisted with French translations for GAC over many years, retired at the end of 2018, and I thank him for his long-term contribution. The eye-catching graphics that appear on the title page of our papers come from the creative 'pen' of Peter Russell, who has also shared his talents with us for many years. Last, but not least, the GAC head office staff (Karen Dawe and Eleanor Penney) assist with many administrative aspects of *Geoscience Canada*, and the support and advice of GAC Book Editor Sandra Barr and former GAC Publications Chair Chris White on several matters have proved invaluable to me. I would also like to thank the new GAC Publications Chair Roger Paulen for his interest in sustaining the Journal's operations. Last, but certainly not least, I wish to thank the Department of Earth Sciences at Memorial University for providing a home for the journal and for supporting this work as part of my adjunct faculty position.

LOOKING BACK TO SEE AHEAD

My own career path in the Earth Sciences started more-or-less at the same time as Geoscience Canada first went to press in 1974. I was in my second year at the University of Southampton and had decided to set aside a program in Environmental Science and study geology instead. The reasons for that choice will be familiar to many - I took an introductory geology course taught by an animated and committed lecturer, and I was hooked for life. That same young lecturer would later persuade me to pursue postgraduate studies in Canada. I owe the late Nick Badham a great deal, and will always feel that I failed to properly thank him. Although I did not come to Canada until 1977, I was already aware of *Geoscience Canada*. Nick had completed his Ph.D. at the University of Alberta, and he used two articles from the very first issue as supplementary reading material for a course on economic natural resources. These two articles, entitled *Trends in the Mineral Industry in the Next Decade* (by Robert J. Uffen and others) and *Energy - Challenge of Man's Future* (by R.E. Follinsbee and A.P. Leech) still make interesting reading. In the mid-1970s, there were dire predictions of the coming exhaustion of all natural resources, and the massive shortages envisioned for the 21st century. That particular version of future history did not come about as predicted, but both papers include prescient observations that are relevant to today's issues. These articles, and the other short papers in Issue 1 of Geoscience Canada, demonstrate that scientific and technical research and reasoned speculation from such data, have lasting value almost half a century beyond their publication. The ideas and conclusions that we have will change over time, but there are many smaller steps in that long process.

Our first issue also contained a message from then-president William Watt Hutchinson (1935–1987), a well-known figure whose name is now attached to GAC's most prestigious medal. Appropriately, he commented that "*The first issue of Geoscience Canada is an historic event for our Association; it marks both the start of a bold new venture and the end of an old one.*" He actually said much more than this, although his introduction only occupied a single page, including its French continuation. His intro-

ductory comments resonated deeply with me in terms of the goals that we hold at *Geoscience Canada*, and I think that others might also benefit from reading them. At the end of this editorial, you will find the complete text of Hutchinson's introduction, which is just as relevant in 2019 as it was in 1974.

The first issue of *Geoscience Canada* also contained a short piece by editor Gerry Middleton. It is worth reiterating some key points from his introduction. Gerry noted our natural focus on general-interest articles about Earth Sciences in Canada, but also our interest in reviewing ideas and developments from beyond our shores. Most importantly, he emphasized that articles *"will be written at a technical level that can be understood not only by specialist research workers but also by non-specialists in other branches of the Earth Sciences."* This is still a key guiding principle for *Geoscience Canada*, but it is also a very difficult objective - which is perhaps why few other technical journals see it as a priority. I think it is even more important in today's environment, in which specialization of research seems to me at times to be a truly blinding obsession. I like to think of *Geoscience Canada* as a journal that bridges the gap between disciplines and specialities, such that geophysicists can learn from glaciologists, and paleontologists from petrologists. Earth Science is amazingly diverse, and there are connections between all of its many facets; the opportunity to learn about new and unfamiliar things is something that we should promote, and not just because it is intrinsically interesting. There are many examples in the history of Earth Science where major advances in one field have come about simply because a far-sighted individual became aware of seemingly unrelated research on another topic.

At this point, a sensible editor would probably conclude that this editorial is already too long, and swiftly bring it to a close. It would be easy to just leave the last words to William Watt Hutchinson, and I admit that I am sorely tempted. However, there are other matters that need to be aired as *Geoscience Canada* approaches its fiftieth anniversary. These topics are not new or unique to us; the world of science publishing is changing rapidly, and most journals are working to adapt and survive in a radically different environment. I see us as a reader- and author-supported scientific journal, and our long-term success depends on the support and participation of our readership, and the wider Canadian geoscience community. In the following short sections, I will quickly touch upon some of these changes and challenges and discuss possible solutions.

IT ALL STARTS WITH A MANUSCRIPT!
Regardless of the mandate or focus of a scientific journal, all have one thing in common - the lifeblood of publishing is *content*. Without the submission of first-draft papers to *Geoscience Canada*, there will not be any published papers. Without submissions to the journal, there will be no journal, period. This may seem self-evident, but it always needs to be repeated. At *Geoscience Canada*, we make a sincere effort to assist authors as they navigate the pipeline - which can be tortuous - and provide them, through the peer-review process, with ideas and suggestions for improvement of their papers. But in the end,

the number of published papers will always be less than the number of submissions received. A major part of my job as editor consists of soliciting contributions and encouraging authors, to ensure that we will have sufficient content for forthcoming issues.

So, if there is one single thing that the readers of the journal can do to help us in our efforts, it is to move from readership to authorship. Consider submitting papers to the journal, or encourage others to write and submit papers. We are always interested in scientific papers that report new research, especially of a regional or interdisciplinary nature, but we are equally interested in review-type papers that have lasting educational value, and in reports connected to geoscience outreach and education activities. If you attended an interesting scientific conference at which topical ideas were discussed, or read a technical book that either impressed you or failed to do so, consider writing us a thoughtful review. We are very much open for business, and our business is also *your* business. If you have published work with us, and had a good experience with that process, please spread the word, and encourage others to contribute. If your experience was less than ideal, then please contact us so we can consider ways to improve things in our system.

THEMATIC SERIES - PAST, PRESENT AND FUTURE
Thematic Series Papers have long been an important part of how Geoscience Canada operates. These are papers that share a common theme in Earth Science, or relate to specific regions or periods in Earth History, and many are later published as stand-alone books by the GAC. The well-known *Facies Models* and *Ore Deposit Models* collections, which are widely used in the educational sector, are examples of previous thematic series. Thematic series papers related to the research pioneered by Paul Hoffman and Harold (Hank) Williams are more recent examples of such compilations. Among the current collection of thematic series, we have some that are very active in terms of papers, notably Igneous Rock Associations (Section Editor, Jarda Dostal), the Andrew Hynes Tectonics Papers (Section Editors, Brendan Murphy and Stephen Johnston) and Economic Geology Models (previous Section Editor, David Lentz). Papers have appeared in several other thematic series over the last few years, but some series are effectively dormant. Over the next year or so, we anticipate bringing some of these dormant thematic series to a close, and replacing them with some new initiatives that we hope will attract more paper submissions. In 2018, we initiated the *Classic Rock Tours* series, and we are actively seeking ideas for other new initiatives. We also need Section Editors to take on the work involved in soliciting and handling papers for any new ventures, and also to replace existing Section Editors who are stepping down. Dave Lentz stepped down from his role with the Economic Geology Models series in 2018, and we are especially keen to fill this gap in the near future. The role of Section Editors is a vital one for the journal, and we are very interested to hear from new candidates with new ideas and visions.

RAISING THE PROFILE OF GEOSCIENCE CANADA

Although the Journal carries the name of our country in its title, we aspire to be much more than a regional journal. Raising our profile and establishing an identity as a source of high quality, diverse material that non-specialist readers can understand and assimilate is an important objective for us. In many respects, the challenges noted above with regard to the submission of new manuscripts are related to the wider issue of the profile of the journal in the Earth Sciences community, especially beyond Canada. A higher profile would obviously encourage more submissions, but raising our profile ultimately depends on publishing more articles, so this is not an easy task. Readers can assist by promoting the journal to colleagues and contacts, and by using materials from our papers in the classroom, and in other ways that increase awareness. Ideally, we would like to add another person to the editorial team to directly address the challenges involved in promoting the journal by any means that we can devise. If you like working hard in support of a good cause, with a reasonable chance of some sense of accomplishment at the end, we would really like to hear from you.

IS OPEN ACCESS IN OUR FUTURE?

In 2016, I wrote a discussion about the growing importance of open access in scientific publishing, and the ways in which we might approach this at *Geoscience Canada*. More recently, as part of a wider change in policy by the Erudit publishing consortium, of which we are a part, *Geoscience Canada* took another step along this road. From 2018 onwards, papers published in Geoscience Canada become open access only 12 months after their formal publication; with the appearance of this issue, papers published in the March issue of 2018 will become fully open access, and can be freely distributed.

Since 2016, we have offered an option for *immediate* open access to all published papers through modest article processing fees. The move to automatic open access after one year has reduced these fees, and several authors of papers published in 2018 opted to make their work immediately available by paying such charges. The current rate for immediate open access is a flat charge of $500, and a page charge of $50 per final published page. So, if you write a paper that ends up being 10 pages long, the total cost is $1000. These fees are significantly less than those charged for open access by other hybrid journals.

The revenue from these open access charges will likely become increasingly important to Geoscience Canada in years to come, should our revenue from subscriptions diminish, which is possible. We encourage authors of papers to consider this option, which will give wider immediate impact to their work, and support the journal in its wider efforts. Many authors and readers will remember 'page charges' from the era of print-only journals, and these still exist for some journals even in this digital age. Page charges were voluntary, and the publication of a given paper was never dependent upon their payment, but authors with adequate support generally made an effort to pay them because they were essential for journals to survive and prosper. Our voluntary open access charges differ from old-style page charges in that they give you something tangible in return. They allow immediate access to and distribution of your work around the world with the click of a mouse. If you publish papers with us in 2019 and have available funding, please consider supporting *Geoscience Canada* by making these payments. The added revenue will also help us with important initiatives such as trying to raise the profile of the journal.

CLOSING REMARKS

When I took on the role of Scientific Editor for the journal in 2015, following my retirement from the Geological Survey of Newfoundland and Labrador, I was not really sure what to expect. I discovered that working as an editor provides an unparalleled opportunity to learn about new topics and connect topics from different disciplines; as a learning opportunity, there are few things that compare to it. When a paper finally appears in Geoscience Canada and I read through the proofs, the ups and downs of the publication process seem worthwhile, and the occasional frustrations are quickly forgotten. If a mere editor is happy to see the final product of work by others, I can only hope that the authors themselves share a greater pleasure, and feel that their much greater efforts were well placed. In conclusion, I hope that 2019 will be another good year for *Geoscience Canada*, and that all involved in every paper will take enjoyment and pride from their accomplishments.

The following message from the GAC Past-President, W.W. Hutchinson, was published in the first issue of Geoscience Canada, V. 1 (1974), No. 1, p. 3.

A Message from the President

This first issue of *Geoscience Canada* is an historic event for our Association; it marks both the start of a bold new venture and the end of an old one. Specifically *Geoscience Canada* replaces our Proceedings which for over 25 years contained formal accounts of scientific studies and of our Association's activities. *Geoscience Canada* will be more broadly based, more topical, will discuss issues and maintain a poise of responsiveness; its appearance is most timely.

The relevance of geology in Canada today is greater than it has ever been. Yet there is substantial polarization of information and views between news media and scientific journals; hopefully *Geoscience Canada* may help fill this gap by providing a forum for informed opinion. But it must do more than this. It must provide for presentation and discussion of concepts which may be ephemeral yet essential to the evolution of science. Perhaps *Geoscience Canada* will even present something of the culture of geology – a rich culture shared by few. It has many elements: love of the outdoors, pioneer spirit of the prospector, disappointment and frustration countered by an underlying enthusiasm and determination for discovery, and the manner in which emotions can be violently stirred as new theories are put forward. *Geoscience Canada* should reflect some of this refreshing vitality but the underlying theme must be the science itself.

Man's evolution is marked by his mastery of minerals and metals; I hope *Geoscience Canada* will convey with impact that geology is not in a backwater but is a rapidly developing science that is exciting, relevant, and well-poised to respond to present and future needs in the world.

Les géologues de l'avenir devront faire face à une carence partielle des richesses naturelles, au souci de protection de l'environnement, ainsi qu'à la complexité croissante des politiques gouvernementales. Espérons qu'ils pourront relever le défi. Leur participation aux débats sur l'actualité et leur contribution à *Geoscience Canada* se doivent de demeurer purement scientifiques. Souhaitons que *Geoscience Canada* saura véhiculer la pensée géologique et ainsi être utile non seulement aux géologues mais aussi à tous ceux qui vivent dans ce gran milieu qu'est la Terre.

Longue vie à *Geoscience Canada* et bonne chance à son rédacteur, G. V. Middleton.

W. W. Hutchison

GEOLOGICAL ASSOCIATION OF CANADA
(2018-2019)

CORPORATE MEMBERS

PLATINUM

MEMORIAL
UNIVERSITY

GOLD

AngloAmerican

Anglo American Exploration (Canada) Ltd.

NORTHWEST TERRITORIES
GEOLOGICAL SURVEY

Northwest Territories Geological Survey

SILVER

ROYAL TYRRELL
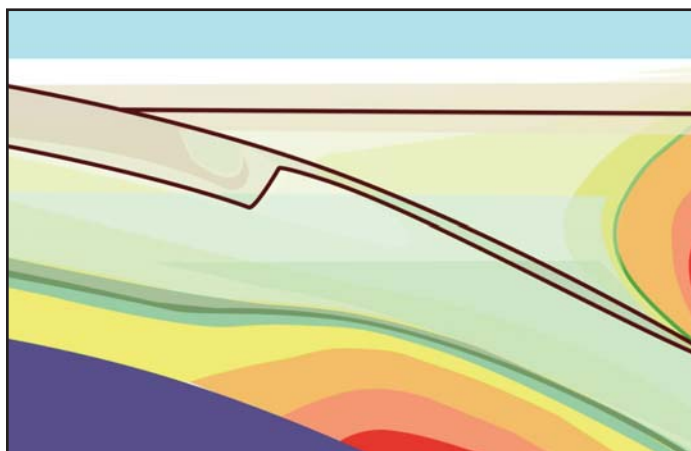**MUSEUM**

YUKON
GEOLOGICAL SURVEY

NICKEL

University of Waterloo

GEOSCIENCE CANADA AND THE GEOLOGICAL ASSOCIATION OF CANADA ARE GRATEFUL TO THE CANADIAN GEOLOGICAL FOUNDATION FOR THEIR FINANCIAL SUPPORT OF THIS JOURNAL.

Canadian
Geological
Foundation

Fondation
Géologique
du Canada

1968

ANDREW HYNES SERIES: TECTONIC PROCESSES

Structural Features of the Central Labrador Trough: A Model for Strain Partitioning, Differential Exhumation and Late Normal Faulting in a Thrust Wedge under Oblique Shortening

E. Konstantinovskaya[1], G. Ivanov[2,3], J.L. Feybesse[3,4] and J.L. Lescuyer[3]

[1]University of Alberta, Earth and Atmospheric Sciences
1-26 Earth Sciences Building, Edmonton, Alberta,
T6G 2E3, Canada
E-mail: konstant@ualberta.ca

[2]IOS Services Geoscientifiques Inc.
1319 Boulevard Saint-Paul, Chicoutimi, Quebec, G7J 3Y2, Canada

[3]senior consulting geologist, formerly with Areva (presently Orano),
Tour Areva , 1 place Jean Millier, 92084 Paris, France

[4]Deceased

SUMMARY
The west-verging fold and thrust belt of the Central Labrador Trough originated as a part of the New Quebec Orogen from rift inversion as a result of oblique collision and dextral transpression between the Archean Superior craton and the Archean block of the Core Zone during the Trans-Hudson orogeny (1.82−1.77 Ga). The structures associated with dextral transpression are well established in the northern segment of the orogen but not in the central part. We present new field structural observations along the ca. 70 km long W−E Minowean-Romanet transect that include not only elements of thrust tectonics but also previously undocumented examples of strike-slip shear zones and late brittle, semi-brittle and ductile extensional structures which occurred both in the frontal and rear parts of the thrust wedge. The newly described low-angle mineral lineation, axes of cylindrical folds and dextral mylonitic shear zones in the footwall of the Romanet Fault are oriented subparallel to the orogen and reflect the early phase of oblique convergence. Mineral lineations and striations on planes of normal faults in the hanging wall of the Romanet Fault are oriented orthogonal to the orogen and correspond to a later phase of exhumation driven by the combined effects of erosion and underplating. To explain the increase in the degree of exhumation along the orogen in the study area from NW to SE, we propose a model of strain partitioning and differential exhumation that resulted from longitudinal variations of shortening and erosion under an oblique convergence setting.

RÉSUMÉ
La partie centrale de la ceinture de plissement et de chevauchement de la Fosse du Labrador de vergence vers l'ouest fait partie intégrante de l'Orogène du Nouveau-Québec, et résulte de la collision oblique avec transpression dextre entre le craton Supérieur archéen et le bloc archéen de la Zone noyau pendant l'Orogenèse trans-hudsonienne (1.82−1.77 Ga). Les structures associées à la transpression dextre sont bien établies dans la partie nord de l'orogène mais pas dans la partie centrale. Nous présentons de nouvelles observations structurales de terrain le long de la traverse ouest−est Minowean-Romanet d'environ 70 km de long, qui comprennent non seulement des évidences de tectonique de chevauchement, mais également des exemples encore non documentés de zones de cisaillement ductile et de structures d'extension fragiles, demi-fragiles et ductiles à la fois dans les parties frontales et arrière du prisme d'accrétion tectonique. La linéation minérale à faible plongement récemment décrite, les axes de plis cylindriques et les zones de cisaillement mylonitique dextre dans le compartiment inférieur de la faille de Romanet sont subparallèles à l'orogène et reflètent une

phase précoce de la convergence oblique. La linéation et les stries minérales sur les plans des failles normales dans le compartiment supérieur de la faille de Romanet sont orientées orthogonalement à l'orogène et correspondent à la phase ultérieure d'exhumation induite par les effets combinés de l'érosion et de l'accrétion basale. Pour expliquer l'augmentation du degré d'exhumation le long de l'orogène du nord-ouest au sud-est dans la zone d'étude, nous proposons un modèle de partitionnement de la déformation et de l'exhumation différentielle résultant des variations longitudinales du raccourcissement et de l'érosion dans un contexte de convergence oblique.

INTRODUCTION

Many collisional orogenic belts developed at oblique convergent plate boundaries are characterized by spatial and temporal distribution of deformation caused by strain partitioning between the two plates. As it has been shown in the south-central Canadian Rockies, the Western Alps, the Variscides of France, and in Taiwan, the regional stretching mineral lineation and axes of cylindrical folds are oriented subparallel to an orogen and were formed in the footwall of a convergent boundary during the earliest phase of deformation and prograde metamorphism as a result of oblique subduction (Ellis 1986; Ellis and Watkinson 1987; Echtler and Malavieille 1990; Matte et al. 1998). The later-formed stretching mineral lineations are oriented transverse to the orogen and occur either at an imbricated hanging wall−footwall transition zone or within the hanging wall. Stretching mineral lineations transverse to the orogen may be associated either with thrust emplacement (Malavieille et al. 1984; Lacassin 1987; Burg et al. 1987) or with normal faulting during the exhumation phase (Ellis 1986; Ellis and Watkinson 1987). Normal faulting may occur in a thrust wedge during shortening and syncollisional exhumation under the combined effect of continuous tectonic underplating (i.e. different decoupling levels acting at different depths within the wedge) and surface erosion (Konstantinovskaia and Malavieille 2005; Malavieille 2010; Konstantinovskaya and Malavieille 2011). On the basis of analog experiments, Malavieille and Konstantinovskaya (2010) have suggested that deep crustal-scale normal shear zones and superimposed brittle normal faults in the uppermost crust may form during compressional tectonics associated with continental subduction.

Longitudinal variation of the amount of shortening along an orogen may too result in strain partitioning in a thrust wedge. This mechanism was suggested for the western Alps where progressively increasing shortening along the orogen is likely associated with changes in the amount of exhumation from the south to the north of the orogen (Rosenberg et al. 2015).

The field structural observations in the Central Labrador Trough presented in this study show that the tectonic evolution of this collisional belt cannot be explained by a two-dimensional model of orogeny but represents an excellent example of strain partitioning and differential exhumation occurring in a thrust wedge during oblique convergence.

The Labrador Trough is a Paleoproterozoic collisional fold and thrust belt of the New Quebec Orogen (NQO) (Fig. 1).
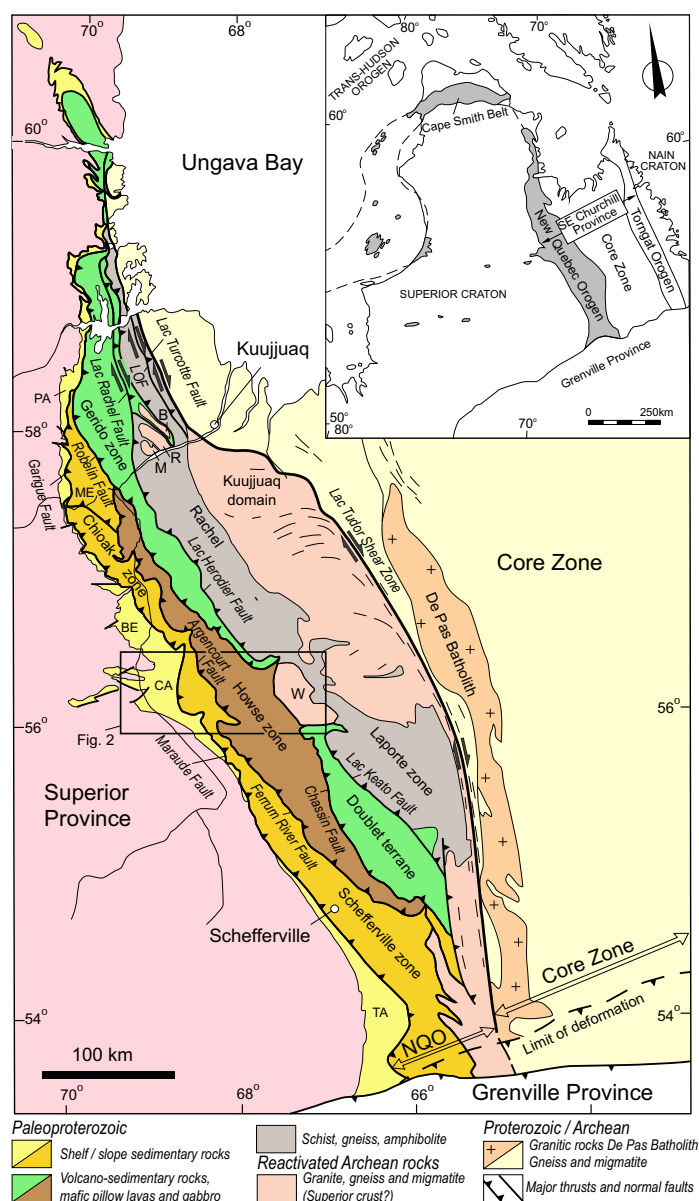

Figure 1. Major tectonic zones of the New Quebec Orogen (NQO) modified after Wardle et al. (2002), Clark and Wares (2004) and Corrigan et al. (2018). BE –Berard, CA –Cambrien, ME –Mélèzes, PA –Payne, TA –Tamarack zones; allochthonous domes of Archean basement gneiss: B –Boulder, M –Moyer, R –Renia, W –Wheeler; *LOF* –Lac Olmstead Fault. The box indicates location of Figure 2a.

The belt extends for about 800 km from the front of the Grenville belt in the south to Ungava Bay in the north. It originated as an incipient rift developed on the eastern margin of the Superior craton in the Paleoproterozoic (Hoffman 1988; Wardle et al. 2002; Clark and Wares 2004). During the rift inversion, voluminous nappes of mafic rocks were thrust over the sedimentary successions of the continental margin of the Superior craton. The rift inversion and formation of the NQO occurred as a result of oblique collision and dextral transpression between the eastern margin of the Archean Superior craton and an Archean block in the Core Zone during the Trans-Hudson orogeny at 1.82−1.77 Ga (Hoffman 1990; Wardle et al. 1990, 2002; Clark and Wares 2004). Strain was partitioned

across the belt between the SW-directed thrusting toward the Superior craton (foreland) and dextral strike-slip faulting in the Rae Province (hinterland) (Hoffman 1990). The dextral component was recognized in some thrust faults, such as Lac Rachel Fault, Lac Olmstead Fault, Lac Turcotte Fault, and Lac Tudor Shear Zone at the rear part in the wedge (Fig. 1), that are considered to accommodate the dextral transpression during the orogeny (Goulet et al. 1987; Girard 1990; Hoffman 1990; Moorhead and Hynes 1990; Goulet 1995; Wardle et al. 2002; Vanier et al. 2017). However, no well-documented ductile strike-slip shear zones that would accommodate strain partitioning during the oblique collision have yet been reported in the Central Labrador Trough between latitudes 56°15' N and 56°30' N (Fig. 2a). Neither the tectonic exhumation phase, nor the associated fault kinematics has been thoroughly studied in the region. The brittle normal faults recognized in the eastern part of the orogen (Romanet horst) were interpreted as small-scale displacement faults, referred to late tectonic adjustments (Clark 1986; Clark and Wares 2004). No late brittle or semi-brittle normal faults have been documented in the foreland zone of the orogen at the latitude of the study area.

In this paper, we present new results of structural analysis carried out during detailed field mapping in selected areas along the 70 km W−E Minowean–Romanet transect across the Central Labrador Trough between latitudes 56°15' N and 56°30' N (Fig. 2a). New evidence for dextral mylonitic shearing and brittle and semi-brittle normal faulting were documented in the frontal part of the orogen. Low-angle stretching mineral lineations and axes of cylindrical folds oriented parallel to the orogen in a dextral mylonitic shear zone, normal brittle faults and shear zones were observed in the hinterland of the orogen. We propose a model of strain partitioning and differential exhumation associated with longitudinal variations of shortening and erosion under an oblique convergence setting to explain the observed structural features.

GEOLOGICAL BACKGROUND
Stratigraphy
The Paleoproterozoic sedimentary succession of the Central Labrador Trough consists of two distinct depositional cycles (Fig. 2b) separated by an erosional unconformity and a possible episode of tectonic disturbance (Dimroth 1978; Le Gallais and Lavoie 1982; Clark and Wares 2004). During the first sedimentary cycle (2169−2142 Ma), the incipient rift was filled with continental deposits and a platform succession (Seward and Pistolet groups) overlain by basin deposits (Swampy Bay Group) closer to the Superior margin, and relatively deeper water sedimentary rocks, basalt (Bacchus Formation) and voluminous gabbro sills−sediment complexes (Montagnais Group) in the rift area (Le Gallais and Lavoie 1982; Clark and Wares 2004). During the second sedimentary Paleoproterozoic transgressive cycle (1884−1870 Ma), the siliciclastic rocks (Wishart Formation), ferriferous shale, siltstone (Ruth Formation), cherty ironstone (Sokoman Formation) of the Ferriman Group and basin turbidites (Menihek Formation) accumulated (Dimroth 1978; Clark and Wares 2004).

The base of the Paleoproterozoic sedimentary succession (Dimroth 1978) in the Central Labrador Trough, known as the Seward Group, includes fluvial conglomerate and arkosic sandstone of the Chakonipau Formation that are overlain by mudstone, dolomitic sandstone and dolomite of the Portage Formation in the west and by dolomite of the Dunphy Formation in the east (Fig. 2b). To the west, conglomerate and fluvial deposits of the Sakami Formation fill graben and half-graben of the Lac Cambrien rift zone and are correlated to the rocks of the Seward Group (Clark 1984; Hoffman 1988). Further to the east, meta-arkose, metaquartzite, quartz−albite−sericite schist and metamorphosed pebble conglomerate of the Milamar Formation overlie Archean gneiss of the Wheeler dome with an erosional contact (Dimroth 1978). Upwards, the Pistolet Group (PI) is composed of pelitic rocks (mudstone and siltstone) with minor dolomite (Lace Lake Formation), quartz arenite, dolomitic sandstone and dolomite (Alder Formation), and mudstone and siltstone (Uvé Formation). The Pistolet Group is overlain by turbidite mudstone, siltstone and sandstone of the Swampy Bay Group (Hautes-Chutes, Savigny and Otelnuk formations) in the west, and by conglomerate, sandstone and slate of the Du Chambon and Romanet formations in the east. Pillowed and massive basalt with subordinate slate interlayers of the Bacchus Formation overlie the Lace Lake Formation in the eastern part of the region. The platform dolomitic reef complex of the Denault Formation records a marine regression at the end of the first sedimentary cycle.

The age of the basal units of the first cycle of the Paleoproterozoic succession is determined on the basis of a granophyre dyke related to the lac Cramolet gabbro sill, which intruded red beds of the Chakonipau Formation (Seward Group) and has a U−Pb zircon age of 2169 ± 4 Ma (Rohon et al. 1993). A rhyolite dyke cutting through basalt in the upper part of the Bacchus Formation was dated by the U−Pb method at 2142 +4/−2 Ma (T. Krogh and B. Dressler, unpublished data cited by Clark 1984). Thus, the onset of rifting on the continental margin of the Superior craton, emplacement of mafic rocks and accumulation of sedimentary succession of the first cycle started prior to 2169 Ma and mostly ended by 2142 Ma (Wardle et al. 1990; Rohon et al. 1993; Clark and Wares 2004). It was suggested by Clark and Wares (2004) that the end of the first cycle could be extended to 2.06 Ga taking into consideration the heavy carbon isotopic composition (δ^{13}C ranging from +5 to +15.4‰) of dolomite of the Alder and Uvé formations (Melezhik et al. 1997), typical for carbonate rocks formed between 2.22 and 2.06 Ga (Karhu and Holland 1996).

The Montagnais Group includes gabbro sills and ultramafic rocks of the Labrador Trough, emplaced within stratigraphic units of the first and second sedimentary cycles (Findlay et al. 1995; Clark and Wares 2004). The Montagnais mafic sills that are coeval with the second sedimentary cycle are considered to indicate transitional MORB-like magmatism during renewed rifting on the Superior margin at about 1.88−1.87 Ga (Skulski et al. 1993).
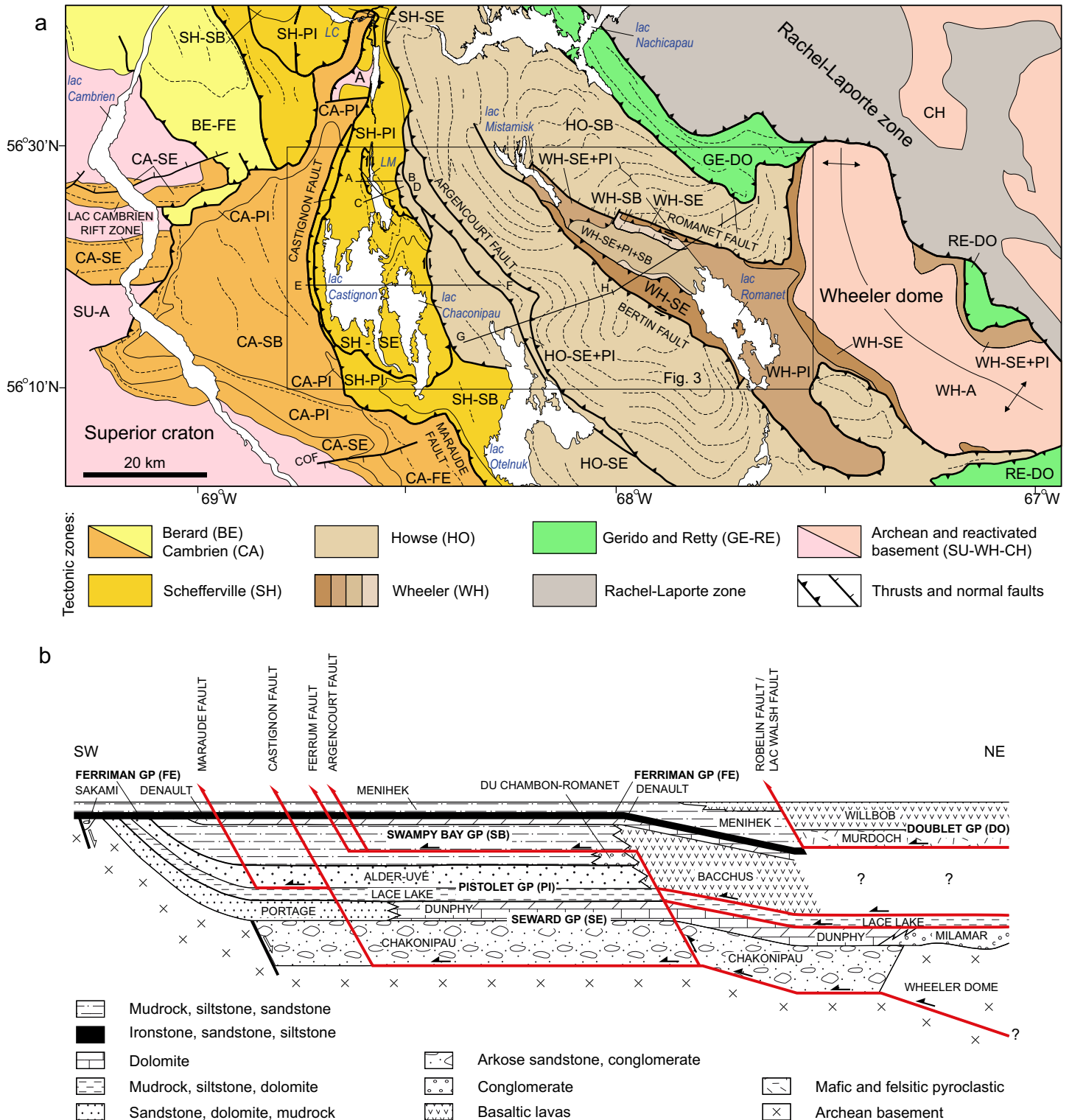
Figure 2. Map of tectonic zones (a) and a generalized pre-thrust reconstruction of Paleoproterozoic sedimentary succession (b) of the Central Labrador Trough, modified after Dimroth (1978), Clark (1986) and Clark and Wares (2004). Tectonic zones: BE –Berard, CA –Cambrien, HO –Howse, SH –Schefferville, WH –Wheeler; SU-WH-CH – Archean (A) rocks of the Superior craton (SU-A) and the Wheeler dome (WH-A) and undivided reactivated Archean rocks of the Southeast Churchill (CH) crustal domain. Stratigraphic groups: DO –Doublet, FE –Ferriman, PI –Pistolet, SB –Swampy Bay, SE –Seward. *COF* –Cambrien-Otelnuk Fault; lac Minowean (*LM*), lac Canichiko (*LC*). The box indicates the location of the study area shown in Figure 3. Solid lines A−B, C−D, E−F, and G−H−I, show the locations of cross-sections in Figures 5 and 6. Dashed lines on the map indicate the structural trend.

The siliciclastic and ferriferous rocks of the Ferriman Group (FE) and basin turbidites of the Menihek Formation of the second sedimentary cycle are present in the western part of the Central Labrador Trough, to the northwest (lac Cambrien) and to the south (the Cambrien-Otelnuk Fault) of the study area (Fig. 2a). The siliciclastic rocks of the Ferriman Group are chrono-stratigraphically correlated with basalt and flysch of the Doublet Group (Fig. 2b) that occur in the eastern part of the orogen (Dimroth 1978; Wardle and Bailey 1981; Le Gallais and Lavoie 1982; Findlay et al. 1995; Clark and Wares 2004). Pyroclastic rocks (tuff and volcanic breccia) of the Murdoch Formation form the base of the Doublet Group are overlain by basalt of the Wilbob Formation east of the Lac Walsh Fault (Fig. 2b), both units being correlated with turbidites of the Menihek Formation (Clark and Wares 2004). The Sokoman Formation in the western part of the orogen is correlated with contemporary intrusive dykes, tuff cones and diatremes of carbonatite and meimechite of the Castignon Complex (Dimroth 1978; Dressler 1979; Chevé 1993; Clark and Wares 2004). The U−Pb age of zircon from a carbonatite dyke of the Castignon complex is 1880 ± 2 Ma (Chevé and Machado 1988). An additional geochronological dataset from the north and south of the NQO referenced in Clark and Wares (2004) indicates the time interval of 1884−1870 Ma for the deposition of the second sedimentary Paleoproterozoic cycle. According to these data, zircon from a glomeroporphyritic gabbro that intruded the Hellancourt Formation gave a U−Pb age of 1874 ± 3 Ma and from rhyodacite in the upper Murdoch Formation yielded an identical U−Pb age of 1870 ± 4 Ma (Machado et al. 1997).

Both the stratigraphic successions of the first and second cycles are characterized by a classic basinward thickening. Each cycle started with a shelf phase of fluvial and/or platformal lithofacies deposited in an oxidized environment (Seward, Pistolet and Ferriman groups), followed by a basin phase with reduced facies (Swampy Bay Group and Menihek Formation) (Le Gallais and Lavoie 1982; Clark and Wares 2004). The sedimentary rocks of the second cycle unconformably overlie (Dimroth 1978) the succession of the first sedimentary cycle and locally Archean basement. This has been interpreted either as a low-angle erosional unconformity resulting from a slight uplift of the Archean foreland (Dimroth 1978), or as an angular unconformity corresponding to the pre-Wishart (Chevé 1993) or proto-Hudsonian (Le Gallais and Lavoie 1982) deformation stage.

Tectonic Structure

The Labrador Trough (Fig. 1) consists of four principal parautochthonous and allochthonous lithotectonic zones composed of Paleoproterozoic sedimentary and/or volcanic and magmatic rocks: Schefferville, Howse, Gerido-Doublet and Rachel-Laporte (Dimroth 1978; Clark and Wares 2004). In the west, these zones are bound by autochthonous zones of sedimentary cover of the Superior craton (Fig. 1): Tamarack, Berard, Cambrien and Payne. The parautochthonous and allochthonous tectonic zones are delineated by major west-verging NW−SE-striking thrust faults extending over 80 km to

250 km, e.g. the Maraude, Ferrum River, Argencourt, Chassin and Lac Herodier faults (Fig. 1).

In the Central Labrador Trough (Fig. 2a), the autochthonous Cambrien zone and parautochthonous Schefferville zone are composed of Paleoproterozoic sedimentary rocks the Seward, Pistolet and Swampy Bay groups (Fig. 2b) with a variable but limited presence of the Montagnais Group gabbro. The ironstone and sedimentary rocks of the Ferriman Group are preserved in the Berard (BE-FE) zone and Cambrien (CA-FE) zones located to the northwest and to the south of the study area, respectively (Fig. 2a).

The autochthonous Cambrien zone is characterized by two different tectonic styles (Fig. 2a). To the west, Archean gneiss basement of the Superior craton is faulted, and the graben and half-graben of the Lac Cambrien rift zone filled by rocks of the Sakami Formation are delimited by the SW−NE normal faults (Clark 1984; Clark and Wares 2004). Some of these normal faults were reactivated as reverse faults during the Trans-Hudson orogeny. The similar SW−NE-striking Cambrien-Otelnuk normal fault (Fig. 2a) delineates an escarpment in the Archean basement to the south of the study area. The Archean gneiss here is overlain with a basal unconformity by the units of the Portage Formation (the Chakonipau Formation is missing). This escarpment was uplifted during the early stages of Paleoproterozoic sedimentation and represents the source terrain for the Chakonipau Formation, accumulated to the north (Dimroth 1978). To the east of lac Cambrien, the Paleoproterozoic sedimentary succession thickens and is composed of units of the Seward, Pistolet and Swampy Bay groups. These rocks deformed in NW−SE-striking folds with limbs dipping to the NE and SW at 25° to 80° and with steep schistosity dipping to the NE at 55°−75° (Dimroth 1978; Chevé 1993). Thrust faults with minimal displacement (Fig. 2a) are mapped in the rocks of the Ferriman Group in the Berard zone (Dimroth 1978; Clark and Wares 2004).

The parautochthonous Schefferville zone is characterized by imbricate structure mostly defined by NW−SE and N−S-striking folds and SW-verging thrust faults. The SW-verging Maraude and Castignon thrust faults separate the rocks of the Cambrien and Schefferville zones (Fig. 2a). These faults join different detachment levels at depth (Fig. 2b); either within or at the base of Paleoproterozoic sedimentary succession and Archean Wheeler dome (Clark and Wares 2004). The detached crustal block of Archean granite-gneiss basement (A) is exposed within the Schefferville zone (Fig. 2a) to the north of the study area, south of the lac Canichiko (Clark and Wares 2004).

The allochthonous Howse zone is composed of voluminous sills of gabbro (Montagnais Group) and pillows and massive flows of basalt with subordinate sedimentary rocks (Bacchus Formation of the Swampy Bay Group, HO-SB). The thick succession of mafic rocks forms nappes emplaced over the rocks of the Schefferville zone along the Argencourt thrust fault. A detached crustal block of Archean granite-gneiss basement is recognized within the Howse zone in the lac Colombet area located about 50 km to the north of the crustal block in the Schefferville zone (Clark and Wares 2004).

The allochthonous Wheeler zone is located in the valley of the lacs Mistamisk and Romanet in the eastern part of the study area (Fig. 2a). The Wheeler zone includes Paleoproterozoic sedimentary rocks of the Seward, Pistolet and Swampy Bay groups and gneiss of Archean basement of the Wheeler dome (Dimroth 1978; Clark and Wares 2004).

The sedimentary units of the Seward (WH-SE), Pistolet (WH-PI) and Swampy Bay (WH-SB) groups of the Wheeler zone are exposed between two nappes of mafic rocks of the Howse zone (Fig. 2a) in a structure known as the Romanet horst delimited by the Bertin and Romanet faults (Le Gallais and Lavoie 1982; Chevé 1985; Clark 1986). These units represent the eastern facies of the sedimentary succession of the Schefferville zone (Le Gallais and Lavoie 1982; Clark and Wares 2004) but are strongly deformed and partially metamorphosed (greenschist facies) and locally contain lenses of the Montagnais gabbro and/or amphibolite and peridotite (Dimroth 1978; Dimroth and Dressler 1978; Clark and Wares 2004). The sedimentary units of the Romanet horst are interpreted as forming an erosional tectonic window below a nappe of mafic rocks of the Howse zone (Dimroth 1978; Clark and Wares 2004). In this study, we propose to rename the Romanet horst to the Romanet antiform in accordance with new data on the kinematics of the bounding faults as explained below.

The Wheeler dome (WH-A) is composed of albite−sericite−biotite gneiss (Fig. 2a) belonging to re-worked Archean basement (Dimroth 1978). A crystallization age of 2668 ± 5 Ma has been recently established for tonalite of the Wheeler dome based on SHRIMP U−Pb geochronological results obtained from zircon (Rayner et al. 2017; Corrigan et al. 2018). In the NE corner of the Wheeler dome, the gneiss has been retrograded to lower amphibolite facies as muscovite−biotite−plagioclase gneiss. Extremely sheared gneiss retrograded to sericite−biotite grade occurs in some zones in the southwest of the dome. According to Dimroth (1978), the Wheeler dome at its southwestern boundary is covered by metamorphosed arkose and arkosic conglomerate of the Milamar Formation (Fig 3) suggesting initially an unfaulted stratigraphic contact between Archean gneiss and Paleoproterozoic sedimentary cover. The Milamar arkosic sandstone and pebble conglomerate, dolomitic sandstone and dolomite are metamorphosed under greenschist facies (quartz−albite−sericite and calcite−epidote−tremolite schist and marble) and strongly deformed displaying undulatory extinction in quartz grains and mylonitic folded schistosity (Dimroth 1978). Clark and Wares (2004) suggested a major decollement is located at the base of the Wheeler dome (Fig. 2b), which implies that the gneissic basement and its sedimentary cover are allochthonous.

The Gerido and Retty zones (GE-RE) in the eastern part of the orogen (Fig. 2a) are composed of pyroclastic and sedimentary rocks with numerous basaltic lava flows (Doublet Group) and sills of mafic and ultramafic rocks of the Montagnais Group. These rocks form a synclinorium overturned to the west and thrust over the succession of the Wheeler zone (Figs. 1, 2) along the Robelin, Lac Walsh and Chassin faults (Clark and Wares 2004).

The hinterland of the Central Labrador Trough is composed of gneiss, migmatite, migmatized metasedimentary schist and amphibolite of the Rachel-Laporte zone (Figs. 1, 2a), grading into reworked Archean basement rocks and granitic plutons of the Kuujjuaq domain further to the east (Hoffman 1988; Wardle et al. 1990, 2002; Charette et al. 2017; Corrigan et al. 2018). The rocks of the Rachel-Laporte zone are thrust over the volcano-sedimentary succession of the Gerido and Retty zones (Wardle and Bailey 1981; Charette et al. 2017; Rayner et al. 2017).

Deformation and metamorphic events occurred in the NQO during the Trans-Hudson orogeny between > 1.87 Ga and 1.77 Ga (Machado et al. 1989; Machado 1990; Perreault and Hynes 1990; Wardle et al. 1990; Machado et al. 1997; Wardle et al. 2002). In the northern sector of the orogen, two metamorphic events related to crustal thickening and deformation occurred in the inner zone during collision at 1.845 Ga (granulite facies) and 1.83 Ga (amphibolite facies) (Perreault and Hynes 1990). In the central and southern segment of the hinterland of the Labrador Trough, deformation started at 1.82 Ga, following emplacement of magmatic arc rocks of the De Pas batholith (Fig. 1) and driven by the collision of Archean terranes to the west and east of the batholith (James and Dunning 2000). Amphibolite-facies metamorphism associated with crustal thickening was followed by cooling at 1775 Ma based on U−Pb ages obtained on zircon, monazite and rutile (Machado et al. 1989; James and Dunning 2000).

METHODS

Structural features of the Schefferville, Howse, and Wheeler lithotectonic zones (Fig. 2a) were studied in the Central Labrador Trough between the latitudes of 56°15' N and 56°30' N. Detailed structural and lithologic mapping were carried out in selected key areas 1−7 along the ca. 70 km long Minowean-Romanet transect (Figs. 3, 4), from the extreme frontal point of the Castignon Fault on the western shore of lac Castignon to the hanging wall of the Romanet Fault at the eastern shore of the Romanet River. Four cross-sections (Figs. 5, 6) were constructed through the studied areas based on our field observations and available geologic maps and reports. Structural elements (bedding, cleavage, schistosity, intersection and mineral lineations, fold axes and fault striations) were analyzed on stereonet plots (Figs. 5, 6) for each structural domain demonstrating regional tectonic zonation. All structural orientations are given according to the right-hand rule. On the basis of structural analysis, the main phases of tectonic deformation were distinguished and new 2D and 3D models of tectonic evolution of the region are proposed.

RESULTS
Schefferville Parautochthonous Zone

The Schefferville parautochthonous zone is about 30 km wide and is limited by the frontal Maraude and Castignon imbricated thrust faults in the WSW and the Argencourt thrust fault in the ENE (Fig. 2a).
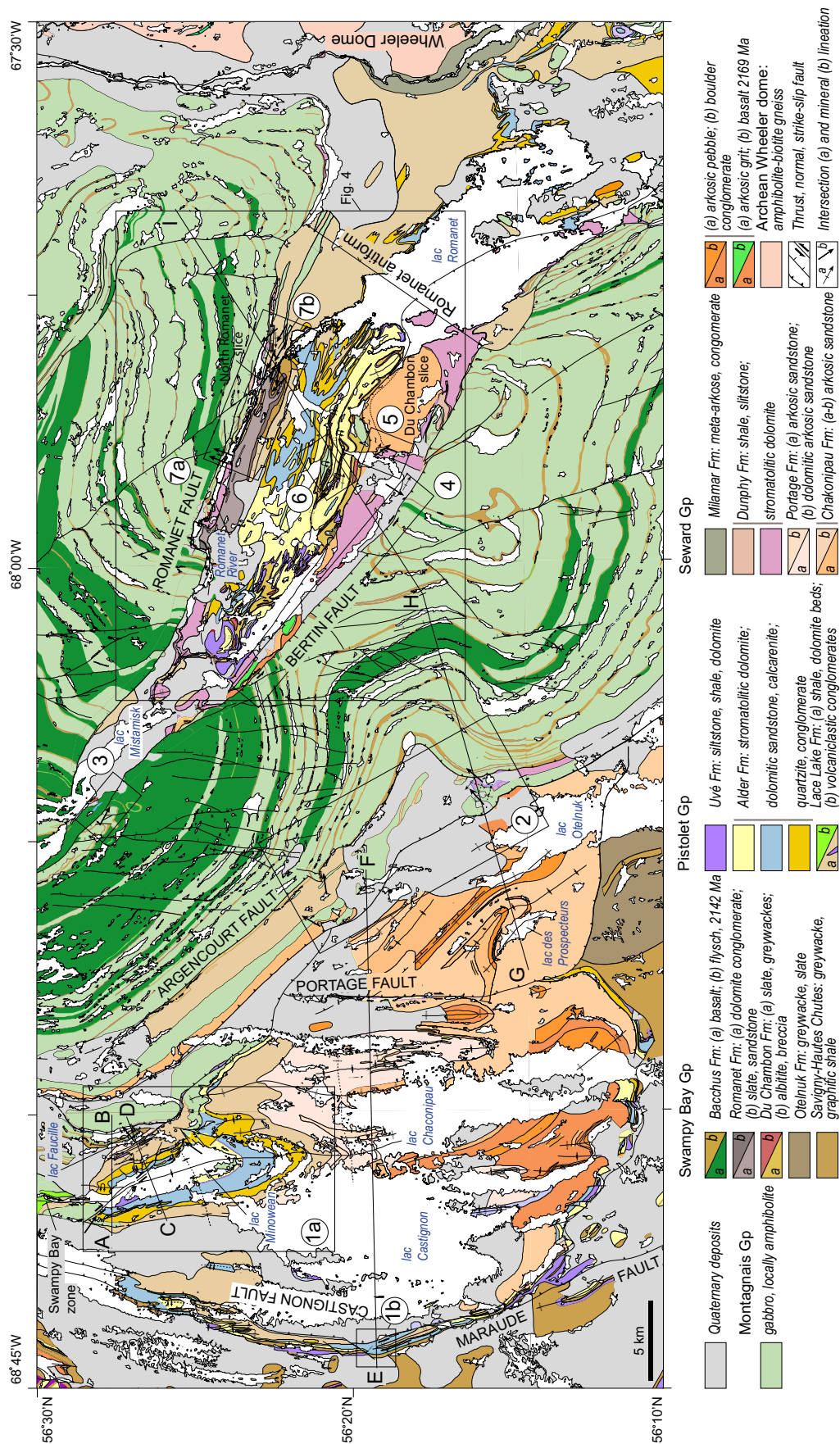
Figure 3. Geological map of the Central Labrador Trough modified after Dimroth (1978) and Clark and Wares (2004). The locations of the cross-sections and areas of structural domains 1−7 used for stereoplots on Figures 5 and 6 are shown.
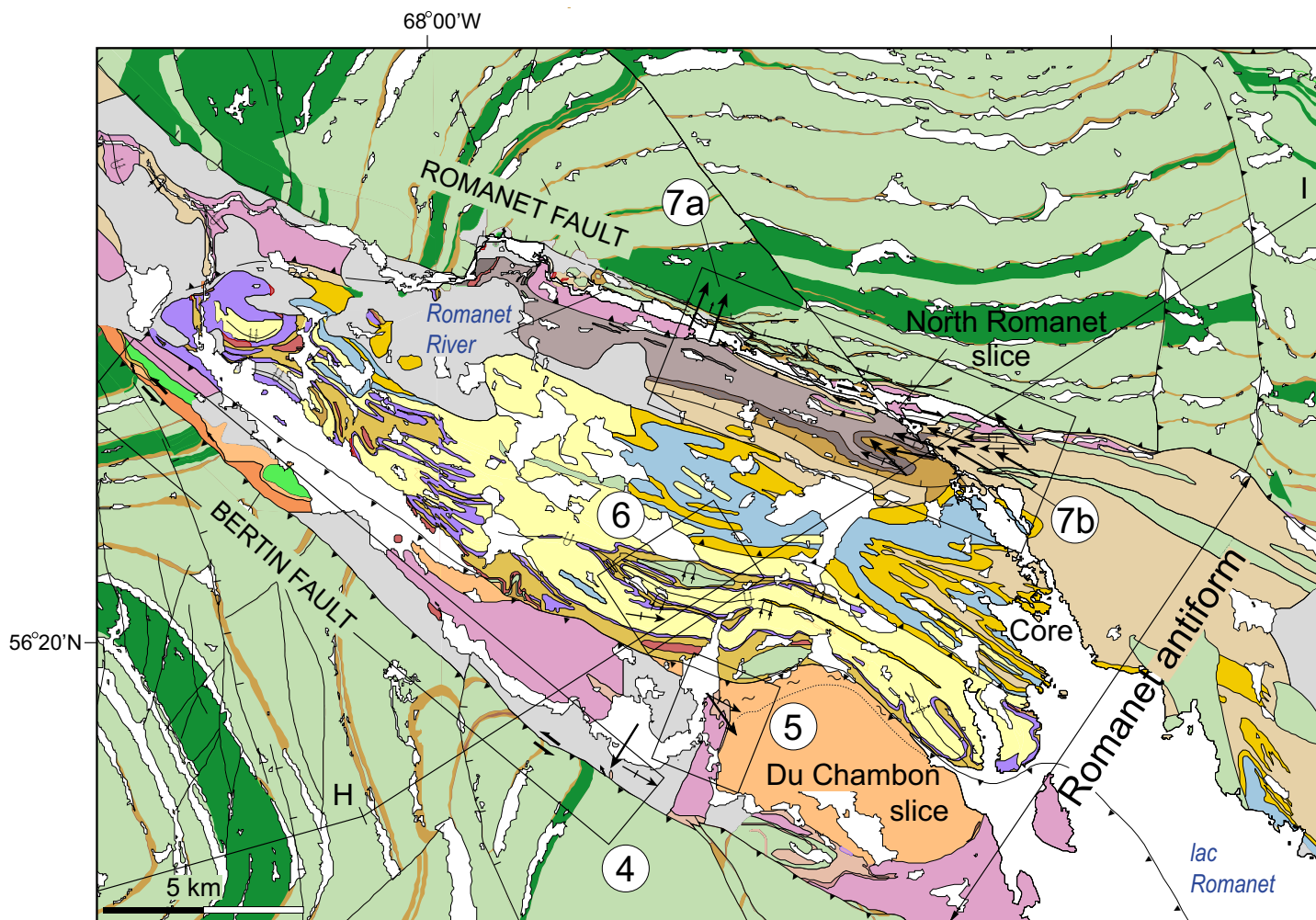
Figure 4. Geological map of the Wheeler zone modified after Dimroth (1978) and Clark and Wares (2004). The locations of cross-section G−H−I and areas of structural domains 4−7 used for stereoplots on Figures 5 and 6 are shown. A coloured legend is shown in Figure 3.

Frontal Thrust Faults

The Maraude Fault extends from north to south for more than 60 km (Fig. 2a). Along this fault, the older parautochthonous units of the Pistolet and Swampy Bay groups were detached along shale of the Lace Lake Formation and thrust to the WSW over the younger autochthonous mudrock of the Hautes Chutes and Savigny formations of the Swampy Bay Group in the west and over the Sokoman Formation of the Ferriman Group in the southwest (Fig. 2b). The more advanced part of the frontal slice is exposed in a 150−200 m high cliff to the west of lac Castignon (Fig. 3, area 1b). Along the cliff, the dolomitic and siliciclastic rocks of the Uvé and Alder formations and pelitic rocks of the Lace Lake Formation are folded in a system of N−S-striking inclined folds verging to the W (Fig. 5, line E−F) and occurring as open synclines (~ 300−400 m wide) and tight anticlines (~ 100−200 m wide). Above the fault contact, the overturned northeastern hanging limb of the frontal inclined syncline dips to the E at about 60° as recognized by the overturned orientation of the stromatolite beds in the limb (Fig. 7a). To the south of lac Castignon, a series of NW−SE-striking overturned synclines and anticlines

are mapped along the Maraude Fault, most probably aligned with the fault deviation caused by a lateral (SW−NE) scarp in the basement along the Cambrien-Otelnuk normal fault (Dimroth 1978; Clark and Wares 2004). The apparent westward displacement along the frontal Maraude and Castignon faults is about 20 km as estimated from the geometry of the erosional thrust front on the map (Fig. 2a).

The Castignon Fault extends from north to south for about 35 km along the western shore of lac Castignon (Fig. 3). This fault delineates the parautochthonous Castignon tectonic slice and corresponds to a detachment at the base of the Paleoproterozoic sedimentary succession (Figs. 2b, 5, line E−F). To the E, the tectonic slice is delimited by the Portage Fault (Fig. 3). The apparent westward displacement along the Castignon Fault is about 20 km (Fig. 5, line E−F).

The parautochthonous Castignon tectonic slice is composed of sedimentary rocks of the Seward Group in the south and Pistolet Group in the north (Fig. 3). The oldest red arkosic sandstone and conglomerate of the Seward Group (Chakonipau and Portage formations) form two anticlinoria in the southern part of the slice. The rocks form NNW−SSE-strik-
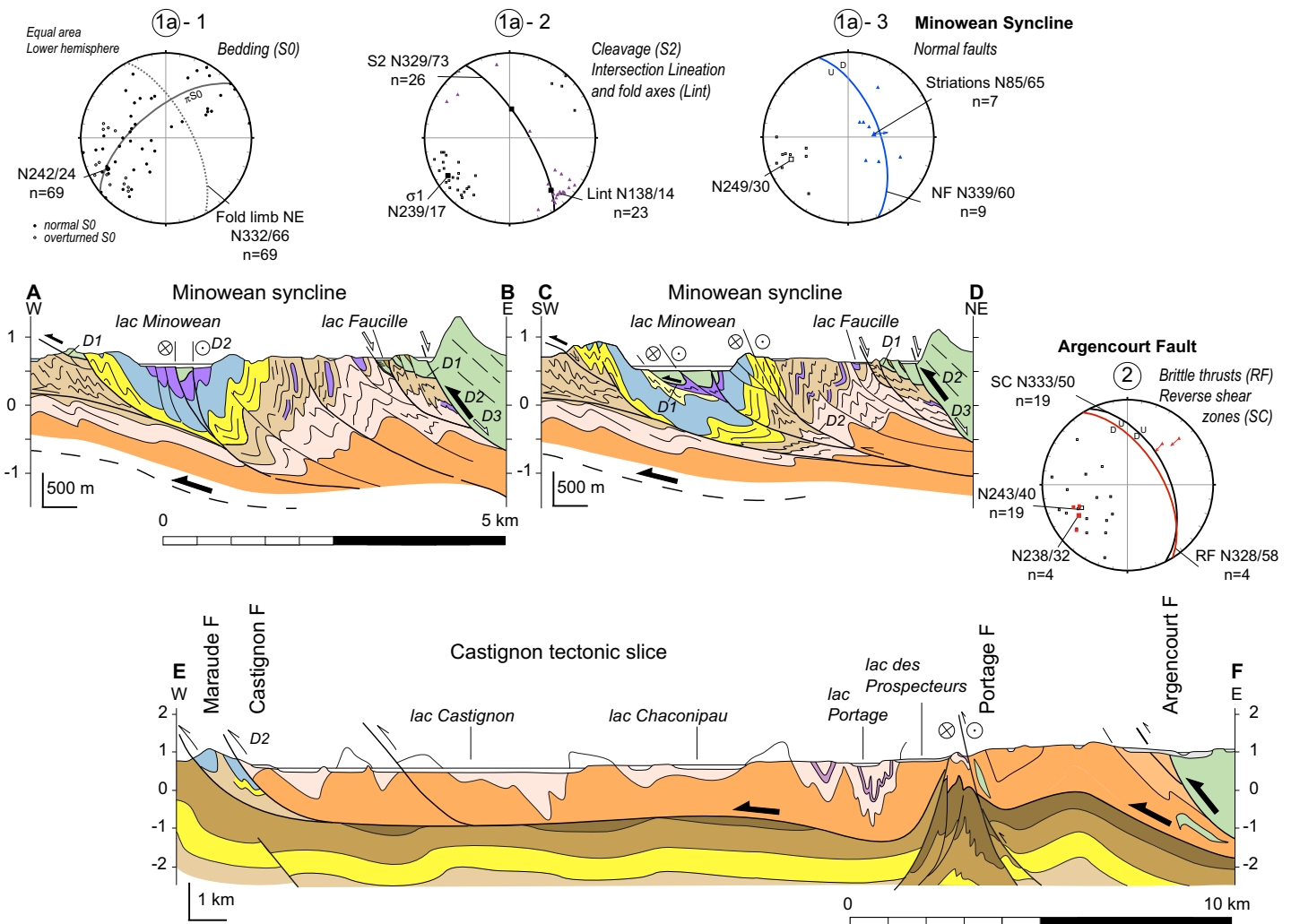
Figure 5. Cross-sections along lines A−B, C−D, and E−F, and stereoplots of principal structural features in studied areas 1−2 along the W−E transect across the Central Labrador Trough. The locations of the cross-sections and coloured legend are shown in Figure 3.

ing, 2−4 km wide open folds, upright in the east and inclined, verging to the WSW, in the frontal part of the slice (Fig. 5, line E−F). The argillaceous, siliciclastic and dolomitic rocks of the Pistolet Group (Lace Lake, Alder, Uvé formations) form the NW−SE-striking Minowean syncline in the north of the slice (Fig. 3, area 1a). The red arkosic sandstone of the Portage Formation (Seward Group) forms the narrow axial zone of a conjugate NW−SE tight anticline to the east of the Minowean fold, in front of the thick Montagnais gabbro frontal slice of the Howse allochthonous zone (Fig. 5, lines A−B, C−D). The inclined folds are verging to the southwest with one of the limbs found in an overturned position.

The Minowean Syncline
The Minowean syncline is about 5 km wide and 15 km long (Fig. 3). The SW-verging fold is steeply inclined: beds of the SW limb dip gently to the NE, while rocks of the NE limb are overturned (Fig. 7b) and dip steeply to the NE at 66°−90° (Fig. 5, stereonet 1a-1). The predominant S2 cleavage is oriented NW−SE (N329/73), parallel to the axial plane (Fig. 5, stere-

onet 1a-2), and dips at lower angles than bedding in the NE overturned limb (Fig. 7c). The pole of low-angle intersection lineation plunges to the SE (N138/14) and corresponds to the axis of a mesoscopic fold (Fig. 5, stereonet 1a-2). More competent dolomitic sandstone of the Alder Formation is folded in open folds, verging to the SW, second-order synclines that predominantly occur at outcrop scale. The second-order anticlines are rarely observed in outcrops and generally occur as tight cuspate folds in shale of the Uvé and Lace Lake formations. From the analysis of orientations of bedding, cleavage and intersection lineations in the Minowean fold area, the principal compressive stress σ_1 is oriented SW−NE (N239/17) (Fig. 5, stereonet 1a-2).

Fault Sets
Different sets of faults are recognized in the area of the Minowean syncline (Fig. 3). Two sets of the NW−SE-striking thrust faults can be distinguished in the area. D1-phase low-angle thrusts are preserved in the axial zone of the fold and on the eastern and western fold limbs at the contact of gabbro
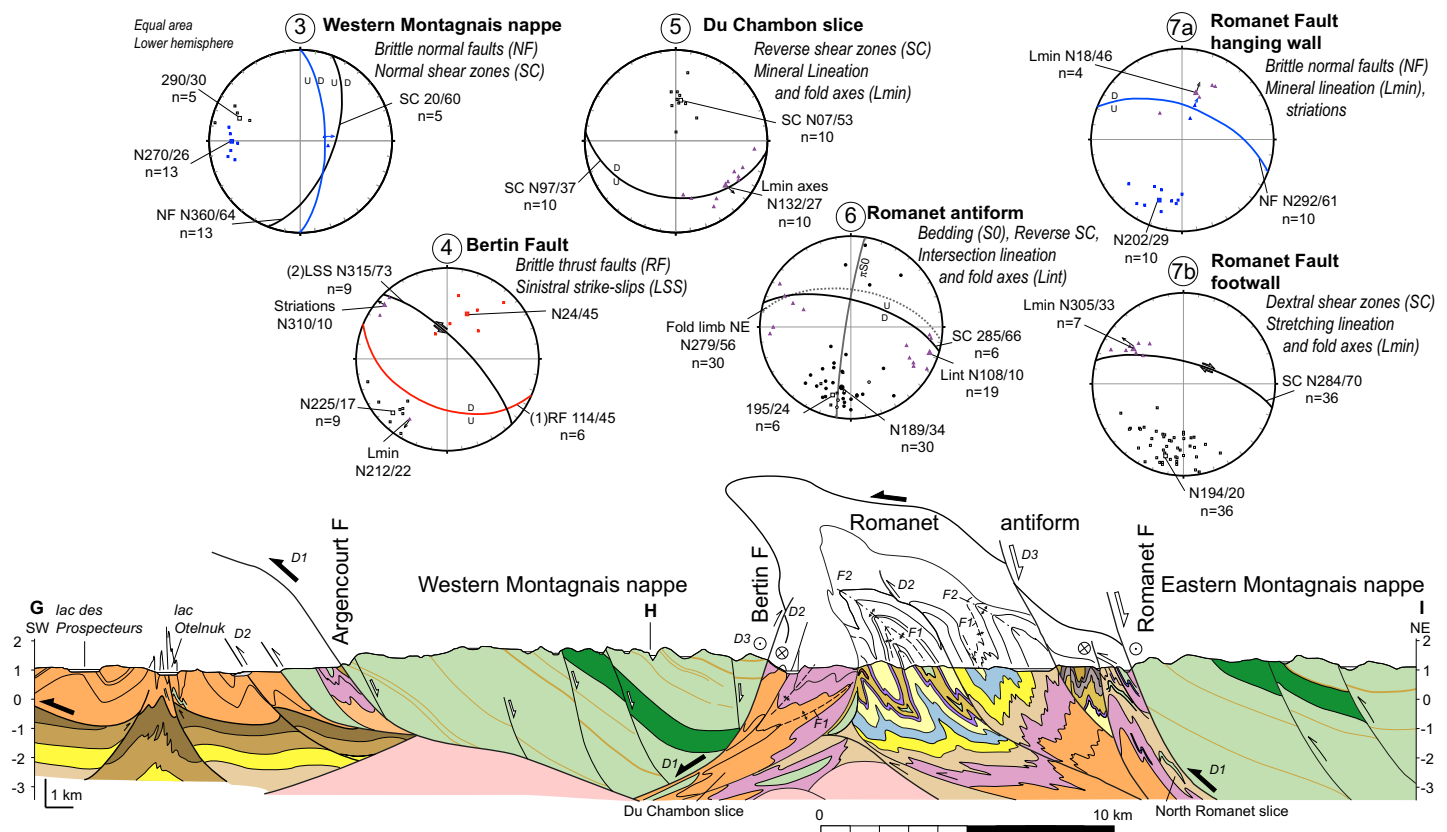
Figure 6. Cross-section along line G−H−I and stereoplots of principal structural features in studied areas 3−7 along the W−E transect across the Central Labrador Trough. The location of the cross-section and colour legend are shown in Figure 3.

slices thrust over shale of the Lace Lake and Uvé formations (Fig. 5, lines A−B, C−D). The D2-phase high-angle thrusts dipping to the northeast mostly affect the northeastern limb. Thrust-related brecciation and boudin rotation (Fig. 7d) were observed in graphitic shale of the Lace Lake Formation below the contact with a gabbro thrust sheet on the western limb of the Minowean fold.

A series of NW−SE right-lateral strike-slip faults with subordinate conjugate left-lateral strike-slip faults (Fig. 7e) and brittle-ductile shear bands of *en echelon* tension fractures affect the northern and northeastern part of the Minowean fold (Fig. 3). These right-lateral strike-slip faults seem to accommodate the dextral displacement along the N−S (N178/80) dextral mylonitic shear zone that runs along the Swampy Bay River at the northern periclinal closure of the Minowean fold (Fig. 3). Along the Swampy Bay dextral mylonitic shear zone, the right-lateral subvertical ductile shear bands SC-C' (Fig. 8a, b) are developed in highly deformed volcaniclastic conglomerate that was previously described as part of the Lace Lake Formation (Brouillette 1989). Pyrite mineralization occurs in the sheared matrix.

Numerous late NNW−SSE-striking near-vertical normal faults (Fig. 7f) of low displacement amplitude (Fig. 5, lines A−B, C−D) cut the NE limb of the Minowean syncline (Fig. 3). The striations on these faults plunge to the ENE with the mean pole oriented N85/65 (Fig. 5, stereonet 1a-3). These faults belong to the same system as the normal faults at the

contact between the Montagnais gabbro frontal slice and shale of the Lace Lake Formation to the east of the Minowean syncline (Fig. 3) that are described in the next section.

Howse Allochthonous Zone
The Howse allochthonous zone extends NW−SE for about 300 km and is delimited by the Argencourt and Ferrum River thrust faults to the west and Robelin and Chassin thrust faults to the east (Fig. 1). The Howse zone includes (Fig. 2a): (i) frontal slices composed of sedimentary rocks of the Seward, Pistolet and Swampy Bay groups and gabbro of the Montagnais Group; (ii) two voluminous Montagnais nappes composed of gabbro (Montagnais Group) and basalt with subordinate sedimentary rocks (Bacchus Formation) (Clark and Wares 2004). The two Montagnais nappes are separated by sedimentary rocks exposed in a tectonic window of the Wheeler zone (Fig. 2a).

Frontal Slices of the Howse Zone
An approximately 600 m thick frontal tectonic slice of Montagnais Group gabbro is thrust over the Paleoproterozoic sedimentary succession of the Schefferville zone in the lac Faucille area, to the east of the Minowean syncline (Fig. 3). Below the main steep thrust contact, a series of gabbro lenses are thrust over the Lace Lake Formation shale (Fig. 5, lines A−B, C−D). Late extensional features overprint compressional structures (Fig. 8c, d). The gabbro lenses contain numerous
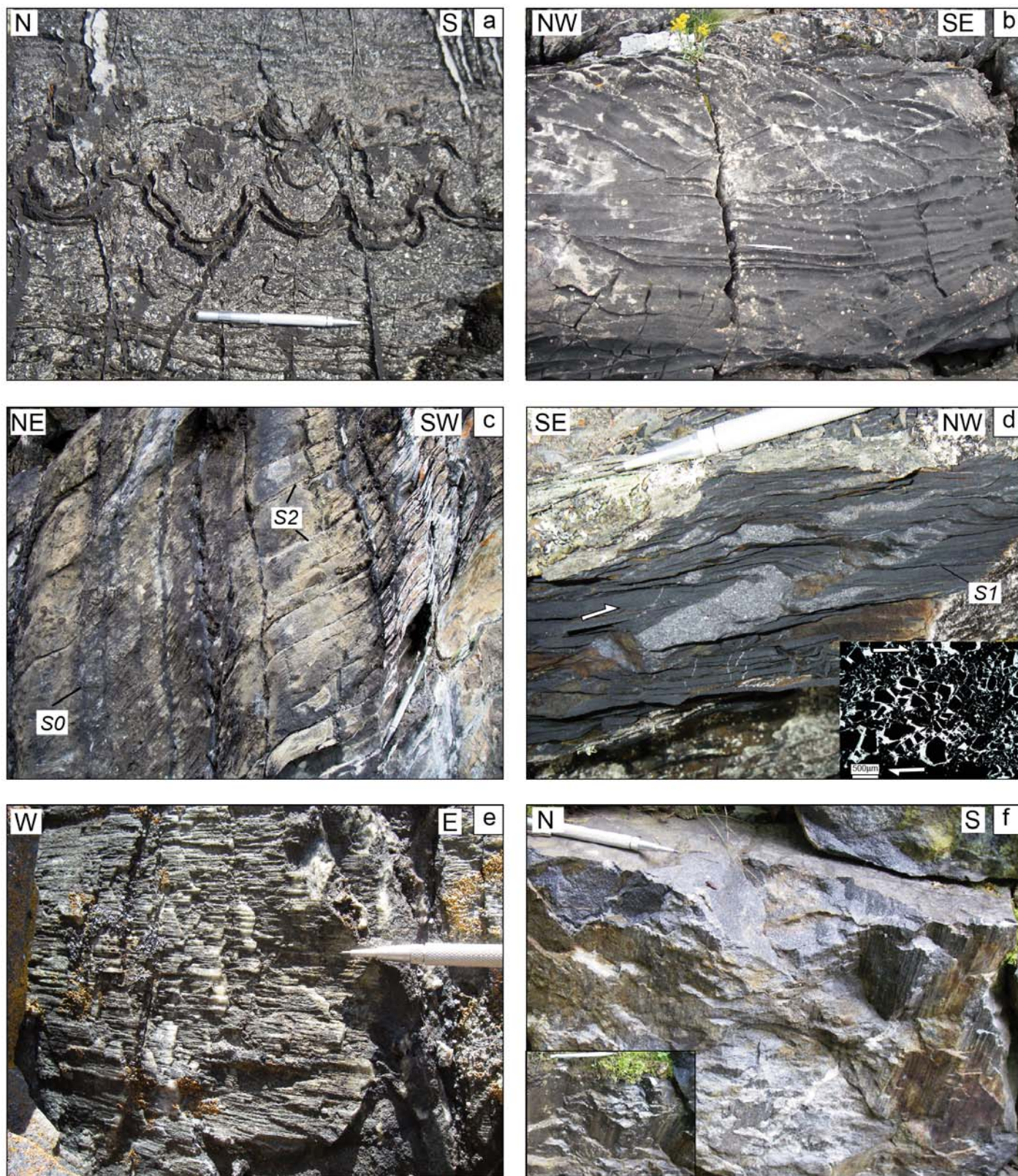
Figure 7. Structural elements of areas of the Schefferville zone (areas 1a and 1b of Figure 3): (a) overturned stromatolite beds in the overturned northeastern limb of a syncline in the hanging wall of the Castignon Fault; (b) overturned cross-bedded stratification in dolomitic quartz sandstone of the Alder Formation, northeastern limb of the Minowean fold; (c) low-angle cleavage and steep bedding dipping to the northeast in the overturned northeastern limb of the Minowean fold; (d) brecciation and boudin rotation in Lace Lake shale below the thrust contact with the Montagnais gabbro in the northwestern part of the Minowean fold; the inset in (d) shows thin section of brecciated graphitic slate from the boudin; (e) striations on a left-lateral strike-slip fault and (f) on normal faults in the northeastern limb of the Minowean syncline.
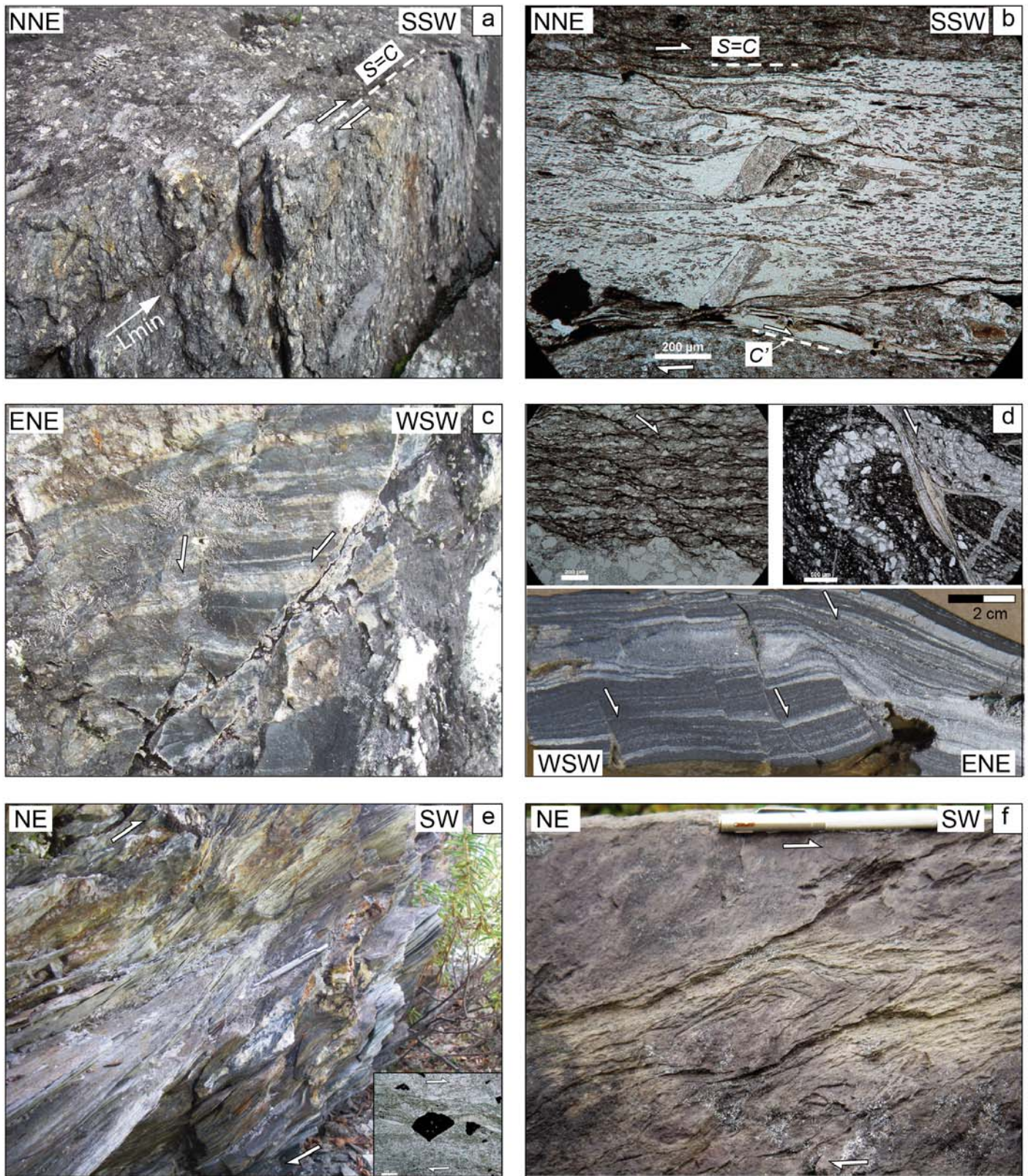
Figure 8. Structural elements of the Schefferville zone (areas 1a and 2 of Figure 3): (a) outcrop and (b) thin-section view of the SC-C' dextral shear bands of the north–south-striking Swampy Bay mylonitic shear zone; (c, d) outcrop, hand specimen and thin sections view of brittle normal faults and semi-brittle normal shear bands in shale of the Lace Lake Formation below the thrust contact with the frontal gabbro tectonic slice at the northeastern limb of the Minowean syncline; (e, f) outcrop views of reverse sheared gabbro of the Montagnais Group in the hanging wall (e) and siltstone of the Lace Lake Formation in the footwall (f) of the Argencourt Fault. The inset in (e) shows stress shadows around a pyrite rotation structure in metasandstone of the Bacchus Formation at the main thrust contact.

steep planes of normal faults with striations dipping to the northeast. Listric normal faults (Fig. 8c), brittle fractures and ductile-brittle shear zones with normal displacement (Fig. 8d) occur in the Lace Lake shale below the contact with massive gabbro. The mean plane of the normal faults (Fig. 5, stereonet 1a-3) is oriented striking NNW−SSE (N339/60) with mean striation plunging ENE (N85/65) indicating a WSW−ENE orientation of late extension.

The Portage Fault delineates the western limit of the frontal slice (Fig. 3), which is mostly composed of red conglomerate and arkosic sandstone of the Chakonipau Formation of the Seward Group (Dimroth 1978). It represents a N−S high-angle thrust fault with a right-lateral strike-slip component that dips steeply (N335/72) to the E (Fig. 5, line E−F). Lenses and sills of gabbro of the Montagnais Group recognized in the sedimentary rocks of the Chakonipau Formation in the eastern part of the slice are considered as *in situ* (Dimroth 1978). The sedimentary rocks in the slice are folded in a series of ca. 1−2 km wide NW−SE open upright synclines and anticlines (Fig. 3). The pole to the NE limb of the mesoscopic fold is oriented N231/12. The high-angle NW−SE schistosity S2 dips to the NE (N326/70). The pole of schistosity corresponds to σ_1 oriented NE−SW (N236/20).

Argencourt Fault

The Argencourt Fault corresponds to a NW−SE regional thrust fault verging to the SW (Figs. 2a, 3) that delineates the western limit of the nappes composed of voluminous gabbro of the Montagnais Group, and basalt and metasedimentary rocks of the Bacchus Formation in the Howse zone (Dimroth 1978; Clark 1986; Clark and Wares 2004). The main thrust contact at the base of the Western Montagnais nappe is localized in metasandstone beds of the Bacchus Formation below the gabbro (Fig. 6, line G−H). The NW−SE reverse SC shear bands (N333/50) dipping to the northeast with mineral lineations plunging to the NE (N40/37) occur in the Bacchus metasandstone (Fig. 5, area 2). The steep S planes in SC shear bands, underlined by oriented mica and fibrous quartz−feldspar−chlorite in oriented pressure shadows around the pyrite grains (Fig. 8e, inset), indicate a reverse sense of displacement and tectonic transport to the SW (N243). The gabbro above the thrust is sheared and transformed into carbonate−chlorite schist (Fig. 8e) characterized by SC reverse shear bands with foliation defined by preferred orientation of chlorite fibers.

Along the frontal part of the Western Montagnais nappe, in the footwall of the Argencourt Fault, relatively thin bodies of strongly sheared gabbro form southwest-verging tectonic lenses in the sedimentary rocks of the Seward and Pistolet groups. Siltstone and sandstone of the Lace Lake Formation and stromatolite dolomite of the Dunphy Formation in the footwall of the Argencourt Fault are characterized by bedding dipping NNE at 35−60° (N290−305/32−58, mean S0 N298/31) and display a strong NW−SE S2 schistosity (Fig. 8f) dipping to the NE (N333/50).

Montagnais Gabbro-basalt Nappes

The gabbro-basalt rocks of the Howse zone form voluminous nappes extending NW−SE for about 300 km (Fig. 2a). A single nappe of mafic rocks, about 30 km wide, in the NW is split southeastwards into two ca. 10 to 20 km wide nappes (Fig. 3), which we name the Western and Eastern Montagnais nappes (Fig. 6, line G−H−I). In the study area, the Western Montagnais nappe is thrust over the sedimentary succession of the Schefferville parautochthonous zone and frontal slices of the Howse zone along the NW−SE Argencourt Fault. In the NE, volcanic and sedimentary rocks of the Gerido zone are thrust to the southwest over the Eastern Montagnais nappe along the NW−SE Robelin thrust fault (Fig. 2a). The Western and Eastern Montagnais nappes are separated by highly deformed sedimentary rocks of the Seward, Pistolet and Swampy Bay groups of the Wheeler zone (Fig. 3) described below as the Romanet antiform and delineated by the NW−SE Bertin and Romanet faults.

The Montagnais nappes are composed of a thick (likely ~ 3−5 km) stratified succession of intercalated Montagnais gabbro sills, Bacchus basalt and relatively thin (a few metres) packages of sedimentary rocks (Fig. 6, line G−H−I). The rocks dip at 15° to 45° to the N−NE in the Western Montagnais nappe and to the N in the Eastern Montagnais nappe (Fig. 3). The gabbro sills are massive or stratified; in some cases the gabbro is affected by retraction fracture systems. The basalt flows are massive or pillowed. Bacchus siltstone and sandstone form 2−5 m-thick layered packages between the gabbro sills and basalt flows.

The Montagnais nappes are affected by different sets of faults. Structural elements related to nappe emplacement are less preserved. Second-order NW−SE-striking thrust faults dipping to the NE (N352/66, striation N82/66) occur in the Montagnais gabbro in the hanging wall of the frontal Argencourt Fault. Horizontal, 3−4 cm-thick veins filled with vertically grown fibrous zeolite occur in basalt at the top of the Western Montagnais nappe (Fig. 3, area 3) and could be associated with the major shortening phase, thus indicating a horizontal orientation of the main tectonic stress. Systems of subvertical, metre-scale displaced N−S right-lateral strike-slip faults and minor W−E left-lateral strike-slip faults were observed in the mafic rocks of the nappes. The most dominant structural features in the Montagnais nappes are the N−S high-angle normal faults (Fig. 9a) and NNE−SSW extensional shear zones (Fig. 9b). The normal faults dip generally to the E in the Western Montagnais nappe and to the W in the Eastern Montagnais nappe (Fig. 3 and Fig. 6, area 3). The N−S high-angle normal faults were likely emplaced during the late extensional tectonic phase as they displace the major faults bounding the Montagnais nappes, such as the Argencourt, Bertin and Romanet faults (Fig. 3).

Wheeler Allochthonous Zone

The Wheeler allochthonous zone (Fig. 2a) includes Paleoproterozoic sedimentary rocks of the Seward, Pistolet and
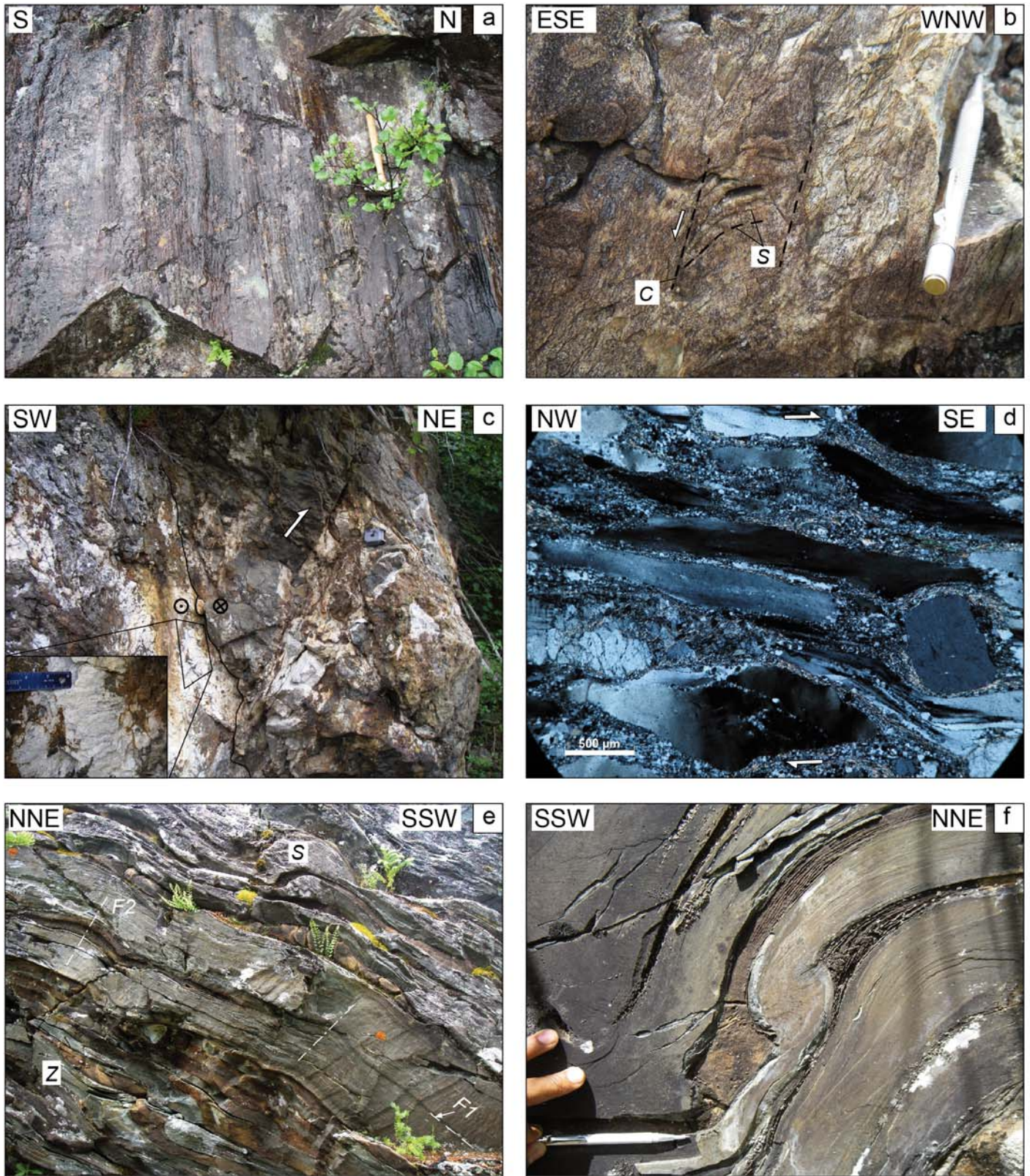
Figure 9. Structural elements of the Howse (a, b) and Wheeler (c, f) zones (areas 3−5 of Figure 3): (a) striations on the north−south-striking brittle normal fault in Bacchus basalt and (b) ductile SC normal shear zone in gabbro of the Western Montagnais nappe; (c) boudinaged fragments of Bacchus basalt in the NE-verging Bertin thrust fault zone that is cut by a subvertical left-lateral strike-slip fault with horizontal calcite striations; (d, e) Du Chambon tectonic slice: (d) strong mylonitic shearing of quartz sandstone of the Chaconipau Formation; (e) mesoscopic tight isoclinal fold F1 dipping to the SSW, slightly refolded by steeply inclined to the NNE folds F2 in dolomitic sandstone of the Dunphy Formation; note S and Z parasitic folds on the limbs of F1 fold; (f) S-type parasitic fold on the limb of F1 fold.

Swampy Bay groups and gneiss of Archean basement of the Wheeler dome (Dimroth 1978; Clark and Wares 2004). Two major faults, the Bertin Fault in the west and the Romanet Fault in the east, delineate the boundaries of the Wheeler zone (Figs. 3, 4). Previously, these faults were interpreted either as converging thrusts (Dimroth 1978) or as diverging normal faults bounding the Romanet horst (Clark and Wares 2004).

Bertin Fault

The Bertin Fault extends NW−SE along the western limit of the Romanet antiform, separating rocks of the Western Montagnais nappe to the SW from arkosic sandstone of the Chakonipau Formation and siliciclastic rocks and dolomite of the Dunphy Formation (Seward Group) that form the Du Chambon tectonic slice to the NE (Figs. 4, 6). The Bertin fault zone includes the NE-verging thrust faults (N114/45) reworked by the NW−SE left-lateral strike-slip faults (N302/86) (Fig. 6, area 4) observed both in the northern and southern segments of the fault zone. The thrust faults mark the contact between gabbro or pillow lavas and sedimentary rocks. Zones of tectonic breccia with boudins of gabbro or basaltic rocks within a carbonate matrix occur below the thrust contact (Fig. 9c). The S-dipping schistosity (N84/32) and mineral lineation plunging to the SW (N212/22) occur in the rocks of the Dunphy Formation in the footwall of the Bertin Fault (Fig. 4, area 4). The subvertical NW−SE left-lateral strike-slip faults (N302/86) are superimposed over the NW−SE thrust structures and display calcite-filled subhorizontal striations on the fault planes (Fig. 9c, inset). Subhorizontal striations and *en echelon* subvertical fracture systems indicating left-lateral displacement were observed at three different outcrops along the Bertin fault zone in area 4 (Figs. 4, 6, area 4). These observations allow us to interpret the Bertin Fault as a refolded thrust fault with initial D1 tectonic transport to the SW, which was reactivated as a top-to-the NE thrust during the D2 shortening phase and then experienced the NW−SE strike-slip left-lateral motion during D3 phase (Fig. 6, line H−I).

Romanet Antiform

The Romanet antiform (former Romanet horst) extends NW−SE for more than 35 km. Its width increases from about 3 km in the northwest to about 12−15 km in the southeast, at the border with the Archean Wheeler metamorphic dome (Fig. 3). The Romanet antiform is composed of a Paleoproterozoic sedimentary succession (Figs. 4, 6, Line H−I) of the Seward, Pistolet and Swampy Bay groups (Dimroth 1978; Clark 1986). Slate and sandstone of the Du Chambon Formation and dolomitic boulder conglomerate of the Romanet Formation (Fig. 2b) represent lateral facies of the Swampy Bay units exposed in the Schefferville and Cambrien tectonic zones to the west. The pelitic rocks of the upper part of the Du Chambon Formation contain albite−carbonate laminated and brecciated rocks of the Mistamisk Complex. The Montagnais gabbro and amphibolite form extended lenses of variable size in the sedimentary succession.

The older sedimentary units of the Seward Group (Chakonipau and Dunphy formations) are exposed in the Du Chambon and North Romanet tectonic slices (1 km to 4.5 km wide) along the southwest and northeast borders of the Romanet antiform dipping respectively to the southwest and northeast below the Western and Eastern Montagnais nappes (Figs. 4, 6, line H−I). The younger units of the Pistolet and Swampy Bay groups are exposed in the central part of the antiform that is about 7 km wide, within which rocks are deformed in a system of tight refolded synforms and antiforms extending WNW−ESE and verging to the SSW (Figs. 4, 6, line H−I).

Du Chambon Tectonic Slice

The Du Chambon tectonic slice (Fig. 4) is exposed in the footwall of the Bertin Fault for 28 km with a width varying from about 800 m in the northwest to 4.5 km in the southeast. The slice is composed of arkosic sandstone of the Chakonipau Formation and siliciclastic rocks and dolomite of the Dunphy Formation (Seward Group) emplaced over the rocks of Du Chambon and Uvé formations in the central zone of the Romanet antiform. Siltstone, dolomitic sandstone and dolomite of the Dunphy Formation in this slice are folded as tight isoclinal mesoscopic F1 folds with fold planes either horizontal or dipping to the SW (Fig. 9e). The mesoscopic folds are about 1−1.5 m wide and about 3−4 m in amplitude. The parallel limbs of the isoclinal folds can be distinguished by the presence of S- and Z-type parasitic folds (Fig. 9e) and microfolds in more ductile dolomitic beds jammed between more rigid siliciclastic sandstone (Fig. 9f). The F1 fold limbs and schistosity SC1 (Fig. 6, area 5) run parallel to the axial plane and are either subhorizontal or dip gently to moderately to the WSW (N97/37), whereas the microfold axes plunge gently to the SE (N145/28). Arkosic sandstone of the Chakonipau Formation underwent ductile shear deformation and is characterized by the presence of SC1 shear bands (Fig. 9d) and mylonitic stretching lineation plunging to the SE (N132/27) (Fig. 6, area 5). Detrital quartz grains are flattened, stretched and bent within a fine-grained quartz−mica matrix. The overturned F1 isoclinal folds are refolded by N−S upright small-amplitude (25−30 cm) F2 folds with subhorizontal axes N96/14 (Fig. 9e) and cut by NNE-verging thrust faults (N95/42) (Fig. 6, line H−I). These observations support our interpretation that the overturned SW-dipping Du Chambon tectonic slice likely represents the sheared base of the sedimentary succession deformed during the D1 deformation phase (Montagnais nappe emplacement) and subsequently refolded during the D2 shortening phase.

Core of the Romanet Antiform

The core of the Romanet antiform is made up of predominantly sedimentary rocks deformed in refolded WNW−ESE-striking antiforms and synforms that plunge to the WNW (Fig. 4). The older units of the Milamar and Lace Lake formations are exposed in the ESE of the core surrounding Archean rocks of the Wheeler metamorphic dome (Fig. 3). The younger units of the Alder-Uvé formations and Du Chambon-Romanet formations occur to the WNW and on the northeast and southwest borders of the core (Fig. 4).

The core of the Romanet antiform represents a large-scale recumbent isoclinal F1 syncline refolded by steeply (65°−76°) inclined SSW-verging F2 folds and cut by the WNW−ESE thrusts and normal faults (Fig. 6, line H−I). The core of the recumbent F1 syncline is composed of graphitic slate and dolomitic quartzite of the Du Chambon Formation containing lenses of the Montagnais gabbro and fragments of albite−carbonate rocks and breccia of the Mistamisk Complex. The upper limb of the F1 syncline is deeply eroded and the lower limb consists of rocks of the Pistolet and Seward groups. The F1 syncline is broken by WNW−ESE faults into three longitudinal segments (Fig. 4); the middle segment is uplifted and thrust over the southwestern one; the northeastern segment is downthrown along a NW−SE normal fault (Fig. 6, line H−I).

The mesoscopic F2 folds are about 600−800 m wide (Fig. 6, line H−I) and are accompanied by about 12−15 m wide secondary folds (Fig. 10a) and by 10−20 cm-scale parasitic folds (Fig. 10b). Normal and reverse bedding (N279/56) on limbs of F2 folds is recognized by stromatolite structures in dolomite, cross-bedding orientation in sandstone and schistosity−bedding relationships in shale units. The intersection lineation and F2 fold axes (Fig. 10b) are subhorizontal and gently plunge to the WNW and ESE (Fig 6, area 6). Rocks on the F2 limbs are sheared to different extents: stromatolite beds or cross-bedded sandstone beds with no grain flattening grade into highly strained rocks. Quartzite and dolomitic quartz sandstone are partially or completely recrystallized showing microstructures of recrystallized elongate quartz grains with quartz directional overgrowths in preferred orientations surrounded by ribbons of newly formed isometric fine quartz grains and/or sub-parallel mica foliae that define the microscopic fabric (Fig. 10c). The boulders (up to 1 m) of dolomitic sandstone and dolomite in conglomerate of the Romanet Formation locally remain undeformed but strongly flattened in high-strain deformation zones (Fig. 10d, e). The dolomitic quartz sandstone matrix of stretched conglomerate is recrystallized with quartz clasts surrounded by fine-grained quartz bands and mica foliae aligned between gravel-size quartz clasts parallel to the schistosity plane. The high-angle reverse schistosity SC2 in the rocks of the Romanet antiform (Fig. 6, area 6) dips to the NNE (N285/66), parallel to the axial planes of the SSW-verging F2 folds and corresponds to the D2 shortening deformation phase.

The high-angle schistosity SC2 dipping to the NNE is overprinted by a subhorizontal crenulation cleavage S3 (Fig. 10f) that occurs in the Lace Lake slate below the Romanet boulder conglomerate in the northeast of the Romanet antiform (Fig. 6, area 7b) and indicates vertical orientation of the main stress during D3 normal faulting (Fig. 6, line H−I).

The Romanet Fault Zone

The footwall of the Romanet fault zone (400−800 m wide) is exposed along the southern and northern shores of the Romanet River and is described here as the North Romanet tectonic slice (Fig. 4). It is composed of folded and sheared slate and mylonitic quartz−mica schist of the Lace Lake Formation and dolomite of the Dunphy Formation that were

emplaced to the southwest over boulder conglomerate of the Romanet Formation (Fig. 6, line H−I). The mylonitic schist of the Lace Lake Formation in the North Romanet tectonic slice is characterized by the development of high-angle dextral ductile shear zones (Fig. 11a−d) and subhorizontal to low-angle mineral lineations (Fig. 11e, f). The dextral SC-C' shear zones are oriented WNW−ESE (SC N284/70, C' N298/66) and the mineral lineations and fold axes plunge to the WNW (N305/33) (Figs. 4, 6, area 7b). The extensional C' shear bands, quartz boudins and microfolds in mylonite indicate a dextral sense of shearing (Fig. 11a, c, d). Axes of cylindrical F1 microfolds gently plunge to the WNW (Fig. 11b). The low-angle mineral lineation is subparallel to the fold axes and to the orogen and indicates top-to-the-east tectonic transport during the early phase of oblique convergence. The dolomite and dolomitic quartz sandstone of the Dunphy Formation in the North Romanet tectonic slice are thrust to the SSW over the mylonitic schist of the Lace Lake Formation (Fig. 6, line H−I) and are characterized by a WNW−ESE high-angle schistosity dipping to the NNE (N290/50−52). W−E extended lenses of amphibolite and phlogopite gabbro with carbonate-altered brecciated zones occur in the North Romanet tectonic slice.

The hanging wall of the Romanet fault zone is exposed on the north shore of the Romanet River (Fig. 4, area 7a). It is characterized by a series of NW−SE high-angle normal faults and shear zones developed in the mafic rocks of the Bacchus Formation and Montagnais Group along the boundary with the sedimentary rocks of the North Romanet slice. The faults dip to the NE (N292/61) (Fig. 6, area 7a), and fault surfaces are characterized by undulations and striations (Fig. 12a) indicating normal-fault displacement. The siliciclastic rocks interbedded with pillowed basalt are affected by semi-brittle normal faulting (Fig. 12b). The steep normal SC shear bands display a low-angle schistosity (S) dipping to the N−NE (N295/64). The gabbro and basalt in the fault zones are stretched and boudinaged; within high-strain normal ductile shear zones basalt (Fig. 12c) and graphitic slate (Fig. 12d) are mylonitized with development of SC-C' extensional shear bands. The normal fault striations, mineral lineations and secondary fold axes plunge to the NNE (N18/46) indicating a SW−NE orientation of extension (Fig. 6, area 7a).

In the transition zone between the footwall and hanging wall of the Romanet fault zone, the initial reverse movement is identified by preserved reverse SC1 shear bands (N270/50) and by micro-folds in quartz−chlorite schist (Fig. 12e, f) of the Lace Lake Formation.

The observations described here allow us to interpret the Romanet Fault as a fault zone with combined kinematics (Fig. 6) of top-to-the SSW thrusting and dextral shearing in the footwall that were likely continuous during the D1−D3 deformation phases and top-to-the NE normal faulting that occurred in the hanging wall during the D3 extensional phase.

Hence, the observations of fault kinematics along the Bertin and Romanet faults and internal structure of the Wheeler allochthonous zone support the interpretation of an antiform, and the Romanet horst is therefore reinterpreted here as the Romanet antiform. This structure is interpreted as
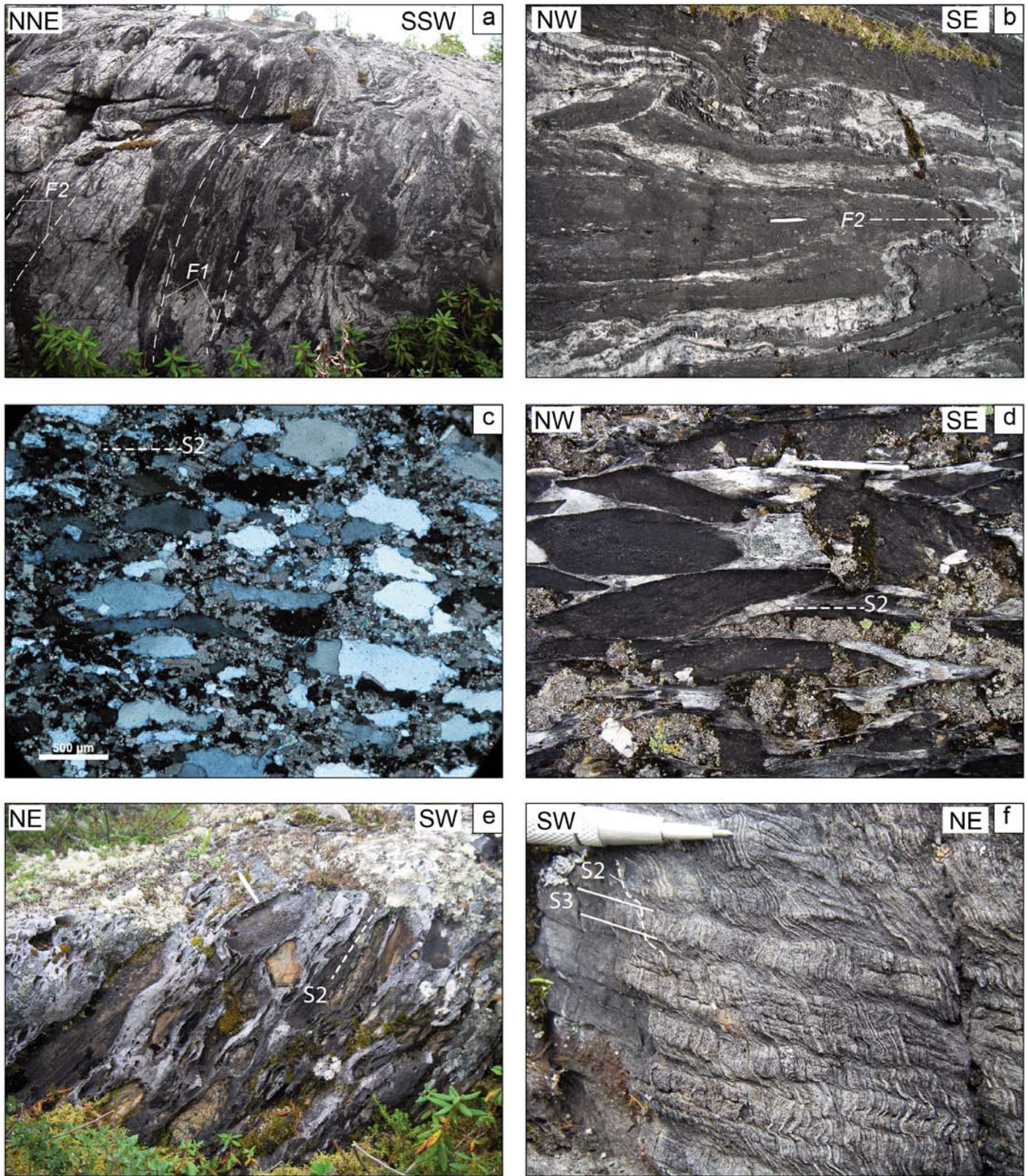
Figure 10. Structural elements of the Romanet antiform (areas 6 and 7b of Figure 4): (a−c) isoclinal folds F1 refolded by SSW-verging steeply inclined F2 folds (a); with sub-horizontal axes (b); formed by dolomitic quartz sandstone of the Alder Formation, area 6; thin section of sheared matrix of Alder dolomitic sandstone (c) is characterized by elongate quartz grains with directional overgrowth in high-strain zones; (d−e) flattened boulders of dolomitic sandstone in Romanet conglomerate (d); with schistosity dipping to the NE (e); (f) subhorizontal crenulation cleavage S3 refolding steep NE-dipping schistosity S2 in slate of the Lace Lake Formation, zone 7b.
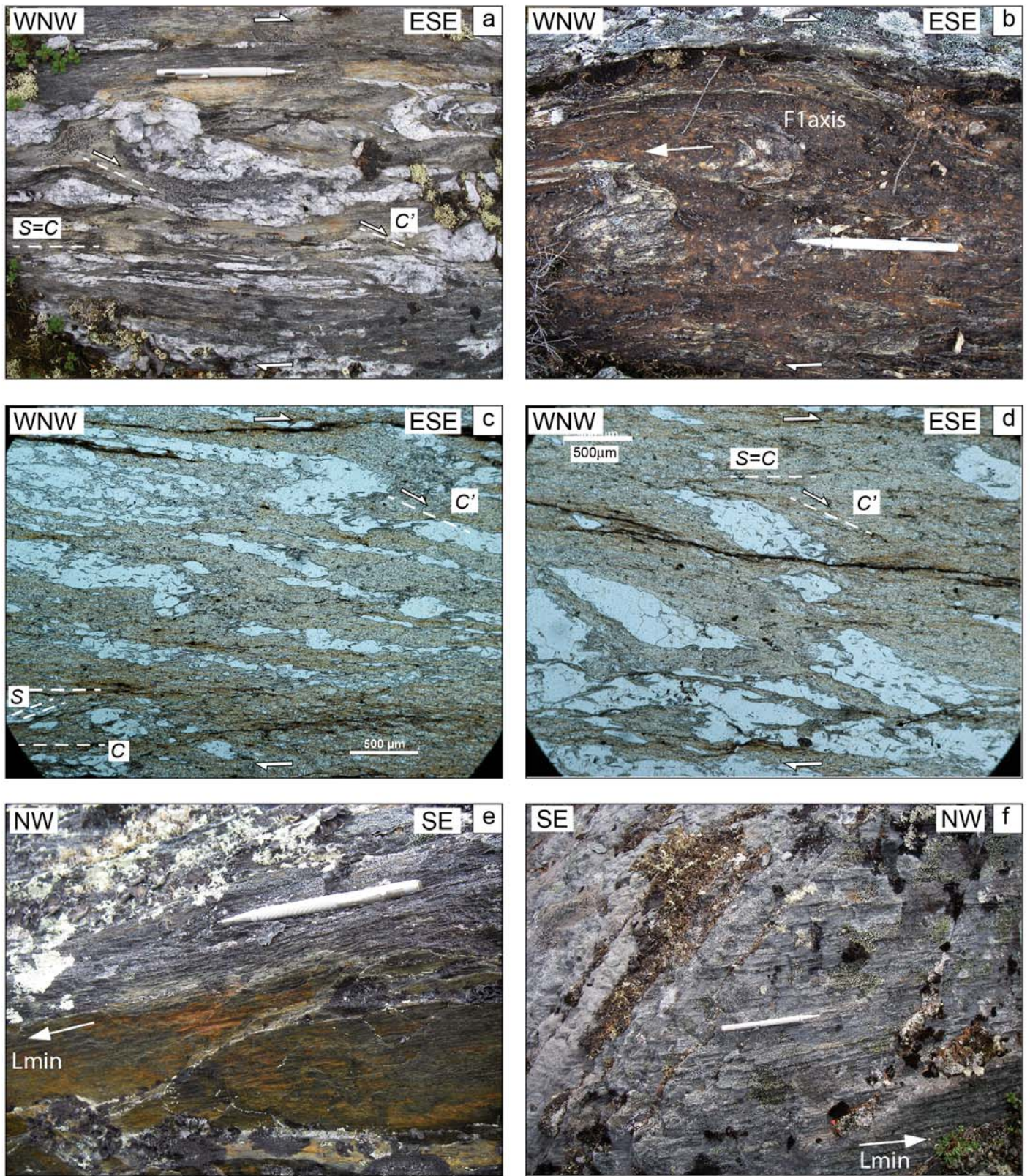
Figure 11. Structural elements of the WNW–ESE dextral mylonitic shear zone in the Lace Lake quartz–mica schist and slate in the footwall of the Romanet Fault (area 7b of Figure 4): (a) SC-C' dextral shear bands and quartz microfolds; (b) cylindrical F1 folds with axes gently plunging to the WNW; (c, d) thin section views of SC-C' dextral shear bands; (e, f) low-angle and subhorizontal stretching mineral lineations plunging to the WNW.
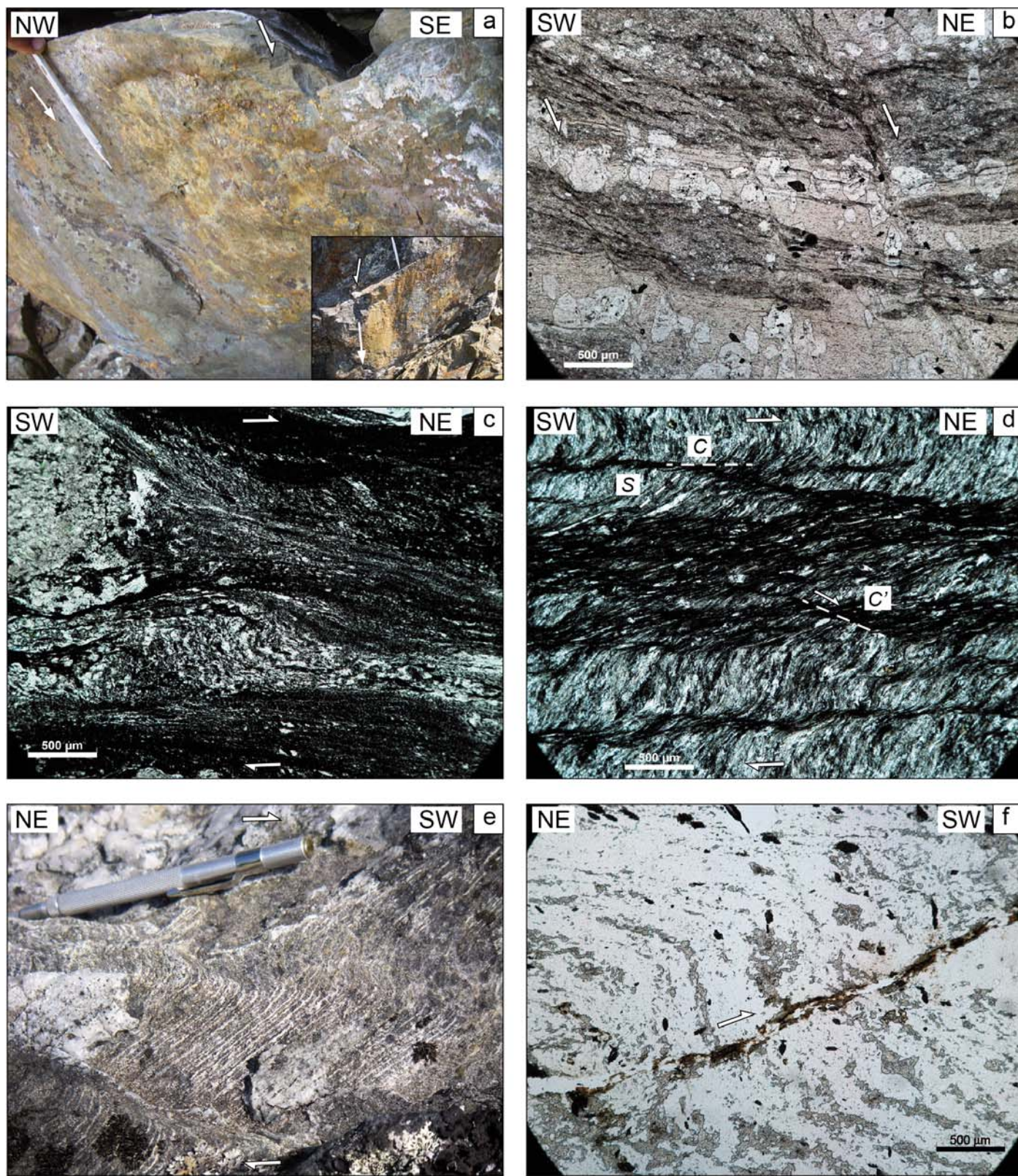
Figure 12. Structural elements of the hanging wall of the Romanet Fault (areas 7a of Figure 4): (a, b) outcrop (a) and thin-section (b) view of normal faults in the sheared Bacchus basalt and sedimentary rocks; (c, d) SC-C' normal shear bands in mylonitized Bacchus basalt (c) and graphitic slate (d); (e, f) outcrop (e) and thin section (f) view of reverse thrusting and microfolding in quartz−chlorite schist of the Lace Lake Formation in the transition zone between the footwall and hanging wall of the Romanet fault zone.
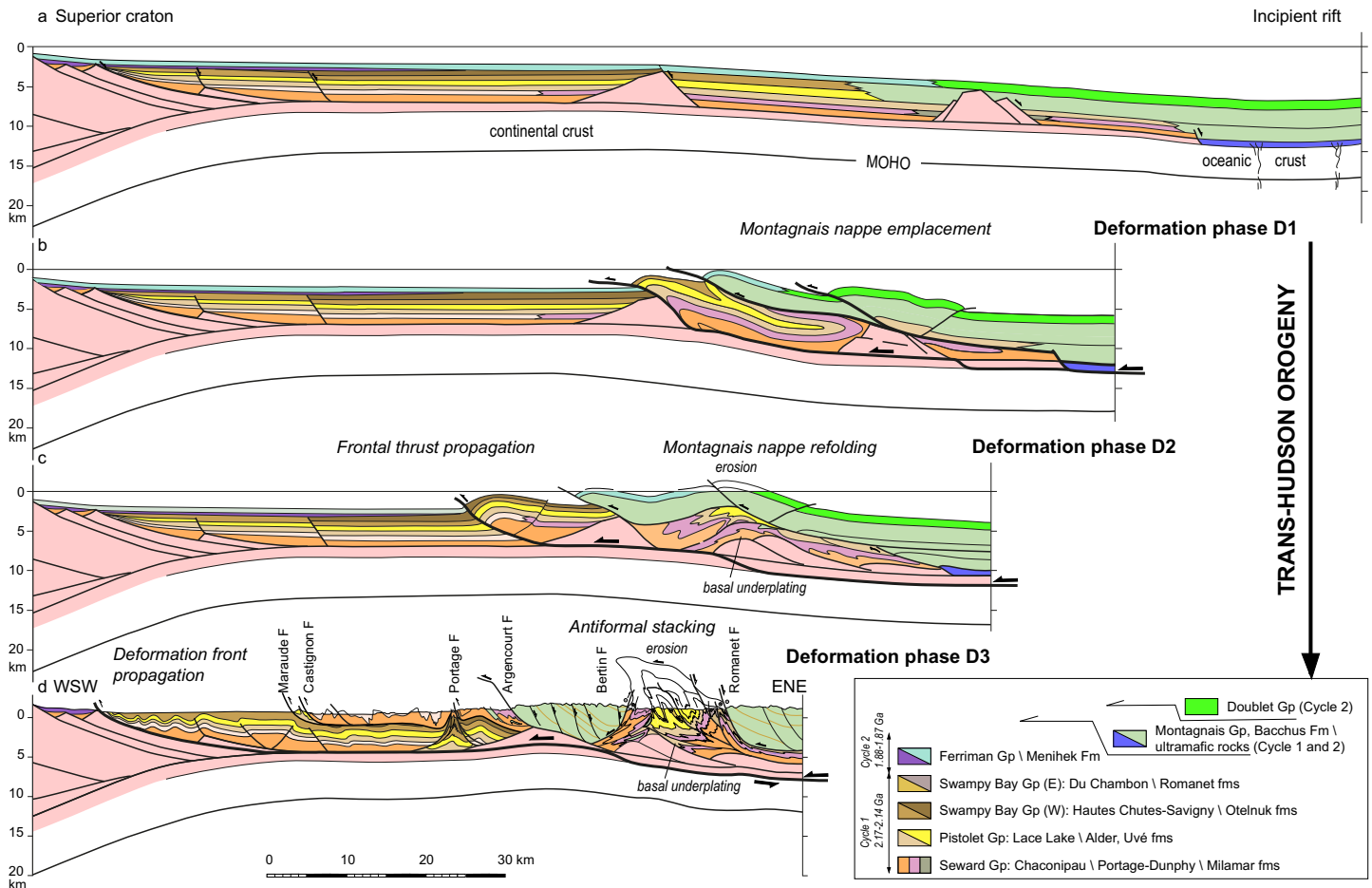
Figure 13. 2D reconstruction of initial settings and principal deformation phases D1−D3 of the Central Labrador Trough during the Trans-Hudson orogeny.

an antiformal stack formed through the combination of basal underplating, erosion and tectonic exhumation of Paleoproterozoic sedimentary rocks below the Montagnais mafic nappe in the rear part of the thrust wedge (Fig. 6). The Western and Eastern Montagnais nappes represent an initial single nappe of mafic rocks emplaced over the Paleoproterozoic sedimentary succession that during the nappe propagation was deformed into a large-scale overturned isoclinal fold with older units of the Seward Group tectonically underplating the mafic rocks in the nappe. This interpretation helps to explain the observation that highly stretched and refolded into isoclinal folds mylonitized rocks of the Chakonipau and Dunphy formations form the Du Chambon and North Romanet tectonic slices located immediately below the nappes (Figs. 4, 6). The younger sedimentary units of the Pistolet and Swampy Bay groups form a large-scale isoclinal F1 syncline in the core of the Romanet antiform that was refolded by the upright F2 folds and cut by WSW-verging thrusts under continuing shortening and basal underplating. Normal faults along the NNE boundary of the Romanet antiform (Fig. 6) likely accommodated antiformal stacking and exhumation in the core of the antiform stimulated by syntectonic erosion. The specific structures resulting from these processes at different deformation phases are described in the next section.

PRINCIPAL PHASES OF DEFORMATION

It is recognized that the principal stages of the tectonic evolution of the NQO involved: (1a) 2.2–2.1 Ga incipient crustal rifting of Superior craton; (1b) 1.88−1.87 Ga renewed rifting phase; (2) 1.82–1.77 Ga initial thrusting and collision between the Archean Superior craton and the Archean block of the Core Zone during a dextral transpression stage (Machado et al. 1989; Perreault and Hynes 1990; Skulski et al. 1993; Machado et al. 1997; Wardle et al. 2002; Clark and Wares 2004; Corrigan et al. 2018).

The tectonic setting during the phase of incipient crustal rifting can be compared to the geometry of the Galicia continental margin (Boillot and Froitzheim 2001) and was likely characterized by the presence of extended and thinned continental crust between individual thicker crustal blocks at the margin of the Superior craton and an open-marine incipient 'rift basin' (Fig. 13a). This suggestion is supported by the faulted structure described above of Archean gneiss basement of the Superior craton in the Lac Cambrien rift zone (Fig. 2a) and presence of the detached crustal blocks of Archean granite-gneiss basement (A) exposed in the lac Canichiko area of the Schefferville zone and lac Colombet area of the Howse zone (Dimroth 1978; Clark and Wares 2004). These blocks can be considered as an analog for the inferred detached basement
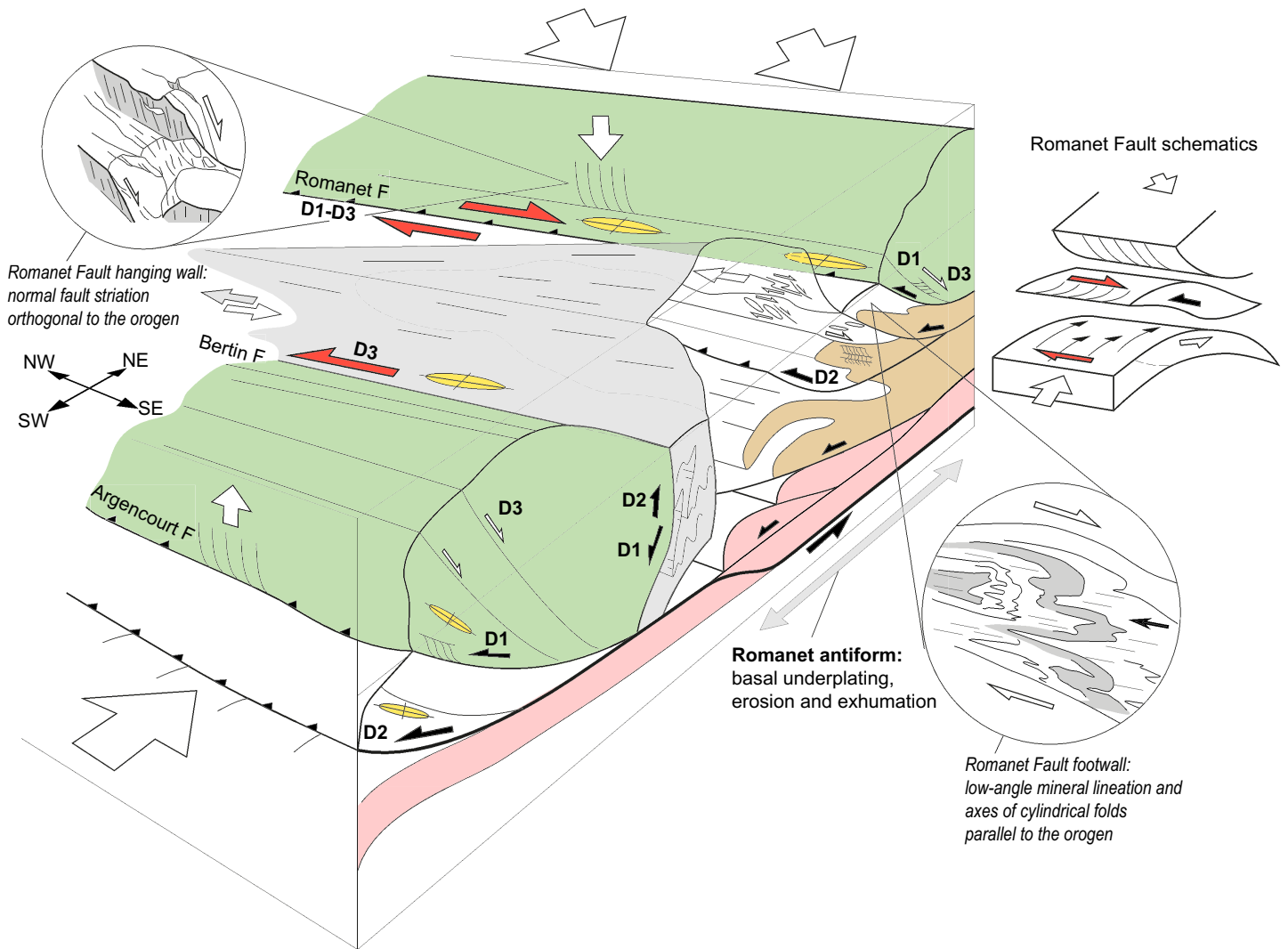
Figure 14. 3D model of tectonic structure of the Wheeler zone showing principal structural elements of the Montagnais nappes and Romanet antiform. The longitudinal progressive increase in the amount of exhumation from the NW to the SE in the antiform is likely related to along-strike variation of shortening and erosion increasing to the southeast.

block below the frontal slices of the Howse zone (Fig. 6). The crustal blocks underplated below the Romanet antiform (Fig. 6) are inferred from the nearby location of the Wheeler dome (Fig. 2a), which is considered to be bounded at the base by a major W-verging decollement (Clark and Wares 2004).

Our structural observations in the Central Labrador Trough support several episodes of thrusting and strike-slip deformation that occurred during the collisional stage followed by extensional shearing and normal faulting during the late phases of syncollisional shortening (Fig. 13b−d).

D1 Nappe Emplacement
The D1 phase is characterized by westward (in present-day coordinates) emplacement of the Montagnais mafic nappe over the Paleoproterozoic sedimentary succession with subsequent decollements along shaly and/or dolomitic units and the formation of a large-scale recumbent isoclinal F1 fold (Fig.

13b). Thrust emplacement under dextral transpressional conditions resulted in the development of right-lateral mylonitic shearing and the top-to-the WNW subhorizontal stretching mineral lineation parallel to the orogen in the footwall of the Romanet Fault (Fig. 6, area 7b), and reverse shearing in the transition zone between the footwall and hanging wall of the Romanet Fault (Fig. 14). These deformation events are recorded in the Lace Lake quartz−mica schist (Figs. 11a−d, 12e, f) of the North Romanet slice in the rear part of the thrust wedge. Mylonitic shearing (Figs. 9d, 10c) and formation of recumbent southwest-dipping isoclinal F1 folds (Fig. 9e) occurred during this stage in the Chaconipau sandstone and Dunphy dolomite of the Wheeler zone (Fig. 14). D1-related relics of the gabbro nappes (Fig. 5, lines A−B, C−D) and associated brecciation and schistosity of the Lace Lake shale in the nappe footwall (Fig. 7d) are recognized in the Minowean syncline (Schefferville zone).

D2 Nappe Refolding and Forward Thrust Propagation

During the D2 phase, the deformation front propagated southwestward with emplacement of SW-verging steep thrusts and moderately inclined folds in the Paleoproterozoic succession (Fig. 13c) in the frontal part of the thrust wedge (Schefferville zone). Top-to-SW reverse SC2 shear bands in the Argencourt Fault (Fig. 8e) and striations at thrust surfaces, steep schistosity SC2 dipping to the NE (Fig. 8f), NW−SE intersection lineation and subhorizontal fold axes (Fig. 5, areas 1, 2) are consistent with a SW (N220°) direction of tectonic transport. Deformation propagation continued during the D3 phase resulting in emplacement of the Portage and Castignon slices along the detachment in shale of the Swampy Bay Group in the Schefferville parautochthonous zone (Fig. 13d). Eventually, minor folding and local thrust faulting affected the autochthonous Cambrien zone. The development of the Swampy Bay dextral mylonitic shear zone (Fig. 8a, b) and dextral transpressional displacement along the Portage Fault (Fig. 3) characterizing the D2−D3 phase may reflect strain partitioning during oblique convergence between the Superior craton and the Core Zone during the Trans-Hudson orogeny.

Continuous underplating at the rear part of the thrust wedge (Wheeler zone) resulted in upward bending of the Montagnais nappe (Fig. 13c), refolding of recumbent isoclinal F1 folds as upright and SSW-verging inclined F2 folds with subhorizontal axes (Fig. 10a, b), and development of a steep schistosity (Fig. 10e) and thrusts dipping to the NNE (Fig. 6, area 6). The Bertin Fault and the shear detachment at the base of the Du Chambon slice were bent, plunging to the SW (Fig. 6, line H−I) and under continuing shortening they were reactivated as NE-verging reverse faults (Fig. 6, areas 4 and 5).

D3 Underplating, Antiformal Stacking, Erosion, Extensional Shearing and Normal Faulting

During the D3 phase, underplating and growth of the antiformal stack combined with localized erosion in the rear part of the thrust wedge resulted in exhumation of sedimentary rocks of the Romanet antiform (Fig. 13d). The amount of erosion and exhumation likely varied along the strike of the orogen in the Romanet area with maximum erosion and uplift occurring in the SE and decreasing to the WNW, where higher structural levels are preserved (Fig. 14). The deeper levels composed of older metasedimentary units of the Lace Lake and Milamar formations are exhumed in the southeast, close to the Archean gneiss basement of the Wheeler dome (Fig. 3). To the NW, lesser amounts of exhumation and erosion resulted in preservation of younger sedimentary units of the Pistolet and Swampy Bay groups. Higher amounts of exhumation in the southeast of the Romanet antiform resulted in superimposed left-lateral strike-slip faulting along the Bertin fault zone (Fig. 9c) and in continued right-lateral displacement in the footwall of the Romanet Fault (Fig. 11a−d).

The continued syncollisional underplating and exhumation in the Romanet antiform resulted in the development of extensional structures along the northeastern antiform boundary (Fig. 13d). A NE-dipping normal fault bounds the downthrown block composed of the Romanet conglomerate (Fig. 6)

at the northeastern limit of the central zone. A subhorizontal S3 crenulation cleavage refolds the steep NNE-dipping S2 schistosity (Fig. 10f) in the Lace Lake slate, northeast of the Romanet antiform. Extensional shear zones and brittle normal faults with northeast-plunging mineral lineations and striations (Fig. 6, area 7a) occur in the hanging wall of the Romanet Fault (Fig. 12a−d).

Late N−S normal faults and shear zones cut mafic rocks of the Montagnais nappes (Fig. 9a, b) and the sedimentary rocks below the nappes in the frontal part of the thrust wedge (Figs. 3, 6, line G−H−I). The NW−SE brittle and semi-brittle normal faults occur in shale of the Lace Lake Formation below the frontal gabbro slice nappe (Fig. 8c, d) and in quartz sandstone of the Alder Formation (Fig. 7f) on the overturned limb of the Minowean syncline (Fig. 5, line A−B). This late normal faulting could result from collapse following the emplacement of the thick gabbro nappe over the parautochthonous sedimentary rocks.

DISCUSSION

Nappe Emplacement and Thrusting

The main phases of deformation related to the Trans-Hudson orogeny in the Central Labrador Trough (Fig. 13b−d) described above can be correlated with synchronous phases in the northern Labrador Trough. The major deformation events related to shortening in the northern Labrador Trough involved: D1 basal decollement, D2 northwest transport of basement-cored Pennine-style nappes, and D3 main stage of compression. The westward transport along D1 decollement planes is estimated to range from 25 to 50 km (Goulet 1995). The SW and WSW direction of transport was probably continuous in the foreland during D2 and D3 and should not be considered as discrete events (Moorhead and Hynes 1990; Wares and Goutier 1990; Goulet 1995). An early episode of low-angle in-sequence thrusting and a later phase of major high-angle out-of-sequence thrusting have been distinguished in the structural evolution of the western foreland both in the northern (Wares and Goutier 1990) and in the central (this study) segments of NQO. In the north, northwest-trending *en echelon* allochthonous domes of Archean (2883−2868 Ma, zircon) basement gneiss (Machado et al. 1989) are exposed in cores of the Boulder and Moyer antiforms and Renia synform (Fig. 1) between the two steep east-dipping Lac Rachel and Lac Olmstead dextral strike-slip faults (Moorhead and Hynes 1990). These structures represent large west-verging, basement-cored nappes developed through the decollement at the basement-cover interface and were refolded during later northwest- and southwest-directed thrust fold phases (Moorhead and Hynes 1990). Similarly, in the Central Labrador Trough, basal underplating and antiformal stacking of sedimentary cover and inferred detached crustal blocks (Fig. 13d) occurred below the Montagnais nappe in the rear part of the thrust wedge and resulted in nappe refolding and out-of-sequence high-angle thrusting during the D2−D3 continuous phases of progressive shortening (Fig. 13c, d). An analog basal detachment is inferred by Clark and Wares (2004) at the base of the

Wheeler dome of Archean basement gneiss (2668 Ma, zircon) (Rayner et al. 2017; Charette et al. 2017).

According to numerical and analog modelling results, the occurrence of frontal and basal accretion in a thrust wedge is influenced by the rheology of the material, surface processes and the balance of material flux (Davis et al. 1983; Selzer at al. 2008; Malavieille 2010; Pfiffner 2017). In sandbox models with a decollement layer, the processes of basal underplating, nappe stacking, syncollisional exhumation and extension above the uplifted core zone are favoured by syntectonic surface erosion (Konstantinovskaia and Malavieille 2005; Bonnet et al. 2007; Konstantinovskaya and Malavieille 2011).

Strike-slip Faulting

A series of NW−SE dextral strike-slip faults, namely the Lac Rachel, Lac Olmstead, Lac Turcotte, and Lac Tudor faults (Fig. 1) is recognized on the eastern border of the NQO (Girard 1990; Moorhead and Hynes 1990; Goulet 1995; Wardle et al. 2002; Simard et al. 2013). In the hinterland of the northern segment of the orogen, the Lac Rachel and Lac Olmstead dextral strike slip faults are interpreted to be related to the D3 deformation phase, during which the D1−D2 structures were refolded to form a series of *en echelon* anticlinoria and synclinoria (Goulet 1995). The Lac Turcotte Fault represents a dextral mylonitic shear zone formed during an early deformation phase of juxtaposition of the Core Zone and Rachel-Laporte zone (Poirier et al. 1990; Perreault and Hynes 1990). The Lac Turcotte Fault probably represents a continuation of the Lac Tudor Fault in the south (Wardle et al. 2002). The Turcotte-Tudor dextral shear zone corresponds to a prominent suture related to the collision between the Superior Craton and the Core Zone (Clark and Wares 2004; Corrigan et al. 2009). The mineral lineation plunging at low angles to the southeast characterizes metamorphic rocks of both the Rachel-Laporte zone and the Core Zone that may reflect the effect of the oblique component during the D3 deformation phase of the collision (Simard et al. 2013). The displacement along the dextral strike-slip fault zones occurred between 1793 and 1783 Ma (Machado et al. 1989; Clark and Wares 2004) as a result of dextral transpression kinematics during the Trans-Hudson orogeny.

The strike-slip faults and shear zones in the Central Labrador Trough described in this study developed during different deformation phases from the hinterland to the frontal parts of the orogen. The dextral shear mylonitic zones and low-angle stretching mineral lineation parallel to the orogen that occur in the footwall of the Romanet fault zone likely record the early stages (D1) of oblique convergence between the Superior craton and the Archean crustal block of the Core Zone (Fig. 14, inset). The basal underplating and nappe refolding through D2−D3 phases resulted in antiformal stacking in the Romanet antiform, continued dextral shearing in the footwall of the Romanet fault zone and top-to-the NE thrusting along the Bertin Fault subsequently reworked as a left-lateral strike-slip fault. The left-lateral strike-slip faulting along the Bertin Fault and continued right-lateral shearing along the Romanet Fault developed as a result of longitudinally heterogeneous exhumation in the Romanet antiform (Fig. 14) during the D2−D3 phase. The Swampy Bay dextral shear zone and right-lateral displacement along the Portage Fault (Figs. 3, 5) of the Schefferville and Howse zones could also be the result of strain partitioning during the late phases (D2−D3) of shortening in the frontal part of the thrust wedge. Thus, the effect of dextral transpression during the oblique Trans-Hudson orogeny was not limited by the hinterland (Rachel-Laporte zone) but was also pronounced in the Labrador Trough (Wheeler, Howse and Schefferville zones).

Along-strike Variation of Exhumation and Shortening

Field observations and structural analysis of the Romanet antiform has shown that deeper structural levels are exhumed in the southeast, near the Wheeler dome, while shallower levels are preserved in the northwest (Fig. 14). This allows us to suggest an along-strike variation of exhumation rate in the rear part of the thrust wedge that can be explained by higher erosion and shortening rates in the southeastern segment of the thrust wedge as compared to the northwestern segment. In other words, higher shortening in the southeastern segment resulted in higher amounts of basal underplating that involved detached crustal blocks of Archean basement below the core of the Romanet antiform (Fig. 13d) and contributed to higher rates of erosion and exhumation in the southeastern segment (Fig. 14). If this interpretation is valid, the Wheeler dome, located at the extreme southeast point of the Romanet antiform (Figs. 2a, 3), may represent a detached and underplated crustal block of Archean basement that, together with its sedimentary cover (Milamar meta-conglomerate), experienced the highest amounts of differential exhumation in the Wheeler zone during the Trans-Hudsonian orogeny. The proposed model requires a validation by further regional structural and geochronological studies. An analog structural model was proposed by Rosenberg et al. (2015) for the Alps. Those authors have shown that along-strike gradients of collisional shortening in the Central and Eastern Alps may result in longitudinal variation of the erosion and exhumation rates. Stronger shortening coincides with a thicker eroded rock column and higher rate of exhumation. This model can be applied to explain the structural features of the Central Labrador Trough.

Late Normal Faulting

Extension in collisional orogens may be related either to late orogenic extension and collapse or to local crustal shortening (Malavieille 1993). The late orogenic extension model involves the development of normal shear zones and the growth of a metamorphic core complex (Van Den Dreissche and Brun 1989; Echtler and Malavieille 1990). Other models consider the occurrence of detachments in collisional orogens during the unroofing and thinning of thickened crust during shortening (Malavieille 1993; Matte 2007).

In the Central Labrador Trough, the D3 extensional phase is recognized for the first time and is related to different processes. Along the Romanet fault zone, normal faults and shear zones in the hanging wall with stretching lineations and striations plunging to the northeast, orthogonal to the orogen, in contrast to the stretching mineral lineation in the

footwall, which gently plunges to the WNW, subparallel to the orogen (Fig. 14). Such structures are typical of orogens with oblique tectonics such as the Western Alps, Taiwan and the Canadian Rockies and are formed during two distinct phases (Ellis and Watkinson 1987): an early footwall deformation with stretching lineation parallel to the orogen reflecting high oblique strain of oblique subduction, and a later hanging wall deformation with structures orthogonal to the orogen reflecting imbrication and exhumation processes.

In the northeastern part of the Romanet antiform, the northeast-dipping normal faults and subhorizontal S3 crenulation cleavage (Figs. 10f, 14) likely reflect a syn-convergent mechanism of extension that combines simultaneous uplift and exhumation induced by local basal underplating of detached units and erosion during convergence. Based on analog experiments (Konstantinovskaia and Malavieille 2005; Malavieille 2010; Malavieille and Konstantinovskaya 2010; Konstantinovskaya and Malavieille 2011), it is possible to suggest that normal faulting could be the result of the kinematic effect of vertical shears induced by strain partitioning in the orogenic wedge. Such partitioning is the direct consequence of upper crustal underplating processes combined with surface erosion and induces strong uplift in discrete areas. Differential motion of underplated crustal units relative to surrounding material induces vertical shearing and as a consequence strong stretching and layer-parallel thinning of the stacked tectonic units. At depth these zones are characterized by the development of normal shear zones that evolved to brittle normal faults when reaching upper crustal domains during continuous syn-convergent erosion assisted by uplift (Malavieille and Konstantinovskaya 2010).

The late brittle normal faulting in the Montagnais nappes and in the sedimentary units below the frontal nappes (Figs. 3, 5) in the frontal (western) part of the thrust wedge (Minowean area) is likely related to stress relaxation after the emplacement of voluminous gabbro nappes over the Proterozoic sedimentary succession.

Further detailed structural, mineralogical and geochronological studies in the Central Labrador Trough would help to quantify timing of the deformation phases, including the antiformal stacking and exhumation phase and the newly defined D3 extensional phase, and to characterize structural control on fluid circulation and mineralization processes relevant for mineral prospecting in the area. In particular, structural and geochronological studies of lenses of amphibolite and phlogopite gabbro in the footwall of the Romanet Fault and greenschist of the Milamar Formation along the southwestern border of the Wheeler dome could contribute to our understanding of the mylonitic deformation during the early D1 deformation phase of nappe emplacement and decollement propagation at the base of the detached Archean basement block.

CONCLUSIONS

Field structural observations carried out along the ca. 70 km long W−E Minowean-Romanet transect in the Central Labrador Trough have helped to recognize three distinct deformation phases during the Trans-Hudson orogeny that include not only southwestward thrusting (D1−D3) but also the newly established strike-slip (D1−D3) and extensional (D3) tectonics that developed under various settings in the frontal (western) and rear (eastern) parts of the orogen.

In the east, the low-angle mineral lineation, the axes of cylindrical folds and the dextral mylonitic shear zones in the footwall of the Romanet Fault are oriented subparallel to the orogen and reflect the early D1 phase of oblique convergence. The mineral lineations and striations of normal faults and shear zones in the hanging wall of the Romanet Fault are oriented orthogonally to the orogen and correspond to the later phase (D3) of exhumation driven by the combined effects of erosion and underplating. The increasing degree of exhumation along the Romanet antiform from northwest to southeast is explained by a model of strain partitioning and differential exhumation resulting from longitudinal variations of shortening and associated higher amount of erosion in the southeast in an oblique convergence setting.

The D3 northeast-dipping normal fault and subhorizontal crenulation cleavage to the northeast of the Romanet antiform likely reflect the syn-convergent mechanism of extension that combined simultaneous uplift, vertical shearing and exhumation induced by local basal underplating and erosion during convergence. The late D3 brittle normal faults, semi-brittle and ductile shear zones in the Montagnais nappes and in the sedimentary units below the frontal nappes of the thrust wedge (Minowean area) are likely related to stress relaxation after emplacement of the voluminous gabbro nappes over the Proterozoic sedimentary succession.

REFERENCES

Boillot, G., and Froitzheim, N., 2001, Non-volcanic rifted margins, continental break-up and the onset of sea-floor spreading: some outstanding questions, *in* Wilson, R.C.L., Whitmarsh, R.B., Taylor, B., and Froitzheim, N., *eds.*, Non-Volcanic Rifting of Continental Margins: A Comparison of Evidence from Land and Sea: Geological Society, London, Special Publications, v. 187, p. 9–30, https://doi.org/10.1144/GSL.SP.2001.187.01.02.

Bonnet, C., Malavieille, J., and Mosar, J., 2007, Interactions between tectonics, erosion, and sedimentation during the recent evolution of the Alpine orogen: Analogue modeling insights: Tectonics, v. 26, TC6016, https://doi.org/10.1029/2006TC002048.

Brouillette, P., 1989, Géologie de métallogénie de la région des lacs Minowean et du Portage (Fosse du Labrador): Ministère de l'Énergie et des Ressources naturelles, Québec, ET 88–06, 74 p.

Burg, J.-P., Bale, P., Brun, J.-P., and Girardeau, J., 1987, Stretching lineation and transport direction in the lbero-Armorican arc during the Siluro–Devonian collision: Geodinamica Acta, v. 1, p. 71–87, https://doi.org/10.1080/09853111.1987.11105126.

Charette, B., Lafrance, I., and Mathieu, G., 2017, Géologie de la région du Lac Jeannin (SNRC 24Bb): Ministère de l'Énergie et des Ressources naturelles, Québec, Rapport géologique. Available from: http://gq.mines.gouv.qc.ca/rapports-geologiques/province-de-churchill/geologie-du-lac-jeannin/.

Chevé, S.R., 1985, Les indices minéralisés du lac Romanet, Fosse du Labrador :

Ministère de l'Énergie et des Ressources naturelles, Québec, ET 83–13, 60 p. Available from: http://sigeom.mines.gouv.qc.ca/.

Chevé, S.R., 1993, Cadre géologique du complexe carbonatitique du lac Castignon, Fosse du Labrador: Ministère de l'Énergie et des Ressources naturelles, Québec, MB 93–64, 100 p.

Chevé, S.R., and Machado, N., 1988, Reinvestigation of the Castignon Lake carbonatite complex, Labrador Trough, New Quebec (Abstract): Geological Association of Canada-−Mineralogical Association of Canada, Joint Annual Meeting, 1988, St. John's, Newfoundland, Abstracts, v. 13, p. 20.

Clark, T., 1984, Géologie de la région du lac Cambrien, Territoire du Nouveau Québec: Ministère de 1'Energie et des Ressources naturelles, Québec, ET 83-02, 71 p.

Clark, T., 1986, Géologie et minéralisations de la région du lac Mistamisk et de la rivière Romanet: Ministère de l'Énergie et des Ressources naturelles, Québec, PRO 87–18, 7 p.

Clarke, T., and Wares, R., 2004, Synthèse lithotectonique et métallogénique de l'orogène du Nouveau-Québec (Fosse du Labrador): Ministère de l'Énergie et des Ressources naturelles, Québec, Rapport MM 2004–01, 182 p.

Corrigan, D., Pehrsson, S., Wodicka, N., and de Kemp, E., 2009, The Paleoproterozoic Trans-Hudson Orogen: a prototype of modern accretionary processes, in Murphy, J.B., Keppie, J.D., and Hynes, A.J., eds., Ancient Orogens and Modern Analogues: Geological Society, London, Special Publications, v. 327, p. 457–479, https://doi.org/10.1144/SP327.19.

Corrigan, D., Wodicka, N., McFarlane, C., Lafrance, I., van Rooyen, D., Bandyayera, D., and Bilodeau, C., 2018, Lithotectonic framework of the Core Zone, southeastern Churchill Province, Canada: Geoscience Canada, v. 45, p. 1−24, https://doi.org/10.12789/geocanj.2018.45.128.

Davis, D.M., Suppe, J., and Dehlen, F.A., 1983, Mechanics of fold-and-thrust belts and accretionary wedges: Journal of Geophysical Research, v. 88, p. 1153–1172, https://doi.org/10.1029/JB088iB02p01153.

Dimroth, E., 1978, Région de la Fosse du Labrador (54˚30'–56˚30'): Ministère de l'Énergie et des Ressources naturelles, Québec, RG–193, 396 p.

Dimroth, E., and Dressler, B.O., 1978, Metamorphism of the Labrador Trough, in Fraser, J.A., and Heywood, W.W., eds., Metamorphism in the Canadian Shield: Geological Survey of Canada, Paper 78–10, p. 215–236, https://doi.org/10.4095/104534.

Dressler, B., 1979, Région de la Fosse du Labrador: Ministère de l'Énergie et des Ressources naturelles, Québec, RG–195, 136 p.

Echtler, H., and Malavieille, J., 1990, Extensional tectonics, basement uplift and Stephano-Permian collapse basin in a late Late Variscan metamorphic core complex (Montagne Noire, Southern Massif Central): Tectonophysics, v. 177, p. 125–138, https://doi.org/10.1016/0040-1951(90)90277-F.

Ellis, M., and Watkinson, A.J., 1987, Orogen-parallel extension and oblique tectonics: The relation between stretching lineations and relative plate motions: Geology, v. 15, p. 1022–1026, https://doi.org/10.1130/0091-7613(1987)15<1022:OEAOTT>2.0.CO;2.

Ellis, M.A., 1986, Structural morphology and associated strain in the central Cordillera (British Columbia and Washington): Evidence of oblique tectonics: Geology, v. 14, p. 647–650, https://doi.org/10.1130/0091-7613(1986)14<647:SMAASI>2.0.CO;2.

Findlay, J.M., Parrish, R.R., Birkett T.C., and Watanabe, D.H., 1995, U–Pb ages from the Nimish Formation and Montagnais glomeroporphyritic gabbro of the central New Québec Orogen, Canada: Canadian Journal of Earth Sciences, v. 32, p. 1208–1220, https://doi.org/10.1139/e95-099.

Girard, R., 1990, Les cisaillements latéraux dans l'arrière-pays des orogènes du Nouveau-Québec et de Torngat: Une revue: Geoscience Canada, v. 17, p. 301–304.

Goulet, N., 1995, Étude structurale, stratigraphique et géochronologique de la partie nord de la Fosse du Labrador: Ministère de l'Énergie et des Ressources naturelles, Québec, MB 95–36, 41 p. Available from: http://sigeom.mines.gouv.qc.ca/.

Goulet, N., Gapiéry, C., Mareschal, J.-C., and Machado, N., 1987, Structure, geochronology, gravity and the tectonic evolution of the northern Labrador Trough: Geological Association of Canada−Mineralogical Association of Canada, Joint Annual Meeting, Saskatoon, Saskatchewan, 1987, Program with Abstracts, v. 12, p. 48.

Hoffman, P.F., 1988, United plates of America, the birth of a craton: Early Proterozoic assembly and growth of Laurentia: Annual Review of Earth and Planetary Sciences, v. 16, p. 543–603, https://doi.org/10.1146/annurev.ea.16.050188.002551.

Hoffman, P.F., 1990, Dynamics of the tectonic assembly of the northeast Laurentia in geon 18 (1.9−1.8 Ga): Geoscience Canada, v. 17, p. 222−226.

James, D.T., and Dunning, G.R., 2000, U–Pb geochronological constraints for Paleoproterozoic evolution of the Core Zone: southeastern Churchill Province,

northeastern Laurentia: Precambrian Research, v. 103, p. 31–54, https://doi.org/10.1016/S0301-9268(00)00074-7.

Karhu, J.A., and Holland, H.D., 1996, Carbon isotopes and the rise of atmospheric oxygen: Geology, v. 24, p. 867−−870, https://doi.org/10.1130/0091-7613(1996)024<0867:CIATRO>2.3.CO;2.

Konstantinovskaia, E., and Malavieille, J., 2005, Erosion and exhumation in accretionary orogens: Experimental and geological approaches: Geochemistry, Geophysics, Geosystems, v. 6, Q02006, https://doi.org/10.1029/2004GC000794.

Konstantinovskaya, E., and Malavieille, J., 2011, Thrust wedges with décollement levels and syntectonic erosion: A view from analog models: Tectonophysics, v. 502, p. 336–350, https://doi.org/10.1016/j.tecto.2011.01.020.

Lacassin, R., 1987, Kinematics of ductile shearing from outcrop to crustal scale in the Monte Rosa Nappe, Western Alps: Tectonics, v. 6, p. 69–88, https://doi.org/10.1029/TC006i001p00069.

Le Gallais, C.J., and Lavoie, S., 1982, Basin evolution of the Lower Proterozoic Kaniapiskau Supergroup, central Labrador miogeocline (Trough), Quebec: Bulletin of Canadian Petroleum Geology, v. 30, p. 150−166.

Machado, N., 1990, Timing of collisional events in the Trans-Hudson Orogen: evidence from U−Pb geochronology for the New Quebec Orogen, the Thompson Belt and the Reindeer Zone (Manitoba and Saskatchewan), in Lewry, J.F., and Stauffer, M.R., eds., The Early Proterozoic Trans-Hudson Orogen of North America: Lithotectonic Correlations and Evolution: Geological Association of Canada, Special Paper 37, p. 433−441.

Machado, N., Goulet, N., and Gariépy, C., 1989, U–Pb geochronology of reactivated Archean basement and of Hudsonian metamorphism in the northern Labrador Trough: Canadian Journal of Earth Sciences, v. 26, p. 1–15, https://doi.org/10.1139/e89-001.

Machado, N., Clark, T., David, J., and Goulet, N., 1997, U–Pb ages for magmatism and deformation in the New Quebec Orogen: Canadian Journal of Earth Sciences, v. 34, p. 716−723, https://doi.org/10.1139/e17-058.

Malavieille, J., 1993, Late orogenic extension in mountain belts: insights from the Basin and Range and the Late Paleozoic Variscan Belt: Tectonics, v. 12, p. 1115–1130, https://doi.org/10.1029/93TC01129.

Malavieille, J., 2010, Impact of erosion, sedimentation, and structural heritage on the structure and kinematics of orogenic wedges: Analog models and case studies: GSA Today, v. 20, p. 4–10, https://doi.org/10.1130/GSATG48A.1.

Malavieille, J., and Konstantinovskaya, E., 2010, Impact of surface processes on the growth of orogenic wedges: Insights from analog models and case studies: Geotectonics, v. 44, p. 541–558, https://doi.org/10.1134/S0016852110060075.

Malavieille, J., Lacassin, R., and Mattauer, M., 1984, Signification tectonique des lineations d'allongement dans les Alpes occidentales: Bulletin de la Société Géologique de France, v. S7-XXVI, p. 895–906, https://doi.org/10.2113/gssgfbull.S7-XXVI.5.895.

Matte, P., 2007, Variscan thrust nappes, detachments, and strike-slip faults in the French Massif Central: Interpretation of the lineations, in Hatcher Jr., R.D., Carlson, M.P., McBride, J.H., and Martínez Catalán, J.R., eds., 4–D Framework of Continental Crust: Geological Society of America Memoirs, v. 200, p. 391–402, https://doi.org/10.1130/2007.1200(20).

Matte, P., Lancelot, J., and Mattauer, M., 1998, La zone axiale hercynienne de la Montagne Noire n'est pas un "metamorphic core complex" extensif mais un anticlinal post-nappe à cœur anatectique: Geodinamica Acta, v. 11, p. 13–22, https://doi.org/10.1016/S0985-3111(98)80025-9.

Melezhik, V.A., Fallick, A.E., and Clark, T., 1997, Two billion year old isotopically heavy carbon: evidence from the Labrador Trough, Canada: Canadian Journal of Earth Sciences, v. 34, p. 271−285, https://www.doi.org/10.1139/e17-025.

Moorhead, J., and Hynes, A., 1990, Nappes in the internal zone of the northern Labrador Trough: Evidence for major early, NW-vergent basement transport: Geoscience Canada, v. 17, p. 241–244.

Perreault, S., and Hynes A., 1990, Tectonic evolution of the Kuujjuaq terrane, New Quebec Orogen: Geoscience Canada, v. 17, p. 238–240.

Pfiffner, O.A., 2017, Thick-skinned and thin-skinned tectonics: a global perspective: Geosciences, v. 7, 71, https://doi.org/10.3390/geosciences7030071.

Poirier, G.G., Perreault, S., and Hynes, A., 1990, Nature of the eastern boundary of the Labrador Trough near Kuujjuaq, Quebec: in Lewry, J.F., and Stauffer, M.R., eds., The Early Proterozoic Trans-Hudson Orogen of North America: Lithotectonic correlations and evolution: Geological Association of Canada, Special Paper 37, p. 397−412.

Rayner, N.M., Lafrance, I., Corrigan, D., and Charette, B., 2017, New U–Pb zircon ages of plutonic rocks from the Jeannin Lake area, Quebec: an evaluation of the Kuujjuaq domain and Rachel–Laporte Zone: Geological Survey of Canada, Current Research, 2017–4, 17 p.

Rohon, M.-L., Vialette, Y., Clark, T., Roger, G., Ohnenstetter, D., and Vidal., Ph., 1993, Aphebian mafic–ultramafic magmatism in the Labrador Trough (New

Quebec): its age and the nature of its mantle source: Canadian Journal of Earth Sciences, v. 30, p. 1582–1593, https://doi.org/10.1139/e93-136.

Rosenberg, C.L., Berger, A., Bellahsen, N., and Bousquet, R., 2015, Relating orogen width to shortening, erosion, and exhumation during Alpine collision: Tectonics, v. 34, p. 1306–1328, https://doi.org/10.1002/2014TC003736.

Selzer, C., Buiter, S.J.H., and Pfiffner, O.A., 2008, Numerical modeling of frontal and basal accretion at collisional margins: Tectonics, v. 27, TC3001, https://doi.org/10.1029/2007TC002169.

Simard, M., Lafrance, I., Hammouche, H., and Legouix, C., 2013, G.éologie de la région de Kuujjuaq et de la baie d'Ungava (SRNC 24J, 24K): Ministère de l'Énergie et des Ressources naturelles, Québec, RG 2013−04, 62 p.

Skulski, T., Wares, R.P., and Smith, A.D., 1993, Early Proterozoic (1.88–1.87 Ga) tholeiitic magmatism in the New Québec Orogen: Canadian Journal of Earth Sciences, v. 30, p. 1505–1520, https://doi.org/10.1139/e93-129.

Van Den Dreissche, J., and Brun, J.-P., 1989, Kinematic model of late Paleozoic extensional tectonics in the southern, French Massif Central: Comptes Rendus - Academie des Sciences, t. 309, Série II, p. 1607−1613.

Vanier, M.-A., Guilmette, C., Harris, L., Godet, A., Cleven, N., Charette, B., and Lafrance, I., 2017, Analyse structurale et microstructures des zones de cisaillement de la Rivière George et du Lac Tudor: Ministère de l'Énergie et des Ressources naturelles, Québec, MB 2017–12, 50 p.

Wardle, R.J., and Bailey, D.G., 1981, Early Proterozoic sequences in Labrador, *in* Campbell, F.H.A., *ed.*, Proterozoic basins of Canada: Geological Survey of Canada, Paper 81–10, p. 331–359, https://doi.org/10.4095/109385.

Wardle, R.J., Ryan, B., and Ermanovics, I., 1990, The eastern Churchill Province, Torngat and New Québec Orogens: An overview: Geoscience Canada, v. 17, p. 217–222.

Wardle, R.J., James, D.T., Scott, D.J., and Hall, J., 2002, The southeastern Churchill Province: synthesis of a Paleoproterozoic transpressional orogen: Canadian Journal of Earth Sciences, v. 39, p. 639–663, https://doi.org/10.1139/e02-004.

Wares, R.P., and Goutier, J., 1990, Deformational style in the foreland of the northern New Québec Orogen: Geoscience Canada, v. 17, p. 244–249.

*For access to the Konstantinovskaya et al. (2019) supplementary files, (an enlarged version of Figure 3 and a Google Earth location map, .kmz format), please visit the GAC's open source GC Data Repository link for the Andrew Hynes Series: Tectonic Processes at: https://GAC.ca/GC-data-repository/.

GEOLOGICAL ASSOCIATION OF CANADA
(2018-2019)

OFFICERS & COUNCILLORS

OFFICERS

President
Dène Tarkyth

Vice-President
Kathryn Bethune

Past President
Stephen Morison

Secretary-Treasurer
James Conliffe

**COUNCILLORS**

Ihsan Al-Aasm	Michael Michaud
Alwynne Beaudoin	Stephen Morison
Kathryn Bethune	Camille Partin
James Conliffe	Roger Paulen
Hendrik Falck	Liz Stock
Andy Kerr	Dène Tarkyth
David Lentz	Deanne van Rooyen

STANDING COMMITTEES

Communications: Kathryn Bethune

Finance: Michael Michaud

GAC Lecture Tours: Alwynne Beaudoin

Publications: Roger Paulen

Science Program: Deanne van Rooyen

ANDREW HYNES SERIES: TECTONIC PROCESSES
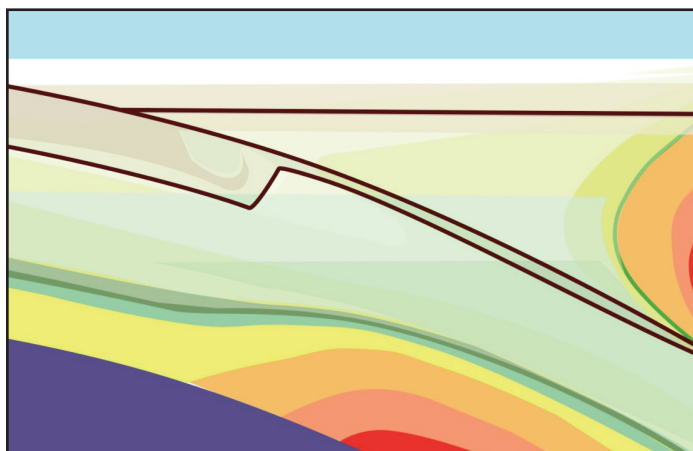
Age, Geochemistry and Origin of the Ardara Appinite Plutons, Northwest Donegal, Ireland

J. Brendan Murphy[1,4], R. Damian Nance[2], Logan B. Gabler[2], Alexandra Martell[1], and Douglas A. Archibald[3]

[1]Department of Earth Sciences, St. Francis Xavier University
Antigonish, Nova Scotia, B2G 2W5, Canada
E-mail: bmurphy@stfx.ca

[2]Department of Geological Sciences, Ohio University
316 Clippinger Laboratories, Athens, Ohio 45701, U.S.A.

[3]Department of Geological Sciences and Geological Engineering
Queen's University, Kingston, Ontario, K7L 3N6, Canada

[4]Earth Dynamics Research Group
ARC Centre of Excellence for Core to Crust Fluid Systems (CCFS)
and The Institute for Geoscience Research (TIGeR), School of Earth
and Planetary Sciences
Curtin University, Bentley, Perth, Western Australia 6102, Australia

SUMMARY

In northwest Donegal, Ireland, a large number of coeval appinitic (hornblende-plagioclase-rich) plutons and lamprophyre dykes occur around the Ardara pluton, a granitic satellite body and one of the oldest phases of the ca. 428–400 Ma composite Donegal Batholith. The appinite units form a bimodal (mafic–felsic) suite in which hornblende is the dominant mafic mineral and typically occurs as large prismatic phenocrysts within a finer grained matrix. Lamprophyre dykes are mafic in composition with a geochemistry that is very similar to that of the mafic appinite bodies. Both mafic rocks are subalkalic, with calc-alkalic and tholeiitic tendencies, and show trace element abundances indicating that the mantle source was contaminated by subduction zone fluids. $^{40}Ar/^{39}Ar$ analysis of hornblende separated from two samples of appinite yield mid-Silurian (434.2 ± 2.1 Ma and 433.7 ± 5.5 Ma) cooling ages that are interpreted to closely date the time of intrusion. Hence, according to the available age data, the appinite bodies slightly predate, or were coeval with, the earliest phases of the Donegal Batholith. Sm–Nd isotopic analyses yield a range of initial εNd values (+3.1 to –4.8 at t = 435 Ma) that, together with trace element data, indicate that the appinitic magmas were likely derived from melting of metasomatized sub-continental lithospheric mantle and/or underplated mafic crust, with only limited crustal contamination during magma ascent. The appinitic intrusions are interpreted to have been emplaced along deep-seated crustal fractures that allowed for mafic and felsic magma to mingle. The magmas are thought to be the products of collisional asthenospheric upwelling associated with the closure of Iapetus and the ensuing Caledonian orogeny, either as a result of an orogen-wide delamination event or as a consequence of more localized slab break-off.

RÉSUMÉ

Dans le nord-ouest du Donegal, en Irlande, un grand nombre de plutons appinitiques (riches en hornblendes ou en plagioclases) et de dykes de lamprophyres contemporains se retrouvent autour du pluton d'Ardara, un corps satellite granitique et l'une des phases les plus anciennes du batholite composite de Donegal, âgé d'environ 428–400 Ma. Les unités de l'appinite forment une suite bimodale (mafique–felsique) dans laquelle la hornblende est le minéral mafique dominant et se présente généralement sous forme de grands phénocristaux prismatiques au sein d'une matrice à grains plus fins. Les dykes de lamprophyres ont une composition mafique dont la géochimie est très similaire à celle des corps d'appinite mafique. Les deux roches mafiques sont subalcaliques, avec des tendances calco-alcalines et tholéiitiques, et elles montrent des teneurs en élé-

ments traces indiquant que la source du manteau a été contaminée par des fluides de zone de subduction. L'analyse $^{40}Ar/^{39}Ar$ des hornblendes provenant de deux échantillons d'appinite donne des âges de refroidissement du Silurien moyen (434,2 ± 2,1 Ma et 433,7 ± 5,5 Ma) qui sont interprétés comme étant proches de la date de l'intrusion. Par conséquent, selon les données d'âge disponibles, les corps d'appinite sont légèrement antérieurs ou contemporains des toutes premières phases du batholite de Donegal. Les analyses isotopiques Sm–Nd aboutissent à une gamme de valeurs εNd initiales (+3,1 à -4,8 à t = 435 Ma) qui, associées aux données des éléments traces, indiquent que les magmas appinitiques sont probablement dérivés de la fusion d'un manteau lithosphérique souscontinental métasomatisé et / ou d'une croûte mafique sousplaquée, avec une contamination crustale limitée lors de l'ascension du magma. Les intrusions appinitiques sont interprétées comme s'étant mises en place le long de fractures profondes de la croûte qui ont permis au magma mafique et au magma felsique de se mélanger. On pense que les magmas sont les produits de la remontée (upwelling) asthénosphérique collisionnelle associée à la fermeture de l'océan Iapetus et à l'orogenèse calédonienne qui s'ensuit, soit à la suite d'un délaminage à l'échelle de l'orogène, soit à la suite d'une rupture plus localisée de la plaque.

Traduit par la Traductrice

INTRODUCTION

In many parts of the Caledonian orogenic belt of Scotland and Ireland, major granitoid bodies, such as the composite Donegal Batholith in NW Ireland, are associated with a distinct suite of relatively small, hornblende-rich plutons formed from water-rich magmas that are 'peri-batholithic' in that they occur around the periphery of the composite batholith (Pitcher and Berger 1972). Known collectively as the appinite suite after the district of Appin in Scotland (e.g. Walker 1927; Bowes and McArthur 1976; Hamidullah and Bowes 1987), these intrusive rocks, which range from mafic to felsic in composition, are unusual in their mineralogy and texture. Those of mafic composition are medium- to coarse-grained melanocratic rocks composed of large, idiomorphic hornblende crystals in a matrix of feldspar and minor quartz (e.g. Pitcher and Berger 1972; Wright and Bowes 1979). Those of intermediate to felsic composition are also rich in idiomorphic hornblende and include syenite, monzonite, diorite and granodiorite. The suite is also characterized by the widespread occurrence of associated breccia intrusions and brecciated metasedimentary rocks.

The appinite suite in both Scotland and Donegal is commonly associated with lamprophyre dykes that show a similar peri-batholithic relationship with respect to major granitoid batholiths (Atherton and Ghani 2002). This temporal and spatial association has been widely interpreted to reflect a genetic linkage between the appinite suite, the lamprophyre dykes and the granitoid batholiths (e.g. Pitcher and Berger 1972), all of which were collectively emplaced towards the end of the Scandian orogeny (e.g. Siegesmund and Becker 2000; Atherton and Ghani 2002).

In Ireland, appinite bodies comprise a sub-group of Caledonian igneous intrusions best exposed around the Ardara pluton at the southwestern end of the composite Donegal Batholith (Fig. 1). The Ardara pluton is one of several intrusive bodies emplaced along the periphery of the Main Donegal Granite (Pitcher and Berger 1972). Available geochronological data suggest that the composite Donegal Batholith contains discrete phases ranging in age from 428 to 400 Ma and that the Ardara pluton is among the oldest of these phases (Condon et al. 2004).

In the Scottish Caledonides, rocks of the appinite suite are also spatially and temporally associated with 430–408 Ma granitoid magmatism (e.g. Neilson et al. 2009). These appinite plutons are geochemically distinct from coeval mafic and granitoid rocks of other associations (Fowler and Henney 1996; Atherton and Ghani 2002). They are typically calc-alkaline and have compositional affinities with shoshonite (basaltic, K-rich trachyandesite composed of olivine, augite and plagioclase phenocrysts), features suggesting emplacement in a volcanic arc tectonic setting (Thompson and Fowler 1986; Macdonald et al. 1986; Fowler 1988). Their distinctive geochemistry and the timing of their emplacement (broadly synchronous with arc–continent collision) has been interpreted to reflect melting of a previously metasomatized lithospheric mantle as a consequence of slab break-off following the termination of subduction (e.g. Atherton and Ghani 2002; Ghani and Atherton 2008; Neilson et al. 2009; Cooper et al. 2013). In addition, recent proposals that large batholiths preferentially form during the waning stages of collision and consequent slab failure (Hildebrand and Whalen 2014a, b; Hildebrand et al. 2018) indicate that rocks of the appinite suite have the potential of contributing significantly to our understanding of collisional processes and the voluminous granitoid magmas with which they are associated.

Despite their potential importance to understanding the genesis and tectonic setting of the Caledonian intrusive rocks, published geochemical data for the appinitic rocks of Donegal are sparse and include only a limited suite of petrogenetically indicative trace elements (e.g. French 1966; Hall 1967), and the precise age of their intrusion is unknown. To further our understanding of these enigmatic rocks and their association with voluminous granitoid batholiths, this paper aims to clarify the intrusive age and petrogenesis of this suite through geochronological ($^{40}Ar/^{39}Ar$ on hornblende), geochemical and isotopic (Sm–Nd) analysis of the appinite bodies associated with the Ardara pluton.

GEOLOGICAL SETTING

The Donegal Batholith of NW Ireland (Fig. 1), made famous by the classical work of Pitcher and Berger (1972), is made up of a suite of Caledonian granitic plutons emplaced into Laurentian crust in the mid-Silurian–early Devonian (428–400 Ma, U/Pb: Condon et al. 2004; 418–397 Ma, Rb/Sr: Halliday et al. 1980; O'Connor et al. 1982, 1987), during the final closure of the Iapetus Ocean (Ghani and Atherton 2008). During the development of the Caledonian orogen, the Laurentian margin
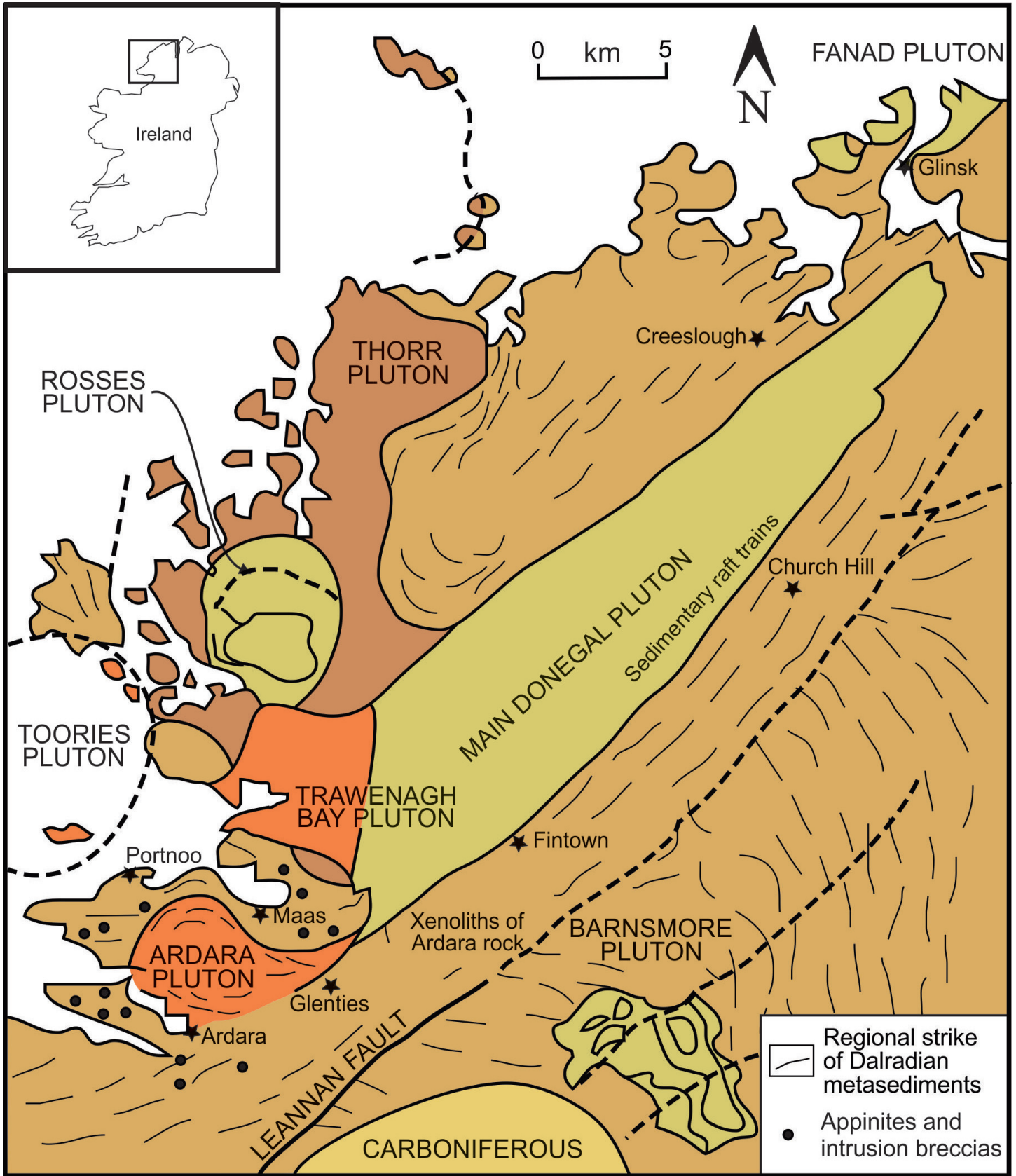
Figure 1. Simplified geological map of the composite Donegal Batholith in northwest Ireland (from Ghani and Atherton 2008).

was affected by two distinct orogenic episodes (e.g. van Staal et al. 1998). The first was the short-lived, mid-Ordovician Grampian event (Dewey and Shackleton 1984; Oliver 2001; Chew and Strachan 2014) linked to arc formation and accretion associated with the subduction of Iapetus oceanic lithosphere below the Laurentian margin at ca. 470–460 Ma. The second and main episode records the final closure of Iapetus and the collision of the Laurentia margin with Baltica-Ganderia (Scandian orogeny) and Avalonia (Acadian orogeny) in mid-Silurian to early Devonian time (e.g. Condon et al. 2006; Chew and Strachan 2014). In Ireland, the resulting Iapetus suture strikes NE–SW from Clogherhead in County Louth to the Dingle Peninsula in County Kerry. Ireland's crust northwest of this suture was originally derived from Laurentia, whereas the crust to the southeast comprises terranes that were originally derived from Gondwana (Todd et al. 1991).

The Donegal Batholith is a composite, predominantly granitoid body made up of the Thorr, Fanad, Trawenagh Bay, Rosses, Barnesmore, Toories and Ardara plutons in addition to the Main Donegal Batholith (Pitcher and Berger 1972; Vernon and Patterson 1993) (Fig. 1). These plutons were emplaced into the Dalradian Supergroup country rock at mid-crustal levels (Siegesmund and Becker 2000) and display distinct differences regarding their shape, internal structures, contact aureoles and emplacement mechanisms. The Dalradian Supergroup itself was deposited along the eastern margin of Laurentia during the late Neoproterozoic and early Cambrian and comprises a thick sequence of lithologically diverse metasedimentary and mafic volcanic rocks (Ghani and Atherton 2008). Dalradian lithologies in Donegal include mica schist, dolomitic schist, and striped and banded siliceous quartzite (Ghani and Atherton 2008).

The Main Donegal Granite (MDG) is the largest pluton within the Donegal Batholith, forming an elongate, steep-walled body with sharp margins that cross-cut intensely deformed Dalradian polymetamorphic schist, quartzite and metabasite (Pitcher and Read 1960; Hutton 1982; Stevenson et al. 2008). Although predominantly granitic, the MDG is internally sheared and varies from mafic to felsic in composition. It is characterized by a foliation and contains inclusions of Dalradian country rock oriented parallel to the length of the pluton (Berger 1971). These features are reportedly the result of stresses superimposed upon the pluton after its emplacement but before complete cooling and consolidation had occurred (French 1976; Hutton and Alsop 1996). The high-K, calc-alkaline granite and granodiorite that make up the MDG are thought to have been emplaced during a phase of major NE–SW sinistral strike-slip faulting that characterizes the final phase of Iapetus closure in the British Caledonides (Atherton and Ghani 2002). The MDG is temporally and spatially associated with both lamprophyre dykes and appinite bodies, the latter being most common adjacent to the Ardara pluton at its southwestern margin (Fig. 1).

Ardara Pluton

Marginal to the MDG, but also contributing to xenoliths within it (Price 1997), the smaller Ardara pluton is a concentrically zoned granodiorite–quartz monzodiorite body (Fig. 2), the outer zone of which is quite strongly deformed (French 1966; Vernon and Patterson 1993). It is a complex, roughly circular body about 10 km in diameter and exhibits sharp contact zones (French 1966). During emplacement, the metasedimentary Dalradian host rocks underwent contact metamorphism and ductile deformation, the latter thought to have provided most of the space for the pluton (Siegesmund and Becker 2000). There were three phases of intrusion; an early outer zone of quartz diorite, an inner zone of coarse potassium-feldspar megacrystic granodiorite and a later core composed of equigranular granodiorite. Unpublished U/Pb data for the Ardara pluton date its intrusion ca. 427 Ma (Condon et al. 2004).

The Ardara pluton has been regarded as a classic example of emplacement by expansion (ballooning) due to the injection of significant volumes of magma into the centre of the body after initial intrusion (Pitcher and Berger 1972). The bulk of the foliation within the pluton is magmatic (apart from a thin rind of solid-state deformation), suggesting that the expansion was accompanied by magmatic flow (Harmon et al. 1984). Flattened microgranitoid enclaves, concentric magmatic flow foliation, and compositional zoning within the pluton are consistent with expansion of magma prior to crystallization (Vernon and Patterson 1993). Mafic enclaves with variable modes of occurrence and texture resemble the lithologies in the appinitic intrusions. Some enclaves within the pluton were sufficiently rigid to fragment without any field evidence of mixing or mingling (Atherton and Ghani 2002). These field relationships suggest the intrusion of appinitic magmas preceded the Ardara pluton, although there may be some temporal overlap between early stages of pluton emplacement and the lamprophyre dykes (Atherton and Ghani 2002).

Appinite Suite

The Ardara pluton is surrounded by a large number of small appinitic intrusions and associated lamprophyre dykes, which are also thought to have been intruded during the final stages of the Caledonian orogeny (Atherton and Ghani 2002). The rocks of appinitic intrusions constitute the appinite suite and are most commonly found in small stocks, sheets, bosses and dykes, commonly closely associated with late to post-tectonic granitoid intrusions (e.g. Fowler and Henney 1996). The suite primarily occurs along the southern edge of the MDG and within 3 km of the Ardara pluton, where it additionally forms small irregular pipes or vents, clustered in large numbers around the plutons and as mafic enclaves within them.

Rocks of the appinite suite are typically coarse-grained and porphyritic with green to brown hornblende in a groundmass with approximately equal proportions of plagioclase and potassium-feldspar (Hall 1967). The appinitic intrusions are predominantly lenticular masses, 100–550 m in width, and most have irregular margins (French 1966) with steeply inclined contacts that truncate regional Dalradian structures and related foliations. Several appinitic masses north of the pluton exhibit a foliation defined by the alignment of felsic minerals interpreted to have formed during their emplacement
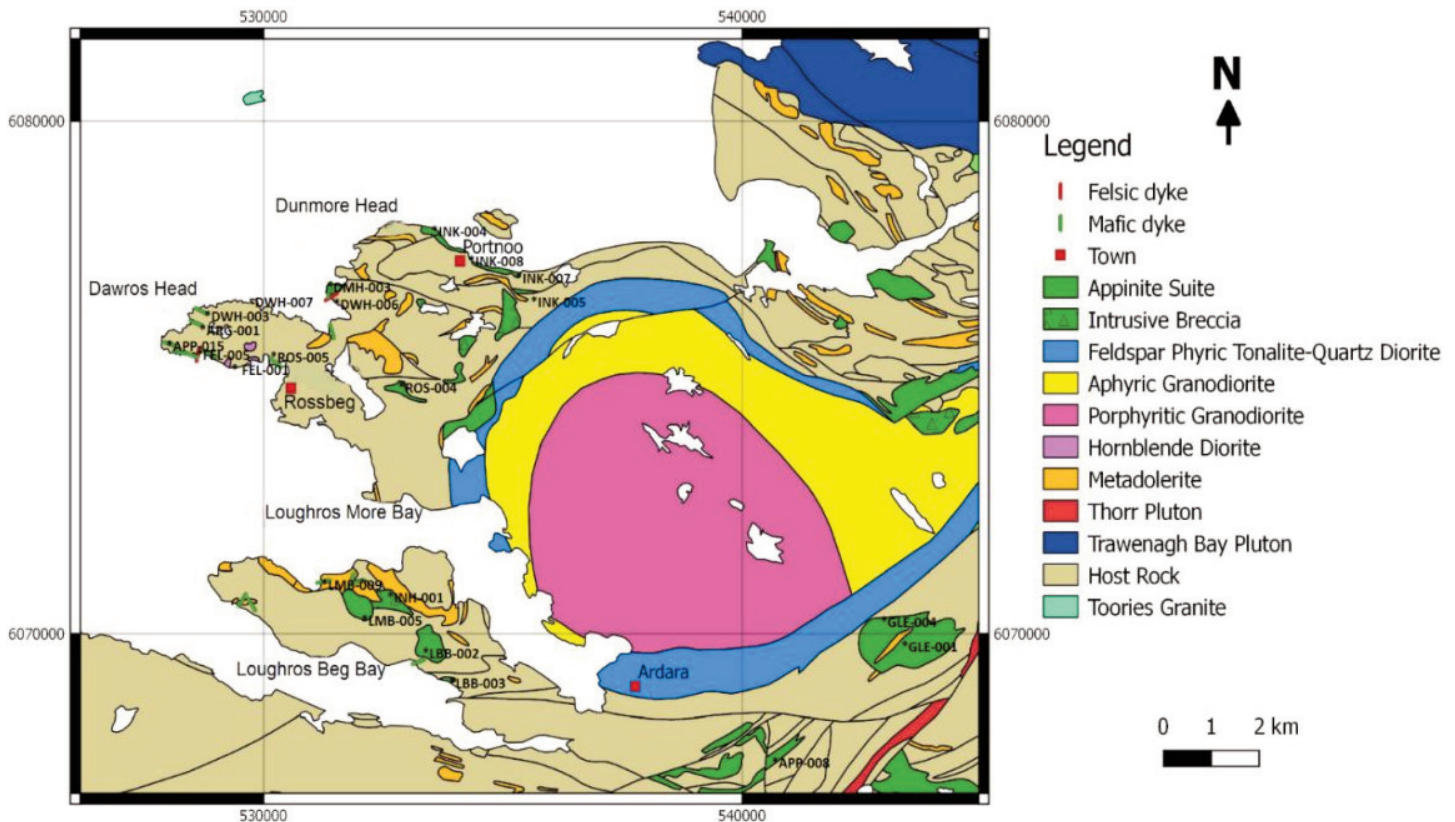
Figure 2. Geological map of the Ardara pluton showing sample locations (after Geological Survey of Ireland 2014). See Table 1 for details of locations.

and cooling (Bowes and McArthur 1976). The presence of xenoliths of appinitic rocks and lamprophyre within the MDG suggests that both were intruded prior to the emplacement of this pluton (French 1976). However, while the Ardara pluton has an early marginal phase lithologically identical to one of the rocks of the appinite suite, and both the appinitic intrusions and lamprophyre dykes crop out close to the pluton, neither cut the pluton itself (French 1976).

Many appinitic bodies are accompanied, particularly along their margins and in roof zones, by masses of disrupted metasedimentary rocks interpreted as intrusion breccias (French 1966). These breccia masses occur in near-vertical conduits that are elliptical in cross section with long axes up to 12 m. The clasts in the breccia are inferred to have been transported upwards to their present positions and comprise fragments of carbonate and quartzitic rocks that are typical of the Dalradian host rock (French 1966).

The appinite suite is made up of coeval plutonic and hypabyssal rocks that range from mafic (gabbro) to intermediate–felsic (diorite, granodiorite) in composition and contain prismatic hornblende in a groundmass of plagioclase, with or without quartz (Fig. 3a, b). The hornblende crystals are typically 3–5 mm in length and, in some cases, are in grain boundary contact with each other.

Although mingling of felsic and mafic lithologies within the appinite suite is rare, some local evidence of hybridization has been observed (Hall 1967). The relationship between the different lithologies is complex with evidence for multiple

intrusion and *in situ* differentiation, as well as complex interactions with the surrounding country rock (Platten 1991). Pitcher and Berger (1972) observed that some outcrops are dominated by intrusion breccia and explosion breccia characterized by angular fragments of quartzite and calc-silicate rock within an appinitic matrix. These features, together with the dominance of hornblende and the wide range of textures, suggest that crystallization of the appinitic magmas occurred under high water vapour pressure (Rock 1991).

Lamprophyre Dykes

The rocks of the appinite suite, along with the breccia intrusions associated with them, intrude and are intruded by lamprophyre dykes (Elsdon and Todd 1989). Lamprophyre (Fig. 3c) occurs as dykes and sills that intruded the Dalradian host rocks and is characterized by phenocrysts of hornblende and phlogopite with lesser amounts of clinopyroxene. The groundmass is diverse and includes plagioclase, biotite, pyroxene and amphibole. Lamprophyre variants include hornblendite, consisting mostly of idiomorphic hornblende within a relatively fine-grained matrix dominated by plagioclase. Less commonly, lamprophyre also contains interstitial quartz (Pitcher and Berger 1972).

^{40}Ar/^{39}Ar THERMOCHRONOLOGY

Analytical Methods

In order to date the emplacement of the Ardara appinite suite, ^{40}Ar/^{39}Ar thermochronology was performed at the
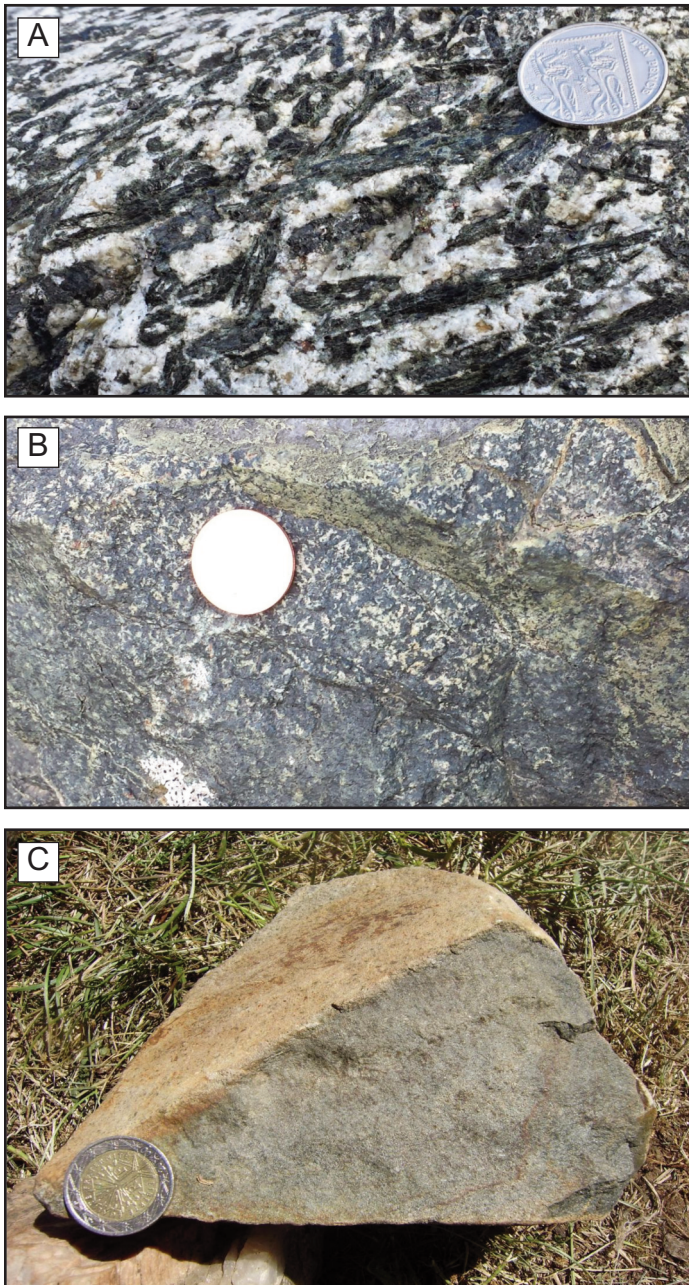
Figure 3. Field photographs of (a) mafic rock of the appinite suite with prismatic amphibole grains within a plagioclase matrix, (b) intermediate–felsic rock of the appinite suite with amphibole clumps within a plagioclase matrix, and (c) a lamprophyre dyke with fine-grained biotite and hornblende grains within a plagioclase-rich matrix.

geochronology laboratory at Queen's University in Kingston, Ontario, on amphibole separated from two representative samples (INK-004 and GLE-004). Electron microprobe analyses and X-ray images of representative hornblende from each sample are shown in the supplemental files SF-1 to SF-5. The amphibole analyses show variations from 39.7 to 42.7 wt.% in SiO_2, 11.8 to 13.9 wt.% in Al_2O_3, 10.8 to 12.4 wt.% in CaO, 2.1 to 4.03 wt.% in TiO_2 and 0.59 to 1.24 wt.% K_2O. Mean Ca/K ratios are between 11.1 and 13.3. Because the water and halogen contents of the amphiboles are unknown, the amphibole

formulae are calculated to 23(O), and the Fe^{2+}/Fe^{3+} ratio determined after the method described by Pe-Piper (1988). According to the classification of Leake et al. (2004), the amphiboles are calcic as they all have $(Ca+Na)^B \geq 1.00$ and NaB > 0.50 apfu (atoms per formula unit). The amphiboles typically have Si^{IV} between 5.9 and 6.4, with Al^{IV} from 2.1 to 1.6 and $Mg/(Mg+Fe^{2+})$ between 0.6 and 0.9. The analyses indicate that the amphibole compositions are typical of tschermakitic hornblende of igneous origin (Leake 1978; Leake et al. 2004).

The sample locations are shown on Figure 2 and listed in Table 1. Both samples were hand-crushed and single grains of hornblende cleavage fragments free of visible overgrowths were selected for analysis. Mineral separates and flux-monitors (standards) were wrapped in Al foil. The resulting disks were stacked vertically into an 8.5 cm long and 2.0 cm diameter Al irradiation capsule, and then irradiated with fast neutrons in position 8C of the McMaster Nuclear Reactor (Hamilton, Ontario) for a duration of 86.4 h (at 2.5 MWH). Packets of flux monitors were located at ~0.5 cm intervals along the irradiation container and the J-value for each of the samples was determined by least-squares, second-order polynomial interpolation using weighted means of replicate analyses of splits of the bracketing monitors position in the capsule.

The samples were loaded into flat-bottomed pits in a copper sample-holder and placed beneath the ZnS view-port of a small, bakeable, stainless-steel chamber connected to an ultra-high vacuum purification system. Following bake-out at 105°C, a 30 W New Wave Research MIR 10-30 CO_2 laser with a faceted lens was used to heat the samples for 3 minutes at increasing percent power settings (2% to 45%; beam diameter 3 mm). After purification using hot and cold SAES C50 getters (for 5 minutes), the evolved gas was admitted to an MAP 216 mass spectrometer, with a Bäur Signer source and an analogue electron multiplier (set to a gain of 100 over the Faraday detector).

Measured Ar isotope peak heights were extrapolated to zero-time and corrected for discrimination using an $^{40}Ar/^{36}Ar$ atmospheric ratio of 298.56 (Lee et al. 2006) and measured ratios of atmospheric Ar. Blanks, measured routinely, were subtracted from the subsequent sample gas fractions. The extraction blanks were typically $< 10 \times 10^{-13}$, $< 0.5 \times 10^{-13}$, $< 0.5 \times 10^{-13}$, and $< 0.5 \times 10^{-13}$ cm^{-3} STP for masses 40, 39, 37, and 36, respectively. ^{39}Ar and ^{37}Ar were corrected for radioactive decay during and after irradiation. Corrections were made for neutron-induced ^{40}Ar from potassium, ^{39}Ar and ^{36}Ar from calcium, and ^{36}Ar from chlorine (Roddick 1983; Onstott et al. 1991). Dates and errors were calculated using the procedure of Dalrymple et al. (1981) and the ^{40}K decay constant of Min et al. (2000; 5.463×10^{-10} 1/y). Plateau and inverse isotope correlation dates were calculated using ISOPLOT v. 3.60 (Ludwig 2008). A plateau is herein defined as 3 or more contiguous steps containing > 50% of the ^{39}Ar released, with a probability of fit > 0.01 and MSWD < 2. If the contiguous steps contain < 50% of the ^{39}Ar released, it is referred to as a plateau segment.

Quoted errors represent the analytical precision at 2σ, assuming that the error in the age of the flux monitor is zero.

Table 1. Lithology, location and analysis of samples selected for geochemical analysis from the Ardara appinite plutons and coeval lamprophyre dykes, Donegal, Ireland.

Sample ID	Rock Type	Location	Northing	Easting	Analysis
Appinite Suite					
APP-008	Mafic Dyke	Ardara	54.7538	-8.3819	REE
APP-015	Mafic Dyke	Dawros Head	54.8333	-8.4552	REE
LBB-003	Mafic Dyke	Loughros Beg Bay	54.7698	-8.4816	REE, Sm–Nd
INK-004	Mafic Dyke	Portnoo	54.8475	-8.4801	REE, Sm–Nd, Ar–Ar
AGR-001	Mafic Dyke	Dawros Head	54.7337	-8.4332	REE, Sm–Nd
GLE-001	Mafic Dyke	Glenties	54.8223	-8.277	REE, Sm–Nd
GLE-004	Mafic Dyke	Glenties	54.7477	-8.2946	REE, Sm–Nd, Ar–Ar
ROS-004	Mafic Dyke	Rossbeg	54.8226	-8.5296	REE
INK-007	Felsic Dyke	Portnoo	54.82575	-8.5603	REE
INK-008	Felsic Dyke	Portnoo	54.84329	-8.4717	REE, Sm–Nd
FEL-005	Felsic Dyke	Dawros Head	54.8254	-8.5544	REE, Sm–Nd
DWH-007	Felsic Dyke	Dawros Head	54.8331	-8.5502	REE
INK-005	Felsic Dyke	Portnoo	54.84436	-8.4724	REE
DWH-006	Intermediate	Dawros Head	54.83297	-8.5532	REE
INH-001	Intermediate Dyke	Loughros Beg Bay	54.82922	-8.5108	REE
Lamprophyre Dykes					
FEL-001	Mafic Dyke	Dawros Head	54.8254	-8.5505	REE, Sm–Nd
LMB-009	Mafic Dyke	Loughros More Bay	54.8365	-8.514	REE, Sm–Nd
LBB-002	Mafic Dyke	Loughros Beg Bay	54.77122	-8.4833	REE, Sm–Nd
DMH-003	Mafic Dyke	Dumore Head	54.8365	-8.5155	REE, Sm–Nd
DWH-003	Mafic Dyke	Dawros Head	54.8308	-8.5548	REE, Sm–Nd
ROS-005	Mafic Dyke	Rossbeg	54.82322	-8.529	REE
LMB-005	Mafic Dyke	Loughros More Bay	54.7870	-8.5143	REE

This precision is suitable for comparing within-spectrum variation and determining which steps form a plateau (e.g. McDougall and Harrison 1988, p. 89). The dates and J-values were referenced to GA1550 biotite (98.5 Ma; Spell and McDougall 2003; McDougall and Wellman 2011; recalculated relative to an FC sanidine age of 28.201 Ma; Kuiper et al. 2008).

Results

A summary of the $^{40}Ar/^{39}Ar$ data obtained is shown in supplemental file SF-6. Step heating of hornblende separates from these two samples resulted in release patterns with initially high ages, decreasing over the first few percent of the ^{39}Ar released, then increasing irregularly to robust well-defined plateaus. In this study, the ISOPLOT plateau dates represent the best estimate of the age of the samples. For both spectra, the plateau steps incorporate those with typical yield Ca/K ratios (12 to 15) calculated from the $^{37}Ar/^{39}Ar$ ratios comparable to those obtained from the electron microprobe analyses (11 to 13).

Sample INK-004 is from an appinitic intrusion into Dalradian host rock taken near the Portnoo coast. This sample contains abundant amphibole, biotite clusters and interpenetrating apatite in a matrix dominated by plagioclase and amphibole. It yielded a ten-step plateau with 90.5% of the ^{39}Ar released and a plateau date of 434.8 ± 1.2 Ma (Fig. 4a), and within error a concordant inverse isochron date of 434.2 ± 2.1 Ma (Fig. 4b). The inverse isochron included 12 of the 14 steps, 94.3% of the

^{39}Ar released, had a slightly non-atmospheric initial $^{40}Ar/^{36}Ar$ ratio (333 ± 18) and an MSWD = 0.63. The ages are essentially the same at each step except for those produced by the argon released (5%–10%) during the initial heating. During the first few steps, traces of loosely bound excess Ar caused the older dates in this part of the spectrum.

Sample GLE-004 is from an appinitic intrusion at Glenties in the contact aureole of the Ardara pluton ~200 m from the exposed contact. This sample is dominated by phenocrysts of olivine, amphibole and augite in a groundmass composed of phlogopite, biotite, plagioclase and orthoclase. The sample yielded a seven-step high-temperature plateau with a date of 440.1 ± 1.4 Ma (65.8% of the ^{39}Ar released) (Fig.5a). Because the inverse isochron ratios for the high-temperature steps were tightly clustered, a reliable ISOPLOT Model 1 solution could not be obtained. A Model 2 solution using all points yielded a date of 433.7 ± 5.5 Ma (Fig 5b) and an initial $^{40}Ar/^{36}Ar$ ratio of 405 ± 14. The initial ratio is well above that for atmospheric argon and suggests that excess Ar was incorporated in the hornblende. As in Sample INK-004, the ages are essentially the same at each step except for those produced by the argon released (5%–30%) during the initial heating. During the first few heating steps, likely traces of excess Ar caused the ages to appear about 50–80 million years older.

Interpretation

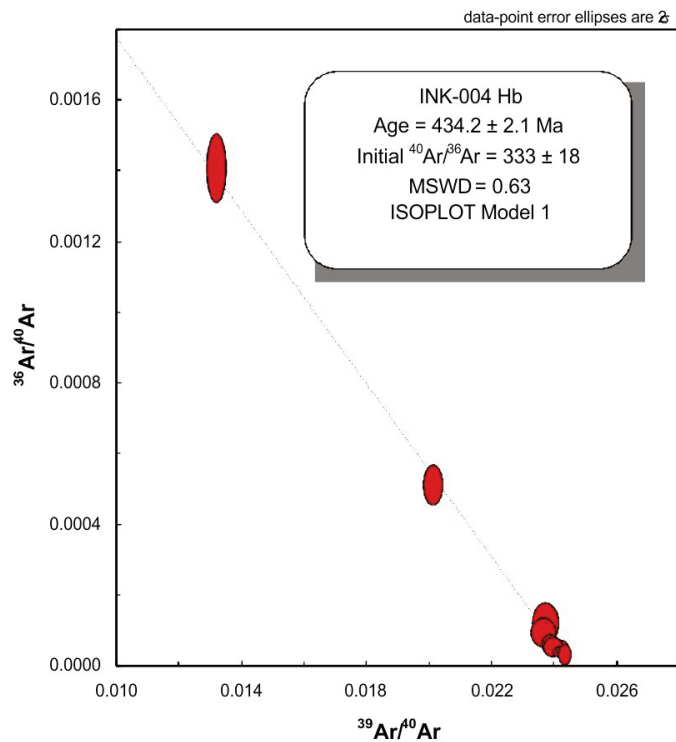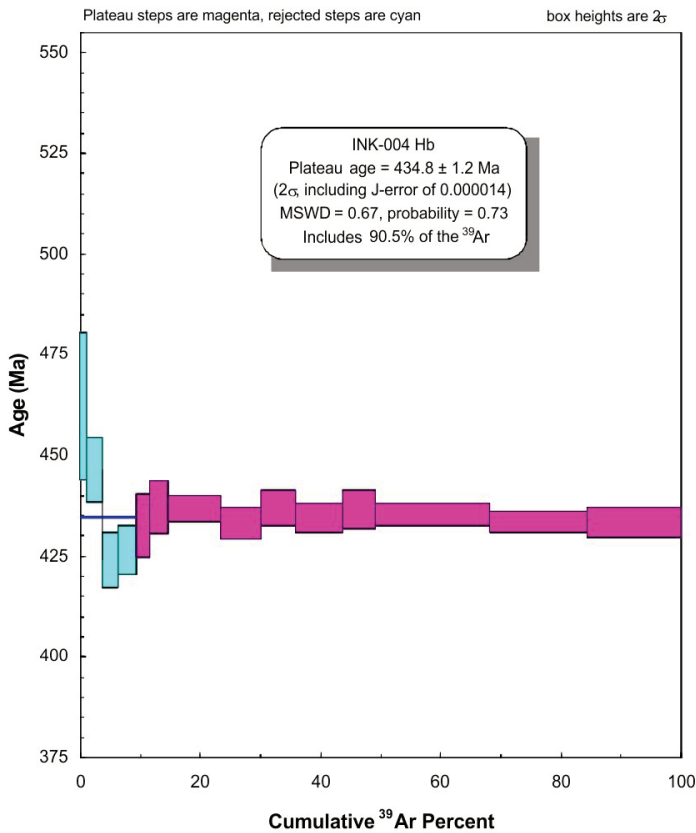The Ar closure temperature for hornblende is variable and

Plateau steps are magenta, rejected steps are cyan   box heights are 2σ

INK-004 Hb
Plateau age = 434.8 ± 1.2 Ma
(2σ, including J-error of 0.000014)
MSWD = 0.67, probability = 0.73
Includes 90.5% of the ^{39}Ar

Plateau steps are magenta, rejected steps are cyan   box heights are 2σ

GLE-004 Hb
Plateau age = 440.14 ± 1.4 Ma
(2σ, including J-error of 0.000014)
MSWD = 0.96, probability = 0.45
Includes 65.8% of the ^{39}Ar

data-point error ellipses are 2σ

INK-004 Hb
Age = 434.2 ± 2.1 Ma
Initial ^{40}Ar/^{36}Ar = 333 ± 18
MSWD = 0.63
ISOPLOT Model 1

data-point error ellipses are 2σ

GLE-004 Hb All Steps
Age = 433.7 ± 5.5 Ma
Initial ^{40}Ar/^{36}Ar = 405 ± 14
MSWD = 4.4
ISOPLOT Model 2

Figure 4. (a) ^{40}Ar/^{39}Ar age spectrum and (b) ^{40}Ar/^{39}Ar inverse isochron plot for sample INK-004.

Figure 5. (a) ^{40}Ar/^{39}Ar age spectrum and (b) ^{40}Ar/^{39}Ar inverse isochron plot for sample GLE-004.

depends on several compositional factors. Because the dated amphibole samples have Mg/(Mg+Fe) ratios in the range of the hornblende investigated by Harrison (1982; 0.6–0.8), it is
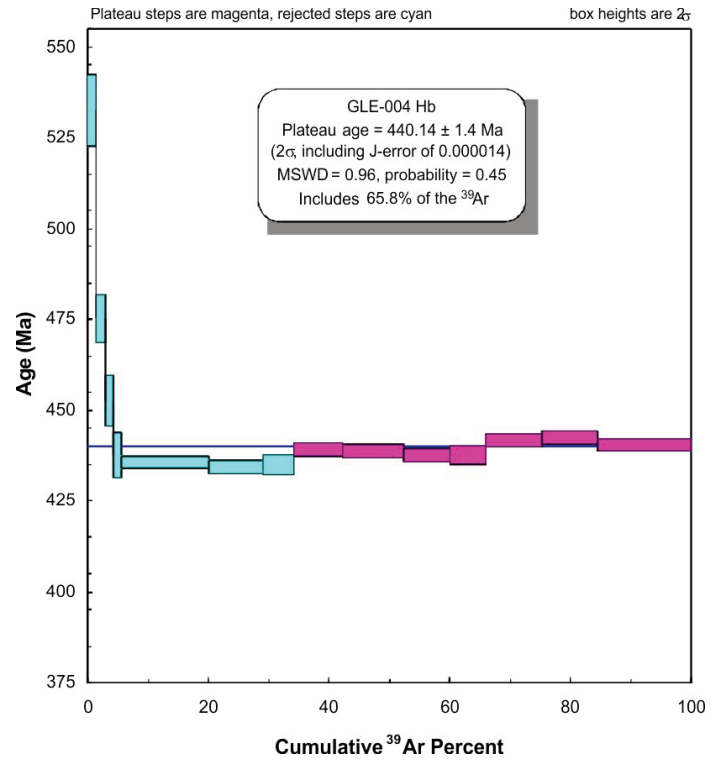
appropriate to calculate a closure temperature based on his experimental diffusion parameters. The relatively small size of both intrusions together with their mid-crustal level of

emplacement, suggests that cooling through the Ar closing temperature for hornblende was rapid. Using Dodson's (1973) iterative expression for closure temperature and a conservative cooling rate of 100°C/m.y. a probable minimum closure temperature of 545°C is obtained. Sample location INK-004 is ~ 2 km from the contact of the Ardara pluton and is not likely to have experienced any reheating from the Ardara pluton. GLE-004 is within ~ 500 m of the southern contact of the Ardara and may have been reheated. However, based on geothermometry and geobarometry in pelitic rocks, Kerrick (1987) modelled the thermal gradient across the aureole. Based on his contact temperature profile and pressures of 2–3 kbar, it is unlikely that GLE-004 would have been re-heated to a temperature > 500°C. The calculated closure temperature is significantly higher than the metamorphic temperatures experienced by the Dalradian metasedimentary rocks that host the Ardara appinite suite, which are at regional greenschist facies. The cooling age of 434.2 ± 2.1 Ma (2σ) obtained from the $^{40}Ar/^{39}Ar$ inverse isochron is consequently interpreted to have been acquired during rapid cooling of the appinitic magma. Given the relatively small size and mid-crustal levels of emplacement, both of which would suggest rapid cooling through the Ar closing temperature for hornblende, the ages are considered to date igneous emplacement closely. These data therefore indicate a Silurian (late Llandovery–early Wenlock) crystallization age for the Ardara appinite suite and, when combined with field relationships, suggest that emplacement of the suite slightly preceded emplacement of the earliest Donegal granite plutons, including the Ardara pluton (Fowler and Henney 1996; Atherton and Ghani 2002; Condon et al. 2004).

GEOCHEMISTRY

Twenty-two samples representative of the appinite suite and lamprophyre dykes were collected from all the larger appinitic bodies and several lamprophyre dykes surrounding the Ardara pluton. These were sent to the Bureau Veritas Commodities Canada, Ltd., Vancouver, British Columbia, for major and trace element analysis by X-ray fluorescence (XRF) using a Philips PW2400 X-ray spectrometer. The samples were obtained from fine- to coarse-grained appinitic intrusions and lamprophyre dykes intruding Dalradian host rock at Dunmore Head, Portnoo, Rossbeg, Loughros More Bay, Loughros Beg Bay and Ardara (Fig. 2). Sample locations are given in Table 1 and shown on Figure 2. Rare earth and selected trace elements were analyzed by Inductively Coupled Plasma Mass Spectrometry (ICP–MS), also at the Bureau Veritas Commodities Canada, Ltd., using a Fisons/Applied Research Laboratories 8420+ wavelength dispersive X-ray spectrometer. A subset of the powdered samples was additionally analyzed for Sm–Nd isotopic values at Memorial University using thermal ionization mass spectrometry.

Whole-rock Analysis

Samples of the appinite suite were taken from mafic enclaves within the Ardara pluton and from dykes up to 5 m in width that cut the Dalradian host rocks. Selected major and trace element data for these samples are given in supplementary file SF-7. Loss-on-ignition (LOI) values are variable, ranging from 1.9 to 2.9 wt.% in mafic rocks and 1.1 to 2.6 wt.% in intermediate–felsic rocks of the appinite suite, and from 49.5 to 57.2 wt.% in the lamprophyre dykes.

Appinite Suite

Mafic rocks of the appinite suite have SiO_2 content ranging from 45.8–53.3 wt.%, MgO values from 5–16 wt.%, magnesium numbers (Mg#), (100 x MgO/ (MgO + $0.9FeO_{tot}$) that range from 22 to 57 and variable Al_2O_3 contents (13.0–22.0 wt.%). Intermediate–felsic members of the suite have higher SiO_2 concentrations (64.8–72.1 wt.%) but a similar range in Al_2O_3 (13.3–19.1 wt.%) and much lower MgO values (0.28–0.78 wt.%).

Petrographic evidence for alteration in rocks of the appinite suites necessitates the emphasis on concentrations of less mobile high-field strength elements (HFSE) and rare earth elements (REE) instead of the more mobile large ion lithophile elements (LILE) in the interpretation of petrogenesis and tectonic setting (e.g. Winchester and Floyd 1977). The mobility of alkalis (Na_2O, K_2O) is evident from their scatter on Harker variation diagrams (Fig. 6). The Zr/Ti vs Nb/Y diagram (Pearce 1996) is used to replace the total alkali–silica diagram because Zr/Ti and Nb/Y are respective proxies for the silica and alkali contents (Fig. 7). The mafic rocks of the suite are sub-alkalic and plot in the basaltic andesite to basalt fields. On FeO_{tot}/MgO vs FeO and FeO_{tot}/MgO vs SiO_2 (Miyashiro 1974) discrimination diagrams (Fig. 8a,b), the mafic rocks show a limited range in SiO_2 over a large range in FeO_{tot}/MgO, a feature that is typical of a tholeiitic differentiation trend, but the low FeO_{tot}/MgO ratio exhibited by several mafic samples is typical of calc-alkaline suites.

The mafic rocks are also characterized by generally high MgO (4.1 to 16.7 wt.%), Cr_2O_3 (0.01 to 0.06 wt.%), Ni (98–288 ppm), Ba (233–528 ppm), and V (179–462 ppm) abundances as well as elevated LILE- and light rare-earth elements (LREE), and slightly depleted heavy rare-earth elements (HREE). The high concentrations of Mg, Ni, Cr and Ba are indicative of a mantle source (Atherton and Ghani 2002). On chondrite-normalized REE diagrams, the mafic rocks display a moderate negative Eu anomaly indicating fractionation of plagioclase (Fig. 9a). On multi-element plots (Pearce 1983), the rocks also display moderately negative anomalies in HFS elements such as Nb, P, Zr and Ti (Fig. 10a,b). The overall slope, a general source enrichment of LILE (Fig. 9b), and the negative anomalies in HFS elements are characteristic of a mantle source in a subduction zone setting. The mafic rocks additionally have generally high Zr/Y, a characteristic typical of within-plate tholeiitic basalt. In the Ti/1000 vs V diagram (Fig. 11), the mafic rocks plot in the fields of mid-ocean ridge (MORB) and back-arc basin (BAB) basalt.

On Th/Yb and Ce/Yb vs Ta/Yb plots (Fig. 12a,b), the vertical axis detects subduction components so that rocks formed in a coeval arc environment, or those contaminated by continental crust plot above typical mantle values. The rocks of the appinite suite display calc-alkalic to shoshonitic compositions
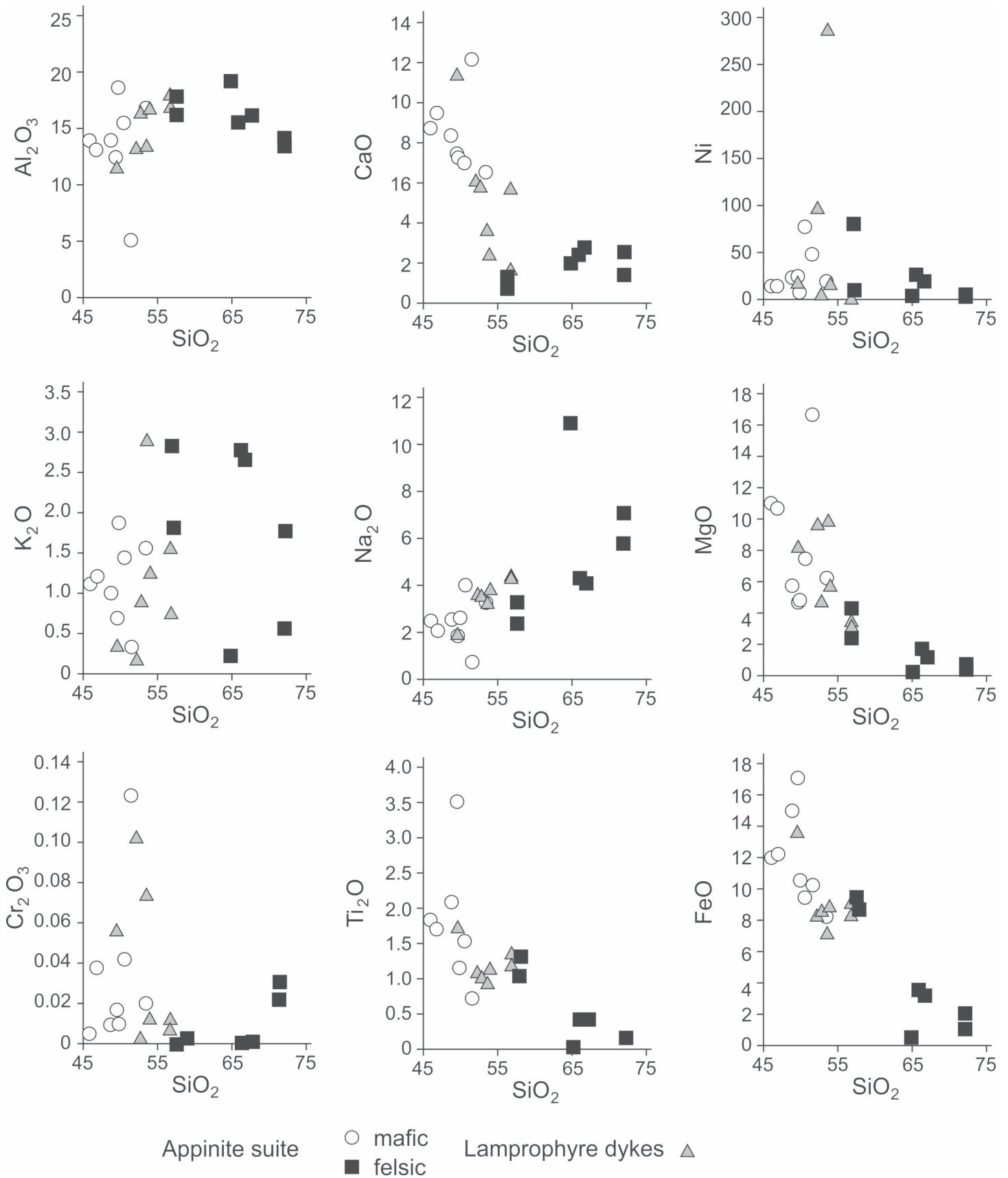
Figure 6. Harker diagrams for major element oxides for the Donegal appinite suite.
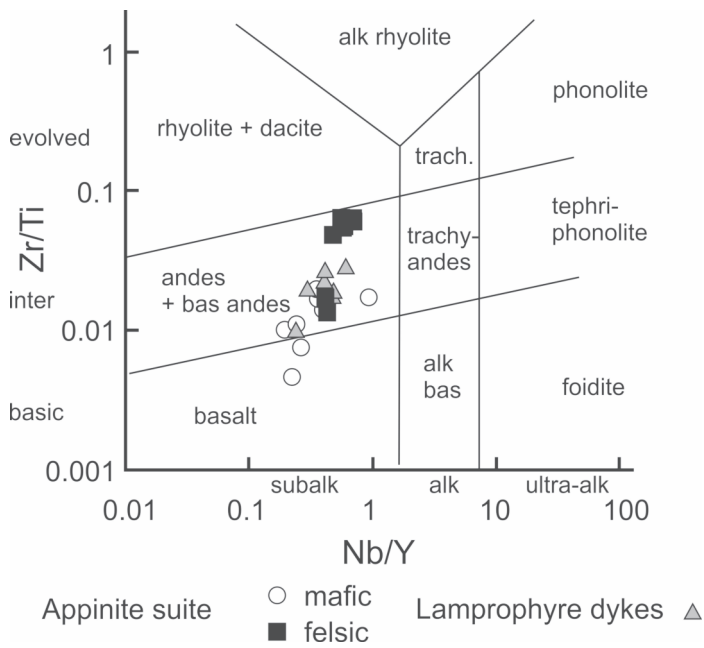
Figure 7. Zr/Ti vs Nb/Y diagram for classifying the Donegal appinites (Pearce 1996 after Winchester and Floyd 1977).

on these plots. On the La/Yb vs Th/Yb plot (Fig. 13), the mafic and intermediate–felsic rocks of the appinite suite display island arc to continental margin arc characteristics. As arc magmas are enriched in Th and depleted in Ta, they plot nearer the Hf–Th join compared to MORB or within-plate basalts on the Hf–Th–Ta diagram (Fig. 14). The rocks of the appinite suite plot as calc-alkaline basalt and have higher Th than typical island arc tholeiite (IAT), plotting closer to the Th apex of this discrimination diagram.

Lamprophyre Dykes
The lamprophyre dykes are mafic to intermediate and range from 49.5 to 56.7 wt.% in SiO_2, 11.5 to 18.0 wt.% in Al_2O_3, and 1.9 to 4.4 wt.% in Na_2O. These rocks are also high in TiO_2, MnO, P_2O_5 and Cr_2O_3.

Using the FeO_{tot}/MgO vs SiO_2 and FeO_{tot}/MgO vs FeO (Miyashiro 1974; Arculus 2003) diagrams, the lamprophyre dykes display small ranges in SiO_2 and FeO contents over a large range in FeO_{tot}/MgO (Fig. 8a,b). The slope evident in this figure is typical of a tholeiitic differentiation trend.

The lamprophyre dykes are moderately enriched in the LREE and LILE relative to HREE. They display a moderate negative Eu anomaly indicating fractionation of plagioclase (Fig. 9c). In the Pearce (1983) multi-element plot, the samples display moderate negative anomalies in HFS elements such as Nb, P, Zr and Ti (Fig. 10c), which is characteristic of a subduction zone setting. All the lamprophyre dykes have high Zr/Y (4.0 to 9.0) and low Nb/Y (0.2 to 0.9), which is typical of within-plate tholeiitic basalt (Fig. 15a,b). In the Ti/1000 vs V diagram (Fig. 11), the lamprophyre dykes are characterized as MORB rocks.

On the Th/Yb and Ce/Yb vs Ta/Yb plots (Fig. 12a,b), the lamprophyre dykes plot as calc-alkaline to shoshonitic. On the La/Yb vs Th/Yb diagram (Fig. 13) they plot as continental
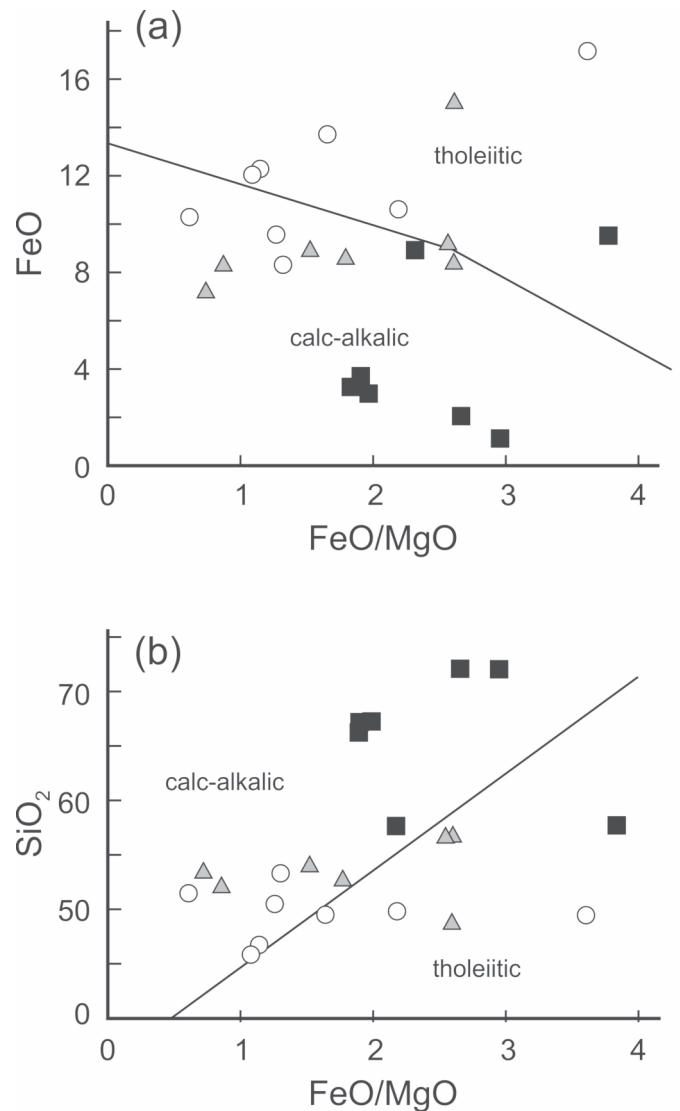

Figure 8. (a) FeO vs FeO_{tot}/MgO and (b) SiO_2 vs FeO_{tot}/MgO for the mafic and felsic rocks of the appinite suite in Donegal (dividing lines after Miyashiro 1974). Symbols as in Figure 7.

margin arc rocks, whereas on the Hf–Th–Ta discrimination diagram (Fig. 14), they plot as calc-alkaline basalt and have higher Th than typical island arc tholeiites (IAT), plotting close to the Th apex.

Sm–Nd Isotopic Analysis
Sm–Nd isotopic data for the Ardara appinite suite and lamprophyre dykes are summarized in Table 2. Nd data are calculated at $t = 435$ Ma, based on the $^{40}Ar/^{39}Ar$ hornblende age determined for the suite. Sm and Nd values for rocks of the appinite suite and lamprophyre dykes lie in the ranges 1.99–6.86 ppm and 8.59–35.84 ppm, respectively. $^{147}Sm/^{144}Nd$ values range from 0.1071 to 0.1536 and $^{143}Nd/^{144}Nd$ values range from 0.512212 to 0.512490. Depleted mantle model ages (T_{DM}) were calculated according to DePaolo (1981, 1988). εNdt values (t = 435 Ma) for the appinite suite range from –4.8 to +3.1 and T_{DM} values range from 805 Ma to 1710 Ma (Fig. 16).
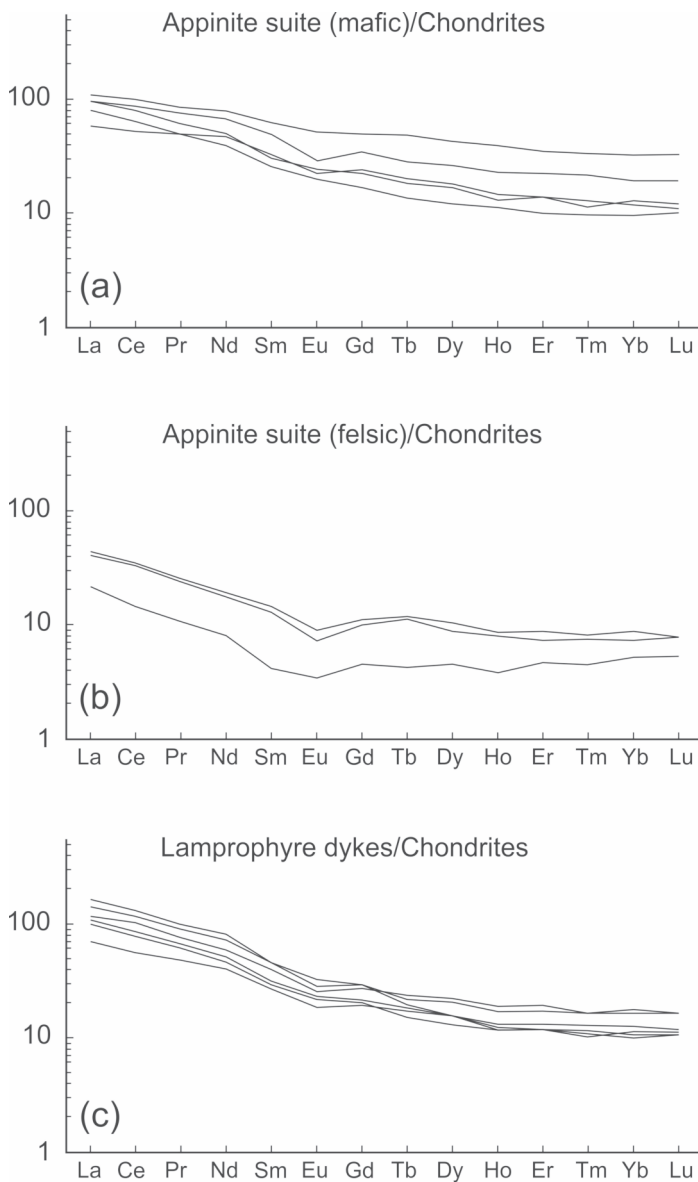
Figure 9. REE plots for representative samples of (a) mafic rocks of the appinite suite, (b) felsic rocks of the appinite suite and (c) the coeval lamprophyre dykes in Donegal (normalizing values from Sun and McDonough 1989).
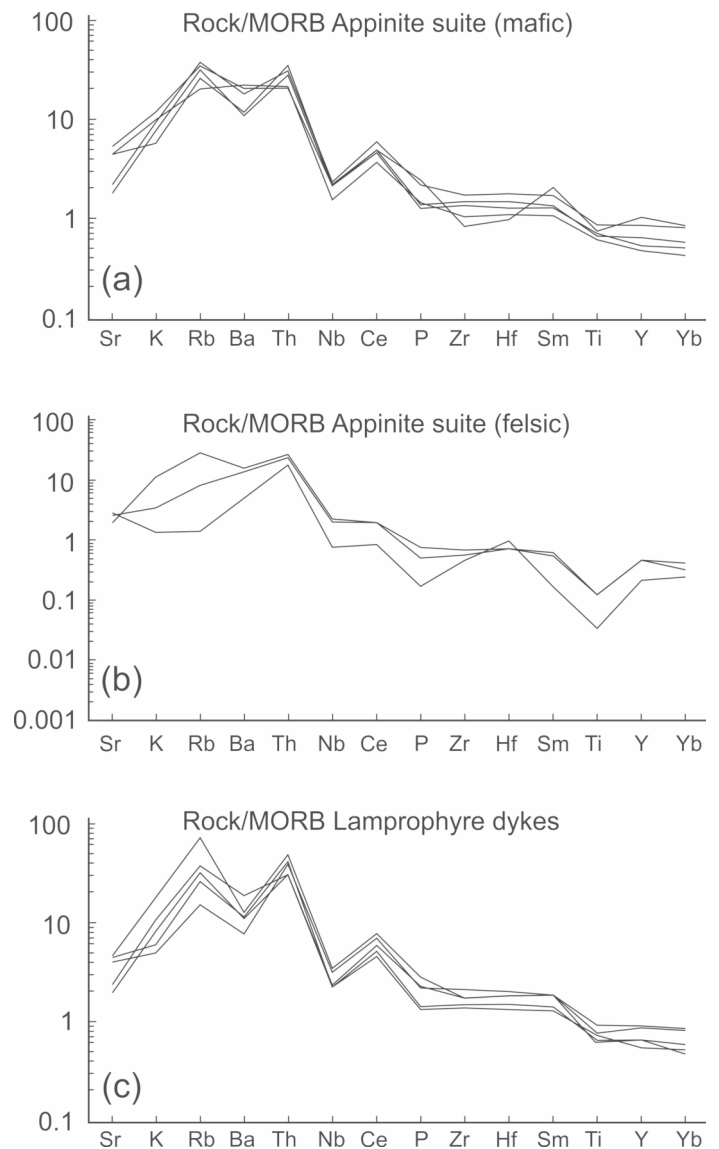

Figure 10. Multi-element plot for representative samples of (a) mafic rocks of the appinite suite, (b) felsic rocks of the appinite suite, and (c) the lamprophyre dykes in Donegal (normalizing values from Pearce 1983).

DISCUSSION

The $^{40}Ar/^{39}Ar$ isotopic data closely constrain the timing of emplacement of the appinite suite. Given that the Ar closure temperature for hornblende is ca. 550°C (Harrison 1982) and that the host Dalradian metasedimentary rocks are at greenschist facies, the cooling ages obtained are interpreted to closely date igneous emplacement at ca. 434 Ma providing supporting evidence for the interpretation that the rocks of the appinite suite slightly predate the emplacement of the Ardara granite, and significantly predate the intrusion of the Main Donegal Granite. This conclusion is similar to that interpreted for the association of granite with appinite and lamprophyre in the Scottish Caledonides (Rogers and Dunning 1991; Fowler and Henney 1996; Atherton and Ghani 2002; Neilson et al. 2009). In the latter case, slab break-off is thought to have induced

asthenospheric upwelling, which induced melting of the lithospheric mantle producing an appinitic mafic layer that underplated the crust (Fig. 17). Heat from underplated mafic crust is inferred to have initiated the production of crustal melts and voluminous granitoid magmatism (e.g. Neilson et al. 2009). The granitoid bodies, in turn, may have been produced by fractional crystallization of appinitic parent magmas (von Blackenburg and Davies 1995; Fowler et al. 2008).

The appinite suite and lamprophyre dykes around the Ardara pluton display similar chemical trends that, together with their field relationships, suggest they are comagmatic. For example, Al_2O_3 varies inversely and displays a systematic correlation with SiO_2, and both rock groups show (i) negative correlations of SiO_2 with CaO, MgO, Fe_2O_3, TiO_2, V, Cr and Ni, and positive correlations of SiO_2 with K_2O and Na_2O, (ii) plot in the andesite to basaltic andesite fields on the Zr/Ti vs
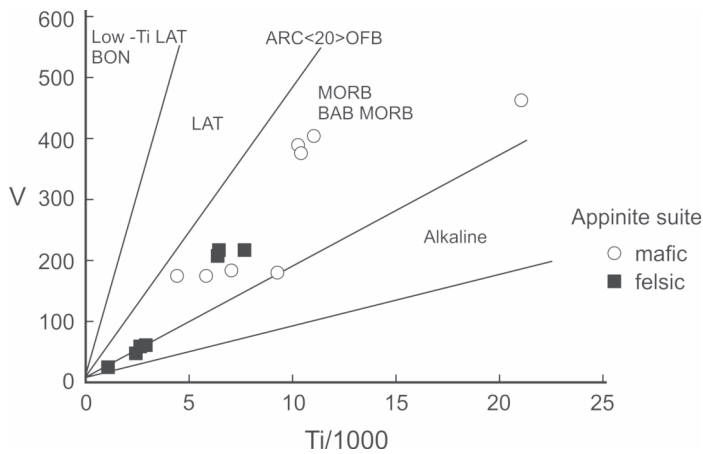
Figure 11. Ti/1000 vs V discrimination diagram for the appinite suite rocks in Donegal (after Shervais 1982). IAT (island arc tholeiite); BON (boninitic basalt); BAB (back-arc basin basalt).

Nb/Y diagrams, and (iii) display very similar trends in REE plots, with elevated LREE and depleted HREE values. The same can be said for both groups of rocks on multi-element plots. Both groups additionally display negative anomalies in Nb, P, Zr and Ti, which are characteristics of a mantle source in subduction zone settings. This interpretation is supported by a 437 ± 5 Ma crystallization age of a lamprophyre dyke to the east of the Leannan Fault in Donegal (Kirkland et al. 2013).

The appinite suite and lamprophyre dykes are also characterized by generally high Mg, Ni, Cr, Ba and V values (typical of mafic rocks), coupled with elevated LILE, and are moderately enriched in LREE with flat HREE profiles, indicating they were generated from partial melting of sub-continental lithospheric mantle. Both also show negative Nb and Ti anomalies, indicating either crustal contamination of the magmas or modification of the original mantle source by subduction zone fluids (e.g. Pearce 1996). If these anomalies were a result of crustal contamination, however, they should also be reflected in the Sm–Nd signature, resulting in a negative correlation between εNd and parameters such as Ce/Yb and Th/Yb. As no such correlation is present (Fig. 18), the trace element contamination presumably occurred at the time of magma generation and so did not affect the isotopic system. Hence, the negative trace element anomalies probably reflect the composition of the metasomatized mantle source, implying that the low εNdt values of the appinite suite and lamprophyre dykes directly reflect the composition of the mantle from which they were derived. But while the low εNdt values are consistent with derivation from the sub-continental lithospheric mantle, the range of εNdt values suggest the additional involvement of a juvenile source.

Rocks of the appinite suite have been described from other orogenic belts of widely ranging age (e.g. Salmon 1998; Castro et al. 2002; Ye et al. 2008; Murphy 2013). Many are associated with major strike-slip faults (e.g. Murphy and Hynes 1990; Murphy 2013) including the appinite suite of Donegal (e.g. Hutton 1982; Hutton and Alsop 1996; Kirkland et al. 2008). In this scenario, the Ar–Ar ages probably reflect the timing of
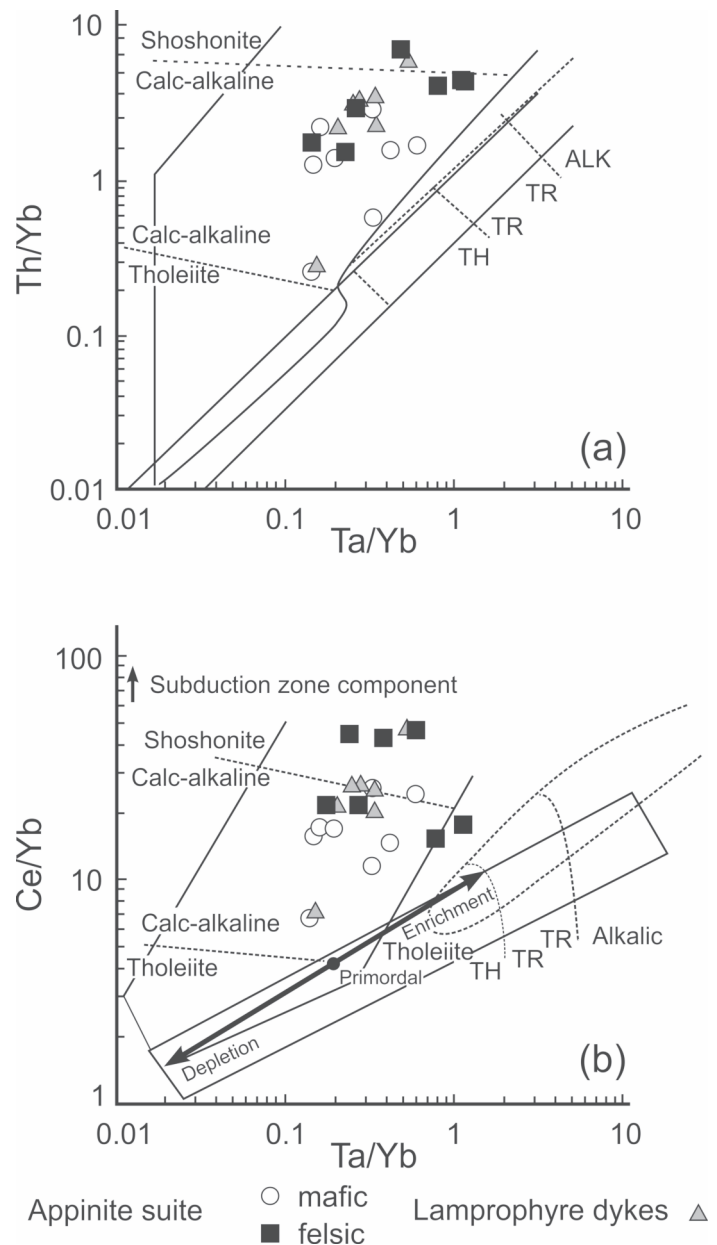

Figure 12. Log-log plots of (a) Th/Yb vs Ta/Yb and (b) Ce/Yb vs Ta/Yb (after Pearce 1982). TH (tholeiitic basalt); ALK (alkali basalt); TR (transition between tholeiitic and alkali basalt) for appinite suite rocks in Donegal.

emplacement of appinitic magma into relatively shallow crustal levels along active strike-slip faults, rather than the duration of appinitic magmatism. Potential sources of the appinitic and lamprophyric magmas include melting of the sub-continental lithospheric mantle (SCLM), melting of individual metasomatic veins within the mantle (Mitchell 1995), and/or melting of metasomatized underplated mafic crust. Only limited fractionation occurred during magma ascent and the magma was chemically modified by (i) the addition of upper crustal material, or (ii) the addition of fluids derived from this upper crustal material.

Regional constraints indicate appinitic and lamprophyric magmatism was coeval with (or shortly followed) collision, for
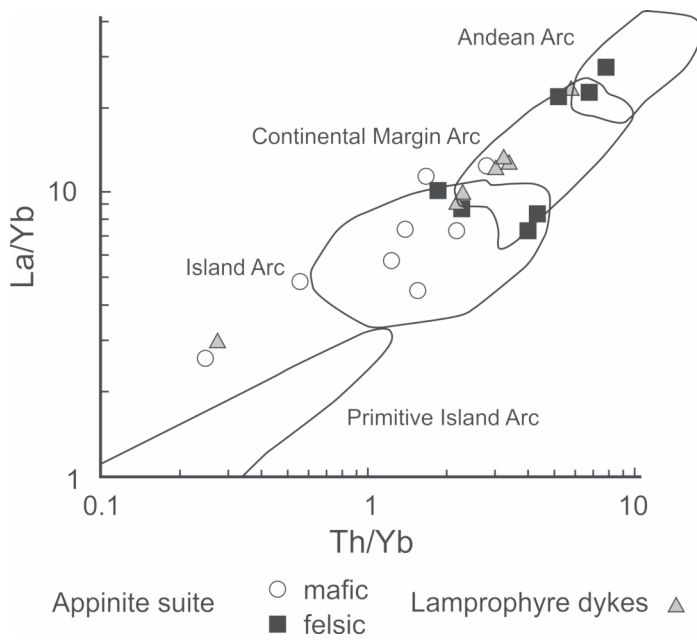
Figure 13. Log-log plot of La/Yb vs Th/Yb (after Condie 1989) for the appinite suite rocks of Donegal.
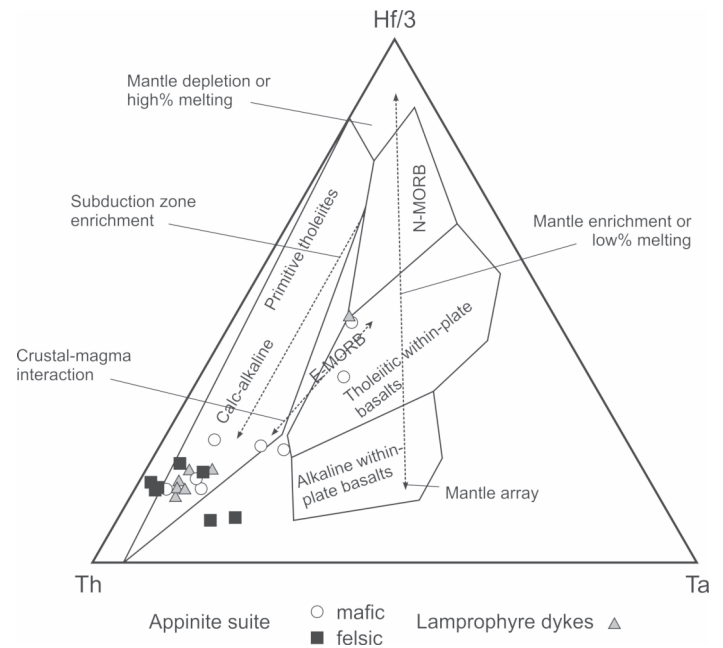

Figure 14. Triangular Hf/3–Ta–Th diagram (after Wood et al. 1979) for the appinite suite rocks of Donegal.
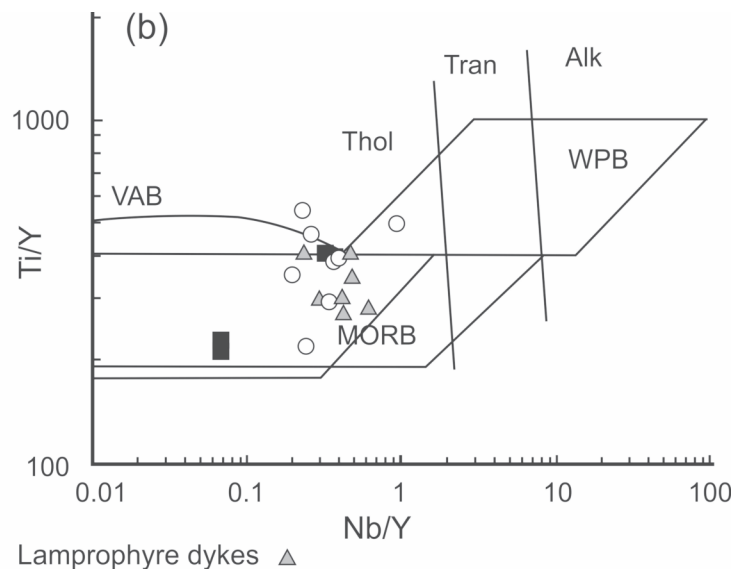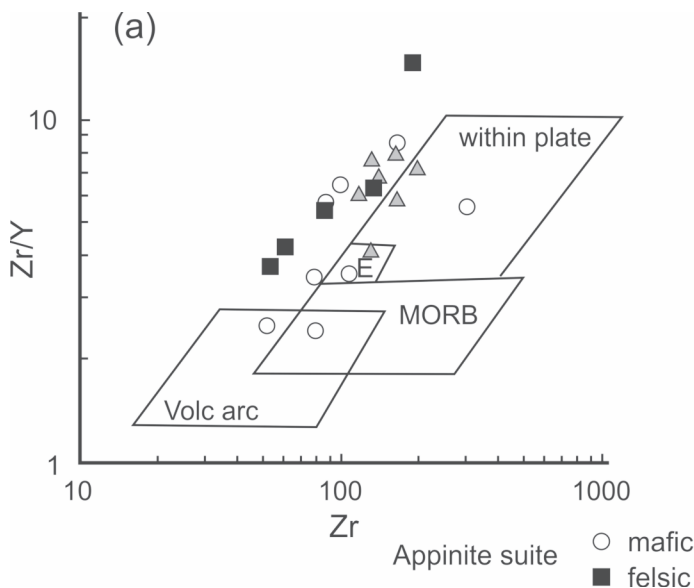

Figure 15. Zr vs Zr/Y discrimination diagram (after Pearce and Norry 1979) for the appinite suite rocks of Donegal. MORB (mid-ocean ridge basalt); E (enriched mid-ocean ridge basalt); VAB (volcanic arc basalt); WPB (within-plate basalt).

which slab break-off magmatism has been inferred (Ghani and Atherton 2008; Oliver et al. 2008; Neilson et al. 2009). Models proposed to account for appinitic and lamprophyric magmas in collisional settings ascribe the heat source to asthenospheric upwelling caused either by extensional tectonics associated with late orogenic events (Seyítoğlu and Scott 1996), such as lithospheric delamination, or by slab break-off (Dilek and Altunkaynak 2009). In both these scenarios, asthenospheric upwelling results in coeval melting of the overlying metasomatized SCLM and at least partial replacement of the SCLM (O'Reilly and Griffin 2006) by younger juvenile mantle (Downes 2001).

Regional Implications

The geochemical data presented here are consistent with previously published data for coeval post-collisional appinite plutons and lamprophyre dykes in the Scottish Highlands (Fowler 1988) whose emplacement also immediately preceded the emplacement of Caledonian granite plutons. These similarities suggest that processes responsible have regional significance. The origin of the rocks of the appinite suite and lamprophyre dykes in the Caledonides has been related specifically to the closure of the Iapetus Ocean, which was immediately followed by subduction of Avalonia beneath Laurentia (Bowes and Košler 1993). Slab break-off is likely to have been a conse-

Table 2. Sm–Nd isotope, εNd and T_{DM} age data for the mafic and intermediate–felsic rocks of the appinite suite and coeval lamprophyre dykes peripheral to the Ardara pluton, Donegal, Ireland.

Sample	Nd (ppm)	Sm (ppm)	$^{147}Sm/^{144}Nd$	$^{143}Nd/^{144}Nd$	2s	εNd (0 Ma)	εNd (435 Ma)	T_{DM}
DWH-003	21.71	4.38	0.1219	0.512347	6	-5.7	-1.5	1156
DMH-003	35.84	6.86	0.1158	0.512454	7	-3.6	0.9	922
FEL-001	18.41	4.07	0.1335	0.512478	7	-3.1	0.4	1076
LMB-009	31.75	6.43	0.1225	0.512318	7	-6.2	-2.1	1210
LBB-002	24.05	4.88	0.1226	0.512257	7	-7.4	-3.3	1311
INK-004	20.25	5.14	0.1536	0.512365	5	-5.3	-2.9	1710
AGR-001	17.90	3.67	0.1239	0.512381	6	-5.0	-1.0	1124
GLE-001	14.76	3.65	0.1496	0.512336	7	-5.9	-3.3	1673
GLE-004	21.18	5.25	0.1500	0.512339	7	-5.8	-3.2	1676
LBB-003	22.03	4.71	0.1294	0.512603	6	-0.7	3.1	805
INK-008	8.59	1.99	0.1400	0.512231	8	-7.9	-5.8	1673
FEL-005	20.39	3.61	0.1071	0.512212	7	-8.3	-3.3	1189

($^{143}Nd/^{144}Nd$) is adjusted from the deviation to JNdi-1 Standard (accepted valve = 0.512115), mean measured value of the standard gives: $^{143}Nd/^{144}Nd$ (0.512105) Std (0.000008) n (22)
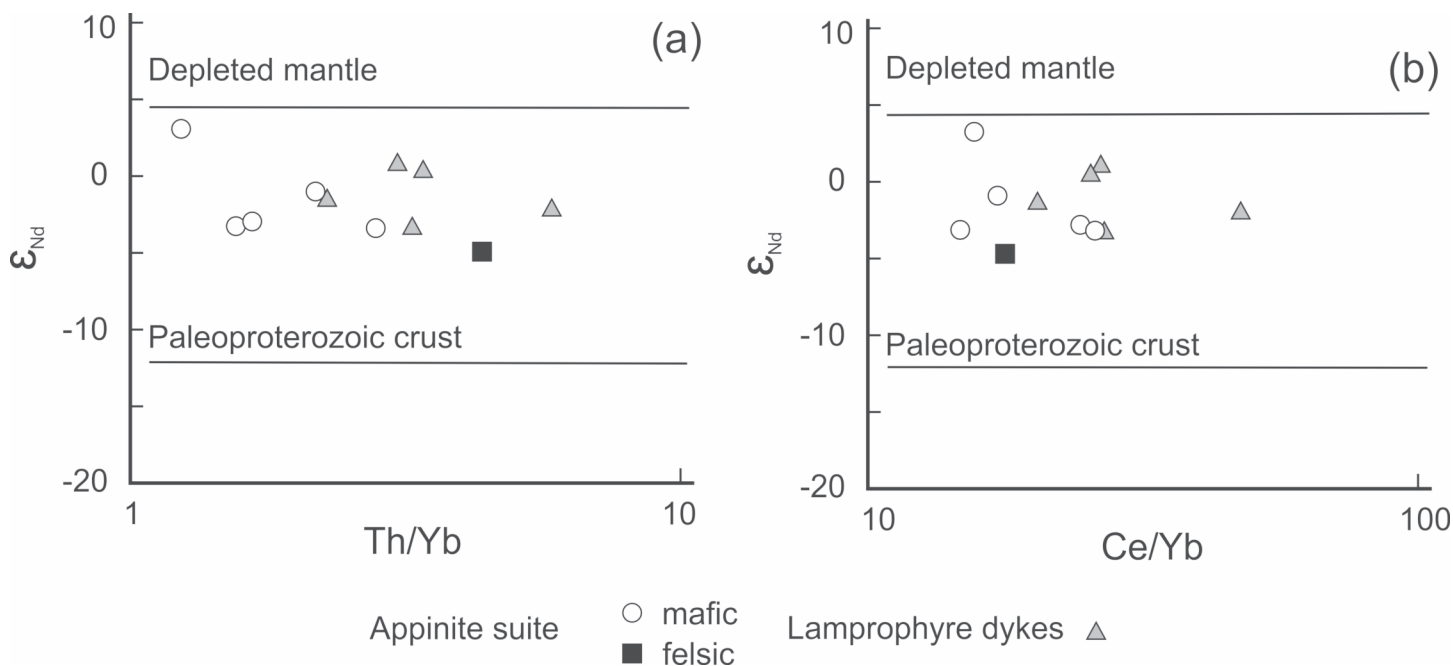

Figure 16. Nd isotope evolution diagram for the appinite suite rocks of Donegal. Values shown on the depleted mantle curve are T_{DM} ages (DePaolo 1981, 1988).

quence of this event. The magmatic association related to this collision (high-K, calc-alkaline, lamprophyric compositions) and the accompanying granitoid magmatism are best interpreted as direct responses to slab-breakoff, an association recently suggested for some late-stage Cordilleran batholiths (e.g. Hildebrand and Whalen 2014a, b). Within the Caledonian orogen in Britain, the association in time and space of appinitic, lamprophyric and voluminous granitic magmas is one in which the mantle components are chemically and isotopically similar and the magmas of all three rock groups are genetically related (Rock and Hunter 1987; Fowler and Henney 1996).

The felsic components include large batholiths that were probably derived by fractionation of shoshonitic magma

(Fowler 1988). Other appinite suites include some, but not all, of these features (Murphy 2013). Some common tectonic traits of appinitic rocks include a tendency to be emplaced soon after the cessation of subduction, and the important role of deep crustal faults as conduits for magmas of various compositions to rise towards the surface. These conduits provide the setting for magmas of diverse composition to mix and mingle (Murphy 2013). The magmas are quite similar to those of lamprophyre dykes and, together with ultrapotassic magma, are considered to have a parental source in potassium-rich phlogopite-bearing mantle. The appinitic and lamprophyric rocks of Donegal may therefore be an example of the products of collisional asthenospheric upwelling that occurred in this area
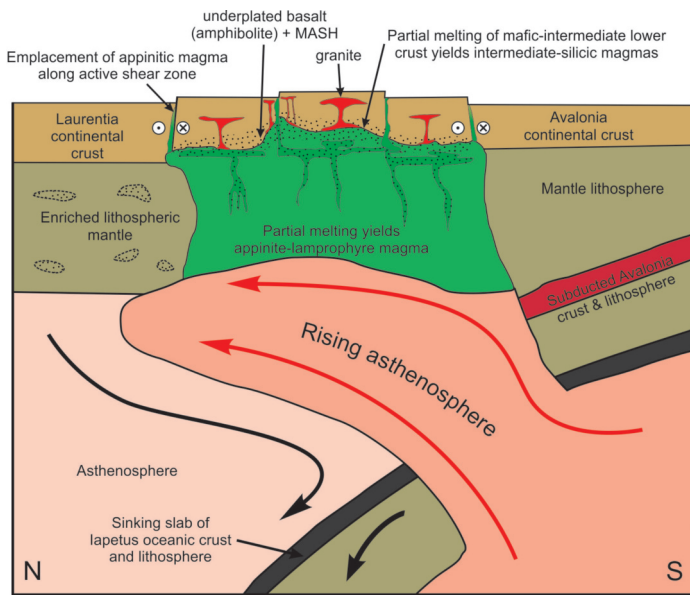
Figure 17. Schematic illustration (modified after Neilson et al. 2009) of a model for magmatism in the Caledonides of Scotland and NW Ireland relating the origin of appinite magma through slab break-off and the consequent upwelling of hot asthenosphere. This upwelling is thought to have caused partial melting of the lithospheric mantle, producing an appinitic–lamprophyre mafic layer that underplated the crust and initiated the production of voluminous granitoid magma. Magma ascent was likely facilitated by major faults (e.g. Jacques and Reavy 1994).

Figure 18. Plots of (a) εNd vs Th/Yb, and (b) εNd vs Ce/Yb (hypothetical evolution of Paleoproterozoic crust shown as reference).

during the Caledonian orogeny. Whether these occurrences can be attributed to an orogen-wide delamination event or to localized zones where slab break-off occurred would require further investigation.

ACKNOWLEDGEMENTS

REFERENCES

Arculus, R.J., 2003, Use and abuse of the terms calcalkaline and calcalkalic: Journal of Petrology, v. 44, p. 929–935, https://doi.org/10.1093/petrology/44.5.929.

Atherton, M.P., and Ghani, A.A., 2002, Slab breakoff: a model for Caledonian, Late Granite syn-collisional magmatism in the orthotectonic (metamorphic) zone of Scotland and Donegal, Ireland: Lithos, v. 62, p. 65–85, https://doi.org/10.1016/S0024-4937(02)00111-1.

Berger, A.R., 1971, The origin of banding in the Main Donegal Granite, N.W. Ireland: Geological Journal, v. 7, p. 347–358, https://doi.org/10.1002/gj.3350070210.

Bowes, D.R., and Košler, J., 1993, Geochemical comparison of the subvolcanic appinite suite of the British Caledonides and the durbachite suite of the Central European Hercynides: Evidence for associated shoshonitic and granitic magmatism: Mineralogy and Petrology, v. 48, p. 47–63, https://doi.org/10.1007/BF01164908.

Bowes, D.R., and McArthur, A.C., 1976, Nature and genesis of the appinite suite: Krystalinikum, v. 12, p. 31–46.

Castro, A., Corretge, L.G., de la Rosa, J.D., Enrique, P., Martinez, F.J., Pascual, E., Lago, M., Arranz, E., Gale, C., Fernández, C., Donaire, T., and López, S., 2002, Palaeozoic magmatism, in Gibbons, W., and Moreno, T., eds., The Geology of Spain: The Geological Society of London, p. 117–153.
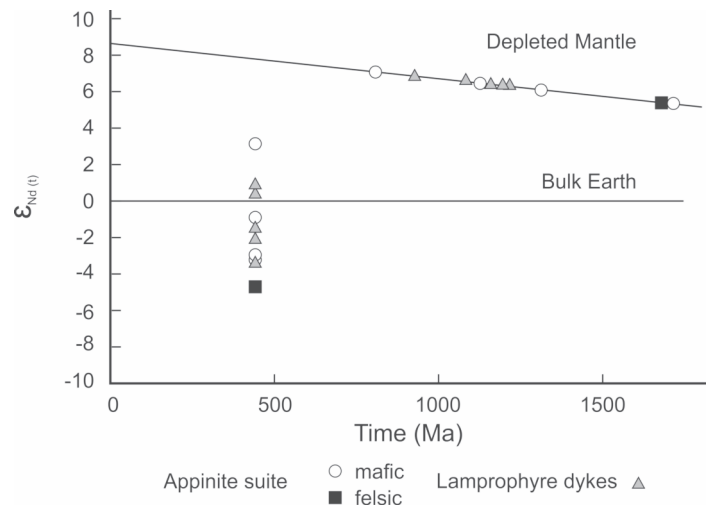
Chew, D.M., and Strachan, R.A., 2014, The Laurentian Caledonides of Scotland and Ireland, in Corfu, F., Gasser, D., and Chew, D.M., eds., New perspectives on the Caledonides of Scandinavia and related area: Geological Society, London, Special Publications, v. 390, p. 45–91, https://doi.org/10.1144/SP390.16.

Condie, K.C., 1989, Geochemical changes in basalts and andesites across the Archean–Proterozoic boundary: identification and significance: Lithos, v. 23, p. 1–18.

Condon, D.J., Bowring, S.A., Pitcher, W.S., and Hutton, D.W., 2004, Rates and tempo of granitic magmatism: a U–Pb geochronological investigation of the Donegal Batholith (Ireland): Geological Society of America, Abstracts with Programs, v. 46, p. 406.

Condon, D.J., Hodges, K.V., Alsop, G.I., and White, A., 2006, Laser ablation 40Ar/39Ar dating of metamorphic fabrics in the Caledonides of north Ireland: Journal of the Geological Society, v. 163, p. 337–345, https://doi.org/10.1144/0016-764904-066.

Cooper, M.R., Crowley, Q.G., Hollis, S.P., Noble, S.R., and Henney, P.J., 2013, A U–Pb age for the Late Caledonian Sperrin Mountains minor intrusions suite in the north of Ireland: timing of slab break-off in the Grampian terrane and the significance of deep-seated, crustal lineaments: Journal of the Geological Society, v. 170, p. 603–614, https://doi.org/10.1144/jgs2012-098.

Dalrymple, G.B., Alexander Jr., E.C., Lanphere, M.A., and Kraker, G.P., 1981, Irradiation of samples for 40Ar/39Ar dating using the Geological Survey TRIGA reactor: United States Geological Survey, Professional Paper, 1176, 55 p., https://doi.org/10.3133/pp1176.

DePaolo, D.J., 1981, Neodymium isotopes in the Colorado Front Range and crust-mantle evolution in the Proterozoic: Nature, v. 291, p. 193–196, https://doi.org/10.1038/291193a0.

DePaolo, D.J. 1988, Neodymium Isotope Geochemistry: An Introduction: Springer Verlag, New York, 187 p., https://doi.org/10.1007/978-3-642-48916-7.

Dewey, J.F., and Shackleton, R.M., 1984, A model for the evolution of the Grampian tract in the early Caledonides and Appalachians: Nature, v. 312, p. 115–121, https://doi.org/10.1038/312115a0.

Dilek, Y., and Altunkaynak, Ş., 2009, Geochemical and temporal evolution of Cenozoic magmatism in western Turkey: mantle response to collision, slab break-off, and lithospheric tearing in an orogenic belt: Geological Society, London, Special Publications, v. 311, p. 213–233, http://dx.doi.org/10.1144/SP311.8.

Dodson, M.H., 1973, Closure temperature in cooling geochronological and petrological systems: Contributions to Mineralogy and Petrology, v. 40, p. 259–274, https://doi.org/10.1007/BF00373790.

Downes, H., 2001, Formation and modification of the shallow sub-continental lithospheric mantle: a review of geochemical evidence from ultramafic xenolith suits and tectonically emplaced ultramafic massifs of Western and Central Europe: Journal of Petrology, v. 42, p. 233–250, https://doi.org/10.1093/petrology/42.1.233.

Elsdon, R., and Todd, S.P., 1989, A composite spessartite-appinite intrusion from Port-na-Blagh, County Donegal, Ireland: Geological Journal, v. 24, p. 97–112, https://doi.org/10.1002/gj.3350240203.

Fowler, M.B., 1988, Ach'uaine hybrid appinite pipes: Evidence for mantle-derived shoshonitic parent magmas in Caledonian granite genesis: Geology, v. 16, p.

1026–1030, https://doi.org/10.1130/0091-7613(1988)016<1026:AUHAPE> 2.3.CO;2.

Fowler, M.B., and Henney, P.J., 1996, Mixed Caledonian appinite magmas: implications for lamprophyre fractionation and high Ba–Sr granite genesis: Contributions to Mineralogy and Petrology, v. 126, p. 199–215, https://doi.org/10.1007/s004100050244.

Fowler, M.B., Kocks, H., Darbyshire, D.P.F., and Greenwood, P.B., 2008, Petrogenesis of high Ba–Sr plutons from the Northern Highlands Terrane of the British Caledonian Province: Lithos, v. 105, p. 129–148, https://doi.org/10.1016/j.lithos.2008.03.003.

French, J.W., 1966, Appinitic intrusions clustered around the Ardara Pluton, County Donegal: Proceedings of the Royal Irish Academy, v. B64, p. 303–322.

French, W.J., 1976, The origin of leucodiorites associated with the appinitic intrusions of County Donegal: Proceedings of the Yorkshire Geological Society, v. 41, p. 107–126, https://doi.org/10.1144/pygs.41.1.107.

Geological Survey of Ireland, 2014, Bedrock Geology of Ireland, 1:1,000,000 scale (map).

Ghani, A.A., and Atherton, M.P., 2008, The chemical character of the Late Caledonian Donegal Granites, Ireland, with comments on their genesis: Earth and Environmental Science Transactions of the Royal Society of Edinburgh, v. 97, p. 437–454, https://doi.org/10.1017/S0263593300001553.

Goldstein, S.L., O'Nions, R.K., and Hamilton, P.J., 1984, A Sm–Nd isotopic study of atmospheric dusts and particulates from major river systems: Earth and Planetary Science Letters, v. 70, p. 221–236, https://doi.org/10.1016/0012-821X(84)90007-4.

Hall, A., 1967, The chemistry of appinitic rocks associated with the Ardara pluton, Donegal, Ireland: Contributions to Mineralogy and Petrology, v. 16, p. 156–171, https://doi.org/10.1007/BF00372795.

Halliday, A.N., Aftalion, M., and Leake, B.E., 1980, A revised age for the Donegal granites: Nature, v. 284, p. 542–543, https://doi.org/10.1038/284542a0.

Hamidullah, S., and Bowes, D.R., 1987, Petrogenesis of the appinite suite, Appin District, Western Scotland: Acta Universitatis Carolinae, Geologica, v. 4, p. 295–396.

Harmon, R.S., Halliday, A.N., Clayburn, J.A.P., and Stephens, W.E., 1984, Chemical and isotopic systematics of the Caledonian intrusions of Scotland and Northern England: a guide to magma source region and magma-crust interaction: Philosophical Transactions of the Royal Society London A, v. 310, p. 709–742, https://doi.org/10.1098/rsta.1984.0016.

Harrison, T.M., 1982, Diffusion of ^{40}Ar in hornblende: Contributions to Mineralogy and Petrology, v. 78, p. 324–331, https://doi.org/10.1007/BF00398927.

Hildebrand, R.S., and Whalen, J.B., 2014a, Arc and slab-failure magmatism in Cordilleran batholiths I—the Cretaceous Coastal batholith of Peru and its role in South American orogenesis and hemispheric subduction flip: Geoscience Canada, v. 41, p. 255–282, http://dx.doi.org/10.12789/geocanj.2014.41.047.

Hildebrand, R.S., and Whalen, J.B., 2014b, Arc and slab-failure magmatism in Cordilleran batholiths II—the Cretaceous Peninsular Ranges batholith of Southern and Baja California: Geoscience Canada, v. 41, p. 399–458, http://dx.doi.org/10.12789/geocanj.2014.41.059.

Hildebrand, R.S., Whalen, J.B., and Bowring, S.A., 2018, Resolving the crustal composition paradox by 3.8 billion years of slab failure magmatism and collisional recycling of continental crust: Tectonophysics, v. 734–735, p. 69–88, https://doi.org/10.1016/j.tecto.2018.04.001.

Hutton, D.H.W., 1982, A tectonic model for the emplacement of the Main Donegal Granite, NW Ireland: Journal of the Geological Society, v. 139, p. 615–631, https://doi.org/10.1144/gsjgs.139.5.0615.

Hutton, D.H.W., and Alsop, G.I., 1996, The Caledonian strike-swing and associated lineaments in NW Ireland and adjacent areas: sedimentation, deformation and igneous intrusion patterns: Journal of the Geological Society, v. 153, p. 345–360, https://doi.org/10.1144/gsjgs.153.3.0345.

Jacques, J.M., and Reavy, R.J., 1994, Caledonian plutonism and major lineaments in the SW Scottish Highlands: Journal of the Geological Society, v. 151, p. 955–969, https://doi.org/10.1144/gsjgs.151.6.0955.

Kerrick, D.M., 1987, Fibrolite in contact aureoles of Donegal, Ireland: American Mineralogist, v. 72, p. 240–254.

Kirkland, C.L., Alsop, G.I., and Prave, A.R., 2008, The brittle evolution of a major strike-slip fault associated with granite emplacement: a case study of the Leannan Fault, NW Ireland: Journal of the Geological Society, v. 165, p. 341–352, https://doi.org/10.1144/0016-76492007-064.

Kirkland, C.L., Alsop, G.I., Daly, J.S., Whitehouse, M.J., Lam, R., and Clark, C., 2013, Constraints on the timing of Scandian deformation and the nature of a buried Grampian terrane under the Caledonides of northwestern Ireland: Journal of the Geological Society, v. 170, p. 615–625, https://doi.org/10.1144/jgs2012-106.

Kuiper, K.F., Deino, A., Hilgen, F.J., Krijgsman, W., Renne, P.R., and Wijbrans, J.R., 2008, Synchronizing rock clocks of earth history: Science, v. 320, p. 500–504, https://doi.org/10.1126/science.1154339.

Leake, B.E., 1978, Nomenclature of amphiboles: Canadian Mineralogist, v. 16, p. 501–520.

Leake, B.E., Woolley, A.R., Birch, W.D., and Burke, E.A.J., 2004, Nomenclature of amphiboles: additions and revisions to the International Mineralogical Association's amphibole nomenclature: Mineralogical Magazine, v. 68, p. 209–215, http://dx.doi.org/10.1180/0026461046810182.

Lee, J.-Y., Marti, K., Severinghaus, J.P., Kawamura, K., Hee-Soo, Yoo, Lee, J.B., and Kim, J.S., 2006, A redetermination of the isotopic abundances of atmospheric Ar: Geochimica et Cosmochimica Acta, v. 70, p. 4507–4512, https://doi.org/10.1016/j.gca.2006.06.1563.

Ludwig, K.R., 2008, User's Manual for ISOPLOT 3.60 – A geochronological toolkit for Microsoft Excel: Berkeley Geochronological Centre Special Publication Number 4, 54 p.

Macdonald, R., Rock, N.M.S., Rundle, C.C., and Russell, O.J., 1986, Relationships between late Caledonian lamprophyric, syenitic, and granitic magmas in a differentiated dyke, southern Scotland: Mineralogical Magazine, v. 50, p. 547–557, https://doi.org/10.1180/minmag.1986.050.358.01.

McDougall, I., and Harrison, T.M., 1988, Geochronology and Thermochronology by the ^{40}Ar/^{39}Ar Method: Oxford University Press, NY, 212 p.

McDougall, I., and Wellman, P., 2011, Calibration of GA1550 biotite standard for K/Ar and ^{40}Ar/^{39}Ar dating: Chemical Geology, v. 280, p. 19–25, https://doi.org/10.1016/j.chemgeo.2010.10.001.

Min, K., Mundil, R., Renne, P.R., and Ludwig, K.R., 2000, A test for systematic errors in ^{40}Ar/^{39}Ar geochronology through comparison with U/Pb analysis of a 1.1 Ga rhyolite: Geochimica et Cosmochimica Acta, v. 64, p. 73–98, https://doi.org/10.1016/S0016-7037(99)00204-5.

Mitchell, R.H., 1995, Melting experiments on a sanidine phlogopite lamproite at 4–7 GPa and their bearing on the source of lamproitic magmas: Journal of Petrology, v. 36, p. 1455–1474, https://doi.org/10.1093/petrology/36.5.1455.

Miyashiro, A., 1974, Volcanic rock series in island arcs and active continental margins: American Journal of Science, v. 274, p. 321–355, https://doi.org/10.2475/ajs.274.4.321.

Murphy, J.B., 2013, Appinite suites: A record of the role of water in the genesis, transport, emplacement and crystallization of magma: Earth-Science Reviews, v. 119, p. 35–59, https://doi.org/10.1016/j.earscirev.2013.02.002.

Murphy, J.B., and Hynes, A.J., 1990, Tectonic control on the origin and orientation of igneous layering: an example from the Greendale Complex, Antigonish Highlands, Nova Scotia, Canada: Geology, v. 18, p. 403–406, https://doi.org/10.1130/0091-7613(1990)018<0403:TCOTOA>2.3.CO;2.

Neilson, J.C., Kokelaar, B.P., and Crowley, Q.G., 2009, Timing, relations and cause of plutonic and volcanic activity of the Siluro–Devonian post-collision magmatic episode in the Grampian Terrane, Scotland: Journal of the Geological Society, v. 166, p. 545–561, https://doi.org/10.1144/0016-76492008-069.

O'Connor, P.J., Long, C.B., Kennan, P.S., Halliday, A.N., Max, M.D., and Roddick, J.C., 1982, Rb–Sr isochron study of the Thorr and Main Donegal Granites, Ireland: Geological Journal, v. 17, p. 279–295, https://doi.org/10.1002/gj.3350170403.

O'Connor, P.J., Long, C.B., and Evans, J.A., 1987, Rb–Sr whole-rock isochron studies of the Barnesmore and Fanad plutons, Donegal, Ireland: Geological Journal, v. 22, p. 11–23, https://doi.org/10.1002/gj.3350220103.

Oliver, G.J.H., 2001, Reconstruction of the Grampian episode in Scotland: its place in the Caledonian Orogeny: Tectonophysics, v. 332, p. 23–49, https://doi.org/10.1016/S0040-1951(00)00248-1.

Oliver, G.J.H., Wilde, S.A., and Wan, Y., 2008, Geochronology and geodynamics of Scottish granitoids from the late Neoproterozoic break-up of Rodinia to Palaeozoic collision: Journal of the Geological Society, v. 165, p. 661–674, https://doi.org/10.1144/0016-76492007-105.

Onstott, T.C., Phillips, D., and Pringle-Goodell, L., 1991, Laser microprobe measurement of chlorine and argon zonation in biotite: Chemical Geology, v. 90, p. 145–168, https://doi.org/10.1016/0009-2541(91)90040-X.

O'Reilly, S.Y., and Griffin, W.L., 2006, Imaging global chemical and thermal heterogeneity in the subcontinental lithospheric mantle with garnets and xenoliths: Geophysical implication: Tectonophysics, v. 416, p. 289–309, https://doi.org/10.1016/j.tecto.2005.11.014.

Pearce, J.A., 1982, Trace element characteristics of lavas from destructive plate boundaries, in Thorpe, R.S., ed., Andesites: Wylie and Sons, p. 525–548.

Pearce, J.A., 1983, Role of the sub-continental lithosphere in magma genesis at active continental margins, in Hawkesworth, C.J., and Norry, M.J., eds., Continental basalts and mantle xenoliths: Shiva Publications, Nantwich, Cheshire, p. 230–249.

Pearce, J.A., 1996, A user's guide to basaltic discrimination diagrams, *in* Wyman, D.A., *ed.*, Trace Element Geochemistry of Volcanic Rocks: Applications for Massive Sulphide Exploration: Geological Association of Canada Short Course Notes, 12, p. 79–113.

Pearce, J.A., and Norry, M.J., 1979, Petrogenetic implications of Ti, Zr, Y, and Nb variations in volcanic rocks: Contributions to Mineralogy and Petrology, v. 69, p. 33–47, https://doi.org/10.1007/BF00375192.

Pe-Piper, G., 1988, Calcic amphiboles of mafic rocks of the Jeffers Brook plutonic complex, Nova Scotia, Canada: American Mineralogist, v. 73, p. 993–1006.

Pitcher, W.S., Berger, A.R., 1972, The Appinite suite: basic rocks genetically associated with granite, *in* Pitcher, W.S., and Berger, A.R., *eds.*, The Geology of Donegal. A Study of Granite Emplacement and Unroofing: John Wiley and Sons Ltd, New York, p. 143–168.

Pitcher, W.S., and Read, H.H., 1960, The aureole of the Main Donegal Granite: Quarterly Journal of the Geological Society, v. 116, p. 1–36, https://doi.org/10.1144/gsjgs.116.1.0001.

Platten, I.M., 1991, Zoning and layering in diorites of the scottish caledonian appinite suite: Geological Journal, v. 26, p. 329–348, https://doi.org/10.1002/gj.3350260406.

Price, A.R., 1997, Multiple sheeting as a mechanism of pluton construction: the main Donegal granite, NW Ireland: Unpublished PhD thesis, Durham University, Durham, UK, 394 p.

Rock, N.M.S., 1991, Lamprophyres: Blackie, Glasgow, p. 265–285.

Rock, N.M.S., and Hunter, R.H., 1987, Late Caledonian dyke-swarms of northern Britain: spatial and temporal intimacy between lamprophyric and granitic magmatism around the Ross of Mull pluton, Inner Hebrides: Geologische Rundschau, v. 76, p. 805–826, https://doi.org/10.1007/BF01821065.

Roddick, J.C., 1983, High precision intercalibration of ^{40}Ar/^{39}Ar standards: Geochimica et Cosmochimica Acta, v. 47, p. 887–898, https://doi.org/10.1016/0016-7037(83)90154-0.

Rogers, G., and Dunning, G.R., 1991, Geochronology of appinitic and related granitic magmatism in the W Highlands of Scotland: constraints on the timing of transcurrent fault movement: Journal of the Geological Society, v. 148, p. 17–27, https://doi.org/10.1144/gsjgs.148.1.0017.

Salmon, S., 1998, The plutonic igneous complex at Sorel Point, Jersey, Channel Islands: A high level multi-magma assemblage: Geological Journal, v. 33, p. 17–35, https://doi.org/10.1002/(SICI)1099-1034(199801/03)33:1<17::AID-GJ757>3.0.CO;2-E.

Seyítoğlu, G., and Scott, B.C., 1996, The cause of N–S extensional tectonics in western Turkey: Tectonic escape vs back-arc spreading vs orogenic collapse: Journal of Geodynamics, v. 22, p. 145–153, https://doi.org/10.1016/0264-3707(96)00004-X.

Shervais, J.W., 1982, Ti–V plots and the petrogenesis of modern ophiolitic lavas: Earth and Planetary Science Letters, v. 59, p. 101–118, https://doi.org/10.1016/0012-821X(82)90120-0.

Siegesmund, S., and Becker, J.K., 2000, Emplacement of the Ardara pluton (Ireland): new constraints from magnetic fabrics, rock fabrics and age dating: International Journal of Earth Sciences, v. 89, p. 307–327, https://doi.org/10.1007/s005310000088.

Spell, T.L., and McDougall, I., 2003, Characterization and calibration of ^{40}Ar/^{39}Ar dating standards: Chemical Geology, v. 198, p. 189–211, https://doi.org/10.1016/S0009-2541(03)00005-6.

Stevenson, C.T.E., Hutton, D.H.W., and Price, A.R., 2008, The Trawenagh Bay Granite and a new model for the emplacement of the Donegal Batholith: Earth and Environmental Science Transactions of The Royal Society of Edinburgh, v. 97, 455–477, https://doi.org/10.1017/S0263593300001565.

Sun, S.-s., and McDonough, W.F., 1989, Chemical and isotopic systematics of oceanic basalts: implications for mantle composition and processes, *in* Saunders, A.D., and Norry, M.J., *eds.*, Magmatism in the Oceanic Basins: Geological Society, London, Special Publications, v. 42, p. 313–345, https://doi.org/10.1144/GSL.SP.1989.042.01.19.

Thompson, R.N., and Fowler, M.B., 1986, Subduction-related shoshonitic and ultrapotassic magmatism: a study of Siluro–Ordovician syenites from the Scottish Caledonides: Contributions to Mineralogy and Petrology, v. 94, p. 507–522, https://doi.org/10.1007/BF00376342.

Todd, S.P., Murphy, F.C., and Kennan, P.S., 1991, On the trace of the Iapetus suture in Ireland and Britain: Journal of the Geological Society, v. 148, p. 869–880, https://doi.org/10.1144/gsjgs.148.5.0869.

van Staal, C.R., Dewey, J.F., Mac Niocaill, C., and McKerrow, W.S., 1998, The Cambrian–Silurian tectonic evolution of the northern Appalachians and British Caledonides: history of a complex, west and southwest Pacific-type segment of Iapetus, *in* Blundell, D.J., and Scott, A.C., *eds.*, Lyell: The Past is the Key to the Present: Geological Society, London, Special Publications, v. 143, p. 197–242, https://doi.org/10.1144/GSL.SP.1998.143.01.17.

Vernon, R.H., and Paterson, S.R., 1993, The Ardara pluton, Ireland: deflating an expanded intrusion: Lithos, v. 31, p. 17–32, https://doi.org/10.1016/0024-4937(93)90030-G.

von Blackenburg, F., and Davies, J.H., 1995, Slab breakoff: A model for syncollisional magmatism and tectonics in the Alps: Tectonics, v. 14, p. 120–131, https://doi.org/10.1029/94TC02051.

Walker, F., 1927, VII. – The Igneous Geology of Ardsheal Hill, Argyllshire: Earth and Environmental Science Transactions of the Royal Society of Edinburgh, v. 55, p. 147–157, https://doi.org/10.1017/S0080456800016288.

Winchester, J.A., and Floyd, P.A., 1977, Geochemical discrimination of different magma series and their differentiation products using immobile elements: Chemical Geology, v. 20, p. 325–343, https://doi.org/10.1016/0009-2541(77)90057-2.

Wood, D.A., Joron, J.-L., and Treuil, M., 1979, A re-appraisal of the use of trace elements to classify and discriminate between magma series erupted in different tectonic settings: Earth and Planetary Science Letters, v. 45, p. 326–336, https://doi.org/10.1016/0012-821X(79)90133-X.

Wright, A.E., and Bowes, D.R., 1979, Geochemistry of the appinite suite, *in* Harris, A.L., Holland, C.H., and Leake, B.E., *eds.*, The Caledonides of the British Isles – Reviewed: Geological Society, London, Special Publications, v. 8, p. 699–704, https://doi.org/10.1144/GSL.SP.1979.008.01.84.

Ye, H.-M., Li, X.-H., Li, Z.-X., and Zhang, C.-L., 2008, Age and origin of high Ba–Sr appinite–granites at the northwestern margin of the Tibet Plateau: implications for early Paleozoic tectonic evolution of the Western Kunlun orogenic belt: Gondwana Research, v. 13, p. 126–138, https://doi.org/10.1016/j.gr.2007.08.005.

ARTICLE

An Overview of the Karst Areas in British Columbia, Canada

Tim R. Stokes[1] and Paul A. Griffiths[2]

[1]*Earth Science Department, Vancouver Island University*
900 Fifth Sreet, Nanaimo, British Columbia, V9R 5S5, Canada
E-mail: tim.stokes@viu.ca

[2]*544 Springbok Road, Campbell River*
British Columbia, V9W 8A2, Canada

SUMMARY

Karst is a three-dimensional landscape that occurs in soluble bedrock (typically limestone, marble, dolostone, gypsum or halite) and is defined by a solutionally weathered surface, a subsurface drainage system (where conduit-flow dominates), and underground openings and caves. Karst can host unique flora and subsurface fauna, as well as a wide range of other scientific, recreational and cultural values. Karst and potential karst areas underlie approximately 10% of British Columbia (BC), but the distribution and extent of this landscape has yet to be fully explored and delineated. Some of the most extensive and well-developed karst areas occur within the forested limestone areas of coastal BC, such as on Vancouver Island and Haida Gwaii, where numerous surface karst features and caves are known. Karst in the interior plateau regions of British Columbia is less well known, being in part covered by thick deposits of glacial materials. Alpine karst regions are most apparent in the Rocky Mountains where there are limestone plateaus, karst drainages and cave systems that have close connections to past and present glacial systems. Mapping of karst is a critical component for any land-use or resource development activity in all regions of British Columbia, as the environmental impacts on karst and its associated values are potentially significant. The regional distribution of karst in BC is not well mapped, with only an office-based reconnaissance karst potential map (1:250,000-scale) and a related database completed in 1999. A renewed effort should now be made to better map karst across British Columbia using digital bedrock mapping data released in 2017, combined with more recent satellite imagery and improved field knowledge.

RÉSUMÉ

Le karst est un paysage tridimensionnel qui se présente dans le substrat rocheux soluble (généralement calcaire, marbre, dolomite, gypse ou halite) et est défini par une surface altérée par dissolution, un système de drainage souterrain (où l'écoulement par conduit domine) et des ouvertures et cavernes souterraines. Le karst peut abriter une flore et une faune souterraine unique, ainsi qu'une grande variété d'autres ressources scientifiques, de loisir et culturelles. Les zones karstiques et potentiellement karstiques constituent environ 10% de la surface de la Colombie-Britannique, mais la répartition et l'étendue de ce paysage n'a pas été complètement explorées et circonscrites. Certaines des zones karstiques les plus étendues et les mieux développées se trouvent dans les calcaires des zones calcaires boisées de la côte de la Colombie-Britannique, telles que l'île de Vancouver et l'archipel de Haida Gwaii, où l'on connaît de nombreuses caractéristiques karstiques de surface et des cavernes. Le karst des régions des plateaux intérieurs de la Colombie-Britannique est moins bien connu, étant en partie recouvert d'épais dépôts de matériaux glaciaires. Les régions karstiques alpines sont plus apparentes dans les montagnes Rocheuses où se trouvent des plateaux calcaires, des bassins de drainage karstiques et des systèmes de cavernes étroitement liés aux systèmes glaciaires passés et contemporains. La cartographie du karst est une constituante essentielle de toute activité d'utilisation du terrain ou de développement des ressources dans toutes les régions de la Colombie-Britannique, car les impacts environnementaux sur le karst et ses bénéfices associés sont potentiellement importants. La distribution régionale et les caractéristiques des karsts en Colombie-Britannique ne sont pas bien cartographiées, avec seulement une carte de reconnaissance du potentiel karstique établie par

une étude de bureau (à l'échelle de 1/250 000) et une base de données associée, complétées en 1999. Il faut aujourd'hui améliorer la cartographie de karsts en Colombie-Britannique en utilisant les données numériques de cartographie du substrat rocheux publiées en 2017, combinées avec des images satellite plus récentes et à une meilleure connaissance du terrain.

INTRODUCTION

'Karst' is a generic term used to describe a topography that is formed primarily by the dissolution of bedrock and is internally drained. For simplicity, this one word is used in preference to 'karst land' or 'karst landscapes.' It implies not only the physical aspects of the karst system (i.e. soil and bedrock), but also the other attributes of karst: biota, air and water. The primary objectives of this paper are to provide an overview of what is currently known about the distribution and general characteristics of karst in British Columbia (BC), to outline the different karst types across the province, to provide some preliminary ideas on karst development in the region and to identify future needs and approaches for better land-use management of karst in BC (e.g. improved karst mapping and karst inventories). A key goal of this paper is to bring together, in one summary document, the main resources and references for karst in BC and provide a starting point for those wishing to delve deeper into this important and valuable resource. The paper is not intended as an exhaustive bibliography covering *all* aspects of karst in the province but aims instead to identify some of the key facets and issues. As with any review, there is the potential for omissions. The authors would be happy to be informed of these.

It is estimated that 10% of BC is underlain by carbonate bedrock with the potential to develop as karst. This number is derived from an analysis of the proportion of soluble bedrock within the various carbonate units of BC and is detailed in Table 1. It is also possible that some areas of carbonate bedrock are unaccounted for and may occur outside those identified. Overall, the most extensive areas of carbonate bedrock occur in the Rocky Mountains, with lesser amounts in BC's interior and along the west coast.

From geomorphic and hydrologic perspectives, karst is best defined as a three-dimensional landscape (Fig. 1) that develops from the dissolving action of water on soluble bedrock such as limestone, marble, dolostone, gypsum or halite. Theoretically, all bedrock can be considered soluble, but karst rock types are significantly more soluble by several orders of magnitude than non-karst bedrock, such as granite. The resulting landscape is characterized by solutional (fluted and pitted) bedrock surfaces, shafts, karst sinkholes (commonly referred to as dolines in Europe), sinking streams, springs, underground drainage systems, deep flooded (phreatic) networks and subsurface openings of all sizes, including those that we as humans enter, better known as caves.

Karst should be considered as an interconnected and functioning ecosystem within which a delicate balance occurs between the bedrock, soil, water, air and biota (Fig. 2). Karst biota can be highly specialized, ranging from calcium-loving
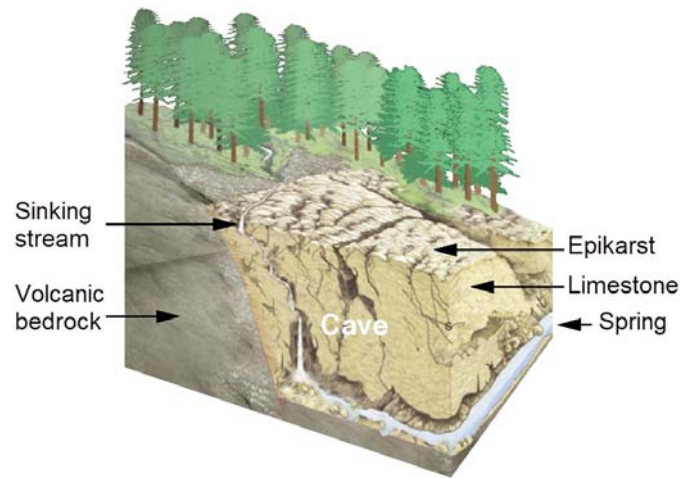

Figure 1. Forest-covered karst of British Columbia can be characterized as a three-dimensional landscape with subsurface openings and drainage. Note that the forest and soil cover is removed on the right side of the image for illustration purposes.
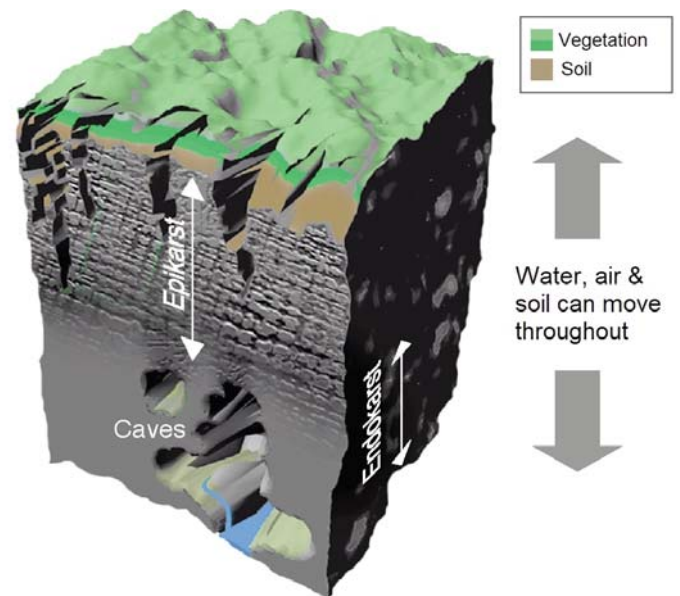
Figure 2. Representation of karst as a functioning system with open connections between surface, epikarst and endokarst, allowing free movement of soil, air, water and biota.

plant life on the surface, specially adapted fauna living in the subsurface environment, to microbes involved in the karstification process (Palmer 2007). Beyond these natural attributes, karst systems can also have considerable historical, cultural, aesthetic, scientific and educational values (Gunn 2003).

The first comprehensive research on karst in BC was initiated in the 1960's by Derek Ford and the Karst Research Group at McMaster University, Ontario. This research was extensive considering the size of the province and covered a broad range of topics across BC and elsewhere in Canada (Ford 1993). Examples of karst investigations in British Columbia include the sinking streams of Mount Tupper (Ford 1967), gypsum karst near Canal Flats (Wigley et al. 1973), alpine karst in the Mount Castleguard-Columbia Icefield area

Table 1. A compilation of rating criteria for 'karst polygons' of British Columbia, as derived from reconnaissance karst mapping (Stokes 1999).

Karst Potential Polygons with Ratings for Criteria #1 and #2[1]	Area of Karst Polygons (km²)	Percent of Total Area	Adjusted Area of Karst Applying Criterion #1[2]	Percent Adjusted Area	Number of Polygons	Percent of Polygons
Primary – High (P^H)	28317.5	23.40%	28317.5	34.03%	2625	34.70%
Primary – Moderate (P^M)	35545.6	29.40%	35545.6	42.72%	1977	26.10%
Primary – Low (P^L)	961.6	0.80%	961.6	1.16%	120	1.60%
Secondary – High (S^H)	1006.7	0.80%	503.4	0.60%	93	1.20%
Secondary – Moderate (S^M)	19145.8	15.80%	9572.9	11.51%	758	10.00%
Secondary – Low (S^L)	3730.2	3.10%	1865.1	2.24%	394	5.20%
Tertiary – High (T^H)	1792.2	1.50%	358.4	0.43%	8	0.10%
Tertiary – Moderate (T^M)	22171.2	18.30%	4434.2	5.33%	932	12.30%
Tertiary – Low (T^L)	8231.4	6.80%	1646.3	1.98%	661	8.70%
Totals	**120,902.2**	**100%**	**83,205.0**	**100%**	**7,568**	**100%**
Percent of Potential Karst in BC Assuming BC Total Land Area of 944,735 km²	**12.80%**		**8.81%**			

[1] Criterion #1 is the proportion of soluble bedrock in the geological unit and included qualitative estimates of Primary (> 50% of unit), Secondary (20–49% of unit), and Tertiary (5–19% of unit). Criterion #2 is the likely intensity of karst development in the soluble bedrock providing ratings of High, Moderate and Low. High indicates a well-developed karst landscape with surface features common and linked to a subsurface drainage system; Moderate some karst development with occasional surface karst features and a definite subsurface drainage system, and Low having minor surface solutional weathering on bedrock surfaces, few to no surface features, with subsurface drainage less evident.

[2] The adjusted total area using Criterion #1 to calculate the polygon areas is based on 100% for Primary, 50% for Seconday and 20% for Tertiary. Note, the percentages for Criterion #1 were originally derived from qualitative estimates provide by geologists familar with bedrock units, map legends and published descriptions of units (Stokes 1999). Hence, there should be care in how data is analyzed and applied.

(Ford 1983b), forested karst in Northern Vancouver Island (Harding and Ford 1993), karst hydrology of White Ridge on Vancouver Island (Ecock 1984), and karst development and groundwater flow on Northern Vancouver Island (Mills 1981). Research on karst caves, such as those on Vancouver Island, provided information on the likely ages of cave sediments and speleothems (cave mineral formations like stalagmites and stalactites), as well as past environmental and climatic conditions (e.g. Ford 1975; Gascoyne et al. 1981; Latham et al. 1982; Zhang et al. 2008; Marshall et. al. 2009). Examples of karst research in the Canadian Rocky Mountains included work on karst springs and regional hydrology (Worthington 1991; Worthington and Ford 1995; Smart 1997), as well as caves and their speleothem materials (e.g. Harmon et al. 1977; Yonge et al. 2014).

Land-use and resource development activities can directly or indirectly impact the surface and the subsurface of karst due to its inherent connectivity and openness. Equally, karst can pose potential hazards for these activities due to subsidence or alteration to subsurface drainage. Forestry is one of the most widespread land-use activities on the karst in BC and is an example of why there has been, and continues to be, a need for an improved understanding of karst. Caves were the prime focus in the protection of forested karst areas until the late 1990s when the BC Ministry of Forests first announced a systems-based approach to karst management (BC Ministry of Forests 1997; Beedle 1997). This was followed by an investiga-

tion into karst inventory systems for BC (Stokes and Griffiths 2000a), and the concurrent development of the *Karst Inventory Standards and Vulnerability Assessment Procedures for British Columbia* (RISC 2003) and the *Karst Management Handbook for British Columbia* (BC Ministry of Forests 2003).

It is now widely accepted that any land-use or resource development activities that occur on or near karst require consideration of the environmental impacts on karst systems (both short and long term disturbances), the effects on karst aquifers and their catchments (including contributing non-karst drainage areas), and the potential for karst-related geohazards (van Beynen 2011). Other resource development activities in BC, such as alternative energy projects, dams, highways, mining and oil and gas extraction now consider karst issues in their planning (Stokes 2013).

KARST AND THE SOLUBLE BEDROCK UNITS OF BRITISH COLUMBIA

Soluble bedrock units (primarily carbonate rocks) are found in all five tectonic regions of BC including the Insular Belt, the Coast Belt, the Intermontane Belt, the Omineca Belt and the Foreland Belt (Fischl 1992; Fig. 3). Each of these tectonic belts is made up of various geologic terranes and super-terranes that were accreted to North America during the Mesozoic and include extensive regions of deformation and magmatism (Wheeler and McFeely 1991). The five tectonic belts closely match the main physiographic areas of BC. From west to east,
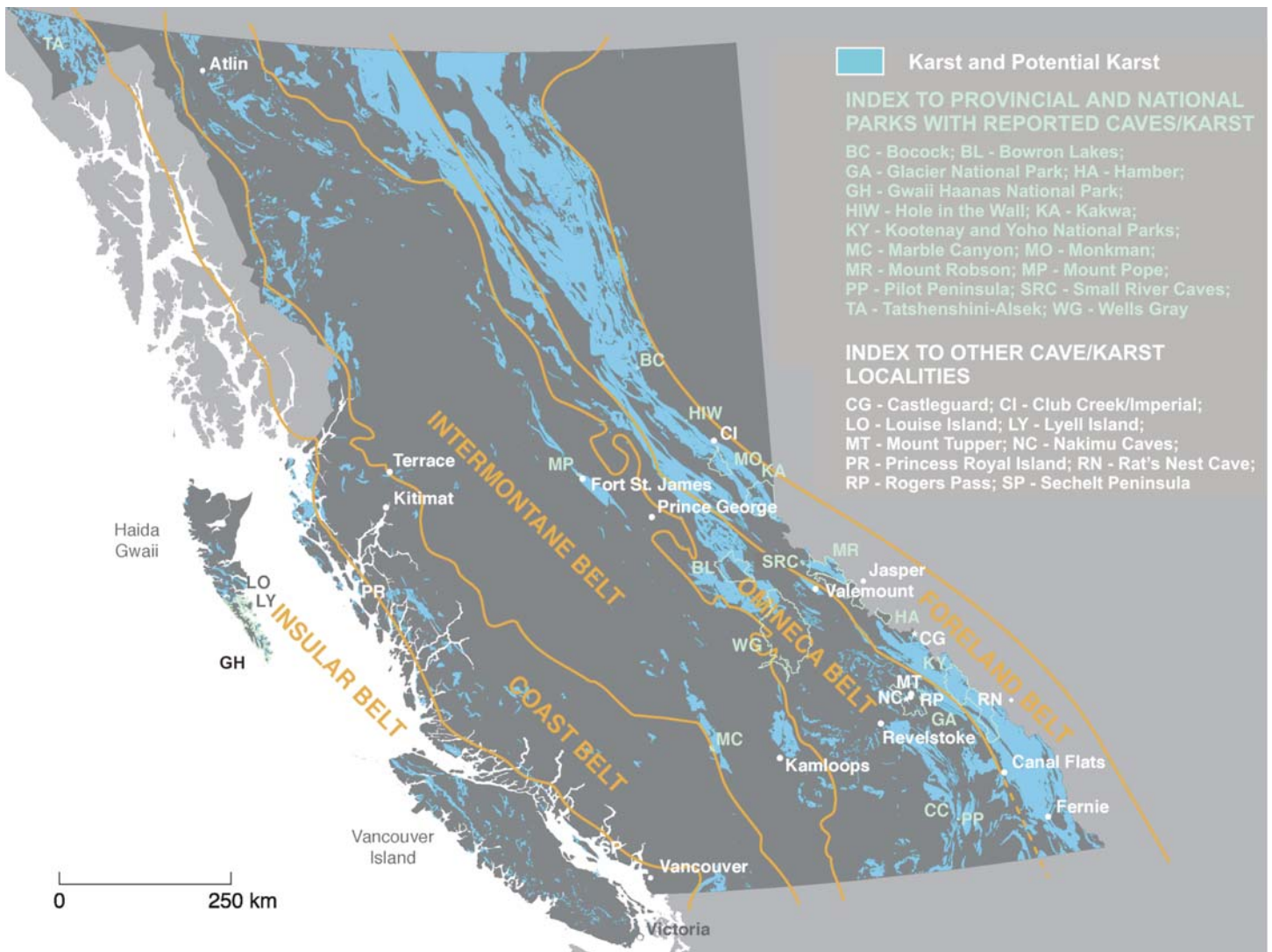
Figure 3. The five major tectonic belts identified in British Columbia showing the areas of carbonate bedrock that contain karst and potential karst.

these are Vancouver Island and Haida Gwaii, the Coast Mountains, the interior plateaus and mountains, the Columbia-Omineca-Cassiar Mountains and the Rocky Mountains (Church and Rider 2010; Fig. 4). Limestone is the most common type of karst bedrock found within all five tectonic belts, and dolostone (often termed dolomite) is generally confined to the Rocky Mountains. Gypsum karst is less common, with occurrences in southeastern BC (mostly in Devonian sequences near Canal Flats), minor amounts in the Rocky Mountains, and some small occurrences in northwest BC. Most of the carbonate units in BC are Triassic, Permian and Carboniferous in age, with older Cambrian to Devonian carbonate units found in the Rocky Mountains (Fischl 1992). Table 2 summarizes the main carbonate-bearing units in which evidence for karst development has been reported, and subdivides them based on their respective tectonic belt, geological age and soluble bedrock type. Note, that not all individual units described below are listed in Table 2 due to space limitations.

The determination as to whether a given carbonate bedrock unit exhibits karst characteristics is not always easy,

and the common term 'karst potential' is often used to describe in a qualitative way the likelihood that a geological unit will develop karst (e.g. Weary and Doctor 2014). For karst to be definitively identified in a given area it should include some if not all of the following elements: a solutionally weathered surface, surface karst features, subsurface openings (which do not have to be caves), and an underground drainage system.

Regional mapping of karst in BC was first carried out on Vancouver Island in 1995 (Stokes 1995), and was followed by reconnaissance (1:250,000-scale) karst potential mapping and inventory for all of BC, which was based on the first available digital bedrock map compilation for the province (Stokes 1999). This study identified 345 soluble bedrock units (formations) in BC with karst potential – a total of 7568 polygons for the whole province (Table 1). These polygons were rated for three criteria. The first criterion was the proportion of soluble bedrock in the geological unit, defined as Primary (> 50%), Secondary (20–50%), or Tertiary (< 20%). The second criterion was the likely intensity of karst development in the soluble
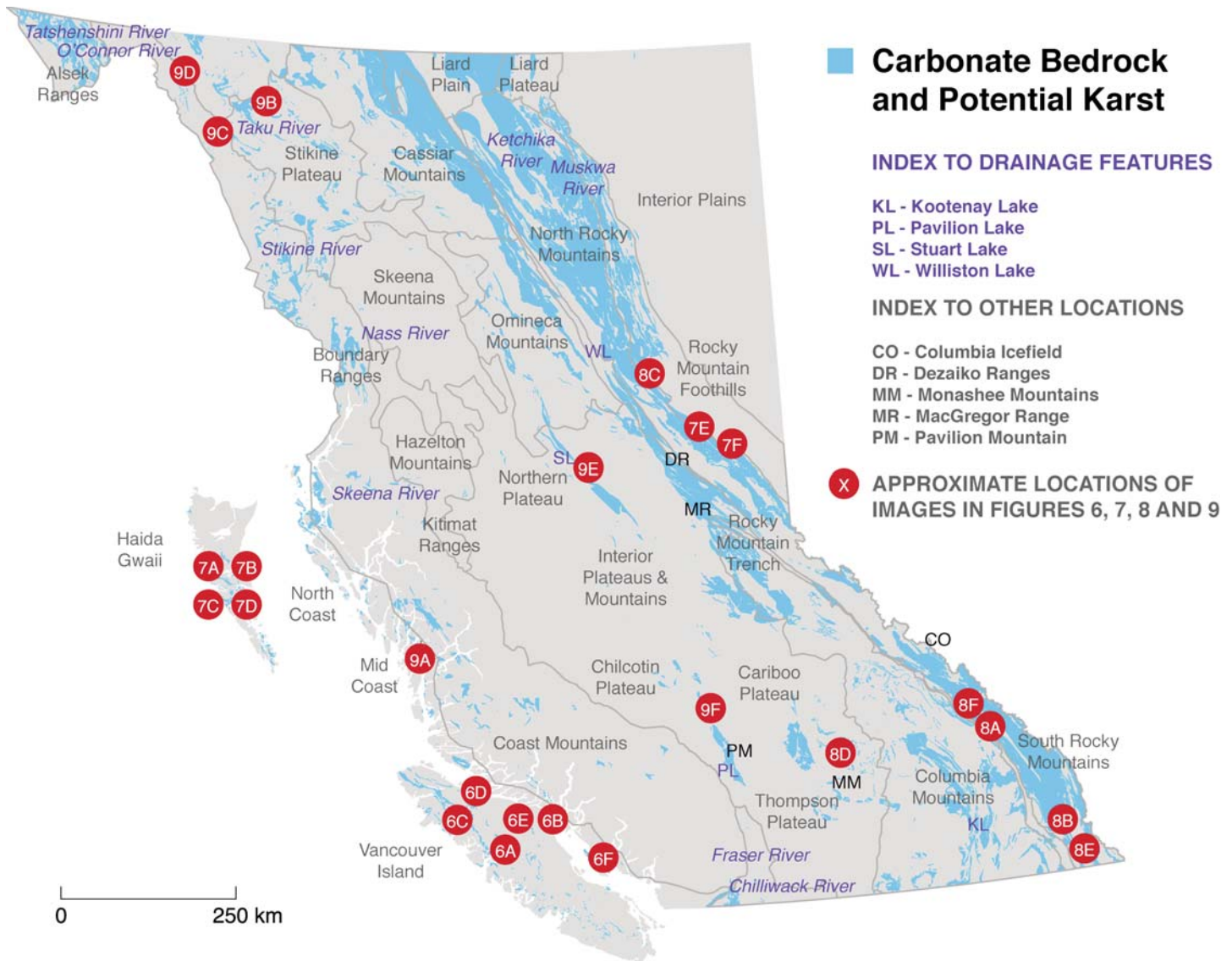
Figure 4. Major physiographic regions of British Columbia, as related to the areas of karst potential indicated in Figure 3. Annotations on the map indicate the approximate locations of photos depicting karst features and landscapes in figures 6, 7, 8 and 9.

bedrock unit, defined as Low, Moderate or High. The third criterion was the presence or absence of caves or other karst landform features. Approximately one-third of the soluble bedrock units identified include > 50% soluble bedrock (Primary) and have a High intensity rating for karst development (see Table 1). However, only 15–20% of these potential karst areas have confirmed karst features or caves, and most occur on the coast or in the southern parts of BC. From this analysis, it is apparent that there are many areas of soluble bedrock in BC that likely have well-developed karst, even though such features have not yet been verified by field work. Geographic data and GIS shapefiles for the reconnaissance karst potential mapping of British Columbia (Stokes 1999) can be directly downloaded from Data BC (https://data.gov.bc.ca/).

The five tectonic belts of BC (Fig. 3) provide a good basis for subdividing the karst areas according to their different geological settings. The physiographic regions of BC that broadly correspond with these tectonic belts vary in terms of their local climate (rainfall and temperature), topography, elevation, surficial materials and vegetation cover. All of these attributes play an important role in the development of karst. In the following sections, the main geological units known to host caves and other karst features within each of the tectonic belts are described, and important examples are then listed and discussed. The level of information and knowledge on karst within individual geological units varies due to the large areal extent of the province, and the dispersed locations of population centres. Areas located close to population centres are generally better known than the more remote areas. In some cases, the evidence for karst development is extensively supported by referenced sources, government documents, and other published or unpublished reports. In other cases, evidence is more fragmentary and based largely on unpublished observations (e.g. field notes and photos) by the authors and/or information

Table 2. A summary of the principal carbonate-bearing units in British Columbia according to tectonic belts and geological age. Note, not all geological units referenced in text are listed.

Age	Insular Belt	Coast Belt	Intermontane Belt	Omineca Belt	Foreland Belt
Triassic	Parson Bay Fm.	Limestone and marble pendants of Wrangellia	Nicola Group		Baldonnel Fm.
	Quatsino Fm.		Sinwa Fm.		Pardonet Fm.
	Upper Karmutsen Fm.				
	Sadler Fm.				
	Peril Fm.				
Permian	Mount Mark Fm.	Limestone and marble pendants of Alexander	Marble Canyon Fm.		
			Teslin Fm.		
			Unnamed Terrace Limestone		
Carboniferous		Chilliwack Formation	Harper Ranch Group	Milford Fm.	Ketchika Group
			Cache Creek Group	Index Fm.	Livingstone Fm.
			Horsefeed Fm.	Broadview Fm	Rundle Group
					Prophet Fm.
					Banff Fm
Devonian					Exshaw Fm.
					Palliser Fm.
					Dunedin Fm
					Stone Fm
Silurian					Whitehorse Fm.
					Mount Wilson Fm.
					Nonda Fm.
Ordovician					Skoki Fm.
					Beaverfoot Fm.
					Chushina Fm.
Cambrian				Mural Fm.	Cathedral Fm
				Cunningham Fm.	Badshot Fm.
				Rosella Fm	Jubilee Fm.
Proterozoic				Espee Fm.	

- Predominately Limestone
- Limestone and Dolostone
- Predominately Dolostone

from other reliable sources. The following sections contain many locality names, and it is difficult to indicate all of these accurately on the page-size maps used in this paper. However, the most important localities are indicated by abbreviations in Figures 3, 4 and 5, and those that are not indicated can be located through examination of more detailed topographic maps. Karst features in British Columbia for each of the tectonic belts are illustrated by photographs in figures 6, 7, 8 and 9.

Insular Belt
The Insular Belt is comprised of the islands and coastal areas of mainland BC (Fig. 3), which are mostly made up of rocks of the Wrangellia Terrane, and to a lesser extent the Alexander Terrane (Wheeler and McFeely 1991). These terranes are bounded to the east by granitoid rocks (e.g. quartz-diorite and granodiorite) of the Coast Belt. The Insular Belt can be subdivided into three geographic areas: Vancouver Island, Haida Gwaii (formerly known as the Queen Charlotte Islands), and by the mid- and north-coast of BC (Fig. 3).

The distribution and extent of karst on Vancouver Island is relatively well known. Most karst occurs within one of three soluble bedrock units – the Quatsino, Parson Bay and Mount Mark formations. These units form linear zones that are typically tens of kilometres long and only a few kilometres wide in the north and central parts of the island (Fig. 5). These rocks are typically moderately dipping, and comprised of thick-bedded, white to light grey limestone of the Quatsino Formation, overlain by interbedded of dark grey limestone and black shale of the Parson Bay Formation. The older Mount Mark Formation occurs as smaller zones comprised of thick fossiliferous beds of crinoidal limestone, which are typically more affected by folding and faulting than the younger units. Much of the karst of Vancouver Island is forest-covered and occurs along lower valley bottoms (e.g. Tashish River), on broad benches and plateaus (e.g. Gibson Plateau) and middle to upper slopes
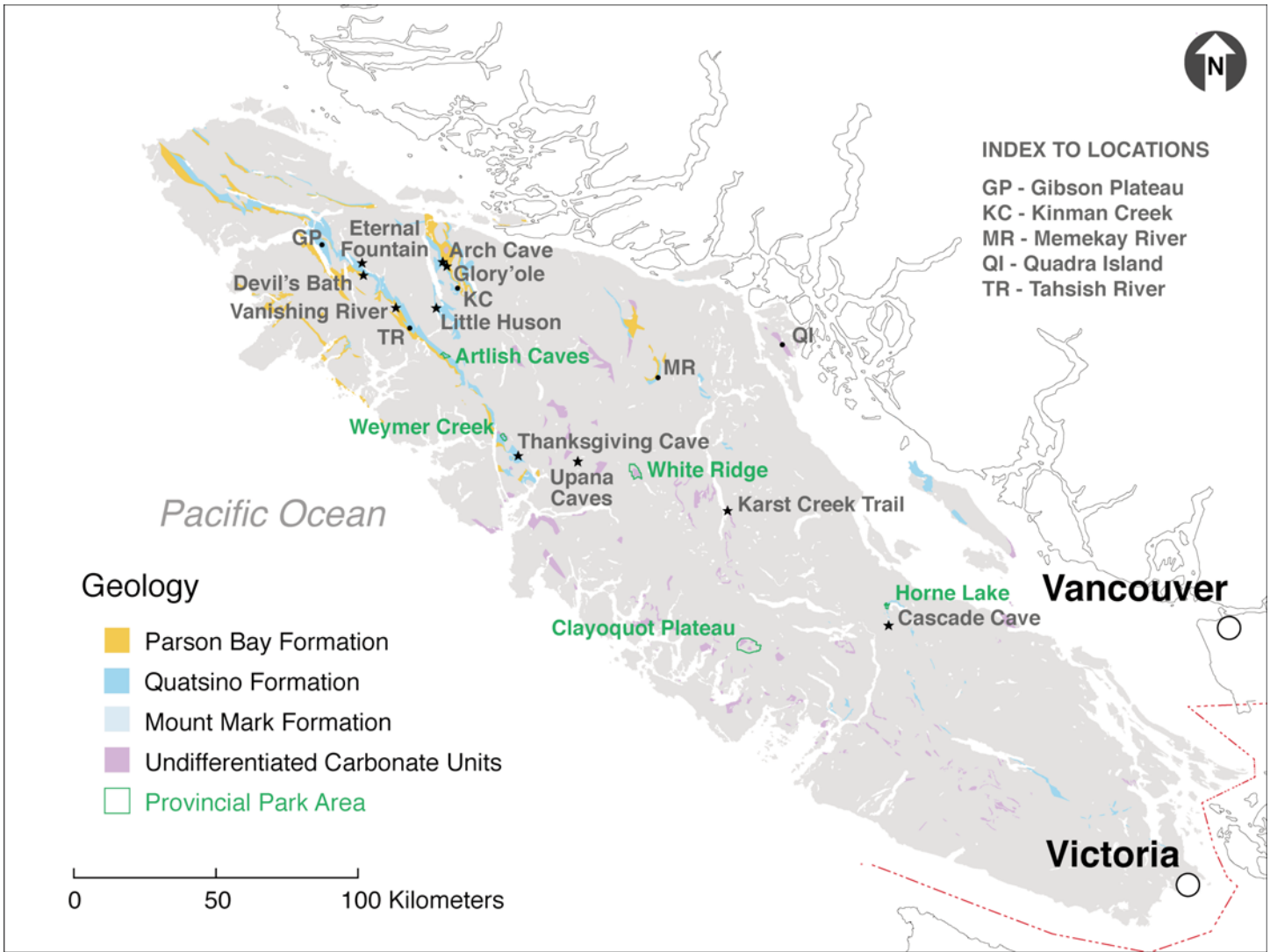
Figure 5. Carbonate units on Vancouver Island, British Columbia, and the locations of important karst areas discussed in the text.

(e.g. Kinman Creek, see Stokes et al. 2010, 2013). A few karst areas occur in alpine regions (e.g. Strathcona Provincial Park; Fig. 6A), whereas others occur near or along shorelines, and represent littoral (shoreline) karst (e.g. Texada Island; Fig. 6F). Karst sinkholes (dolines) of varying dimensions are the most common karst feature encountered (Fig. 6B, D), with sinkhole clusters typically found on benches (Ramsey 2015). Other features include sinking streams (e.g. Vanishing River), karst springs (e.g. Eternal Fountain), karst canyons (e.g. Memekay River; Fig. 6E), and arches (e.g. Little Huson Caves; Fig. 6C). Numerous cave systems occur throughout Vancouver Island, with varying levels of exploration and mapping completed; prominent examples include Thanksgiving Cave, Glory'ole Cave and Arch Cave (Fig. 5). Several provincial parks dedicated to karst landscapes are present on Vancouver Island (e.g. Clayoquot Plateau, Weymer Creek, Artlish Caves, and White Ridge) and Horne Lake Caves Provincial Park. The latter is known for commercially operated cave tours. Several designated sites also highlight various aspects of karst, including the Devil's Bath

and the Eternal Fountain (near Port Alice), Upana Caves (near Gold River), and the Karst Creek Trail in Strathcona Provincial Park.

The karst areas of Haida Gwaii have some similarities to Vancouver Island in that they are mostly forest-covered and occur in bedrock units of equivalent geologic age – the Sadler and Peril formations. The Sadler Formation is comprised of thick-bedded limestone (like the Quatsino Formation), whereas the Peril Formation is comprised of calcareous black shale and limestone (like the Parson Bay Formation). As on Vancouver Island, most of the karst development occurs in thicker-bedded limestone (i.e. the Sadler Formation) with the formation of sinkholes, karst canyons, dry valleys, karst springs, and small-scale solution features (karren) on outcrop surfaces (see Fig. 7A to 7D, and Griffiths and Ramsey 2009). Most of the karst in Haida Gwaii archipelago occurs to the south including areas within the Gwaii Haanas National Park, Lyell Island and Louise Island. Caves in Haida Gwaii (and also on Vancouver Island) are known to contain valuable paleontological remains

Figure 6. Karst features on Vancouver Island, British Columbia. A: Solutionally weathered limestone surface in alpine area near McNally Ridge, Central Vancouver Island. B: Karst spring appearing from the side of a forested sinkhole within second-growth of Quadra Island. C: Disappearing Atluck Creek at Little Huson Regional Park (Credit: Stewart Butler). D: Large sinkhole in Kinman Area with thick primary forest cover. E: Karst canyon along Memekay River during summer months. F: Solutionally weathered limestone on the shoreline of Texada Island.
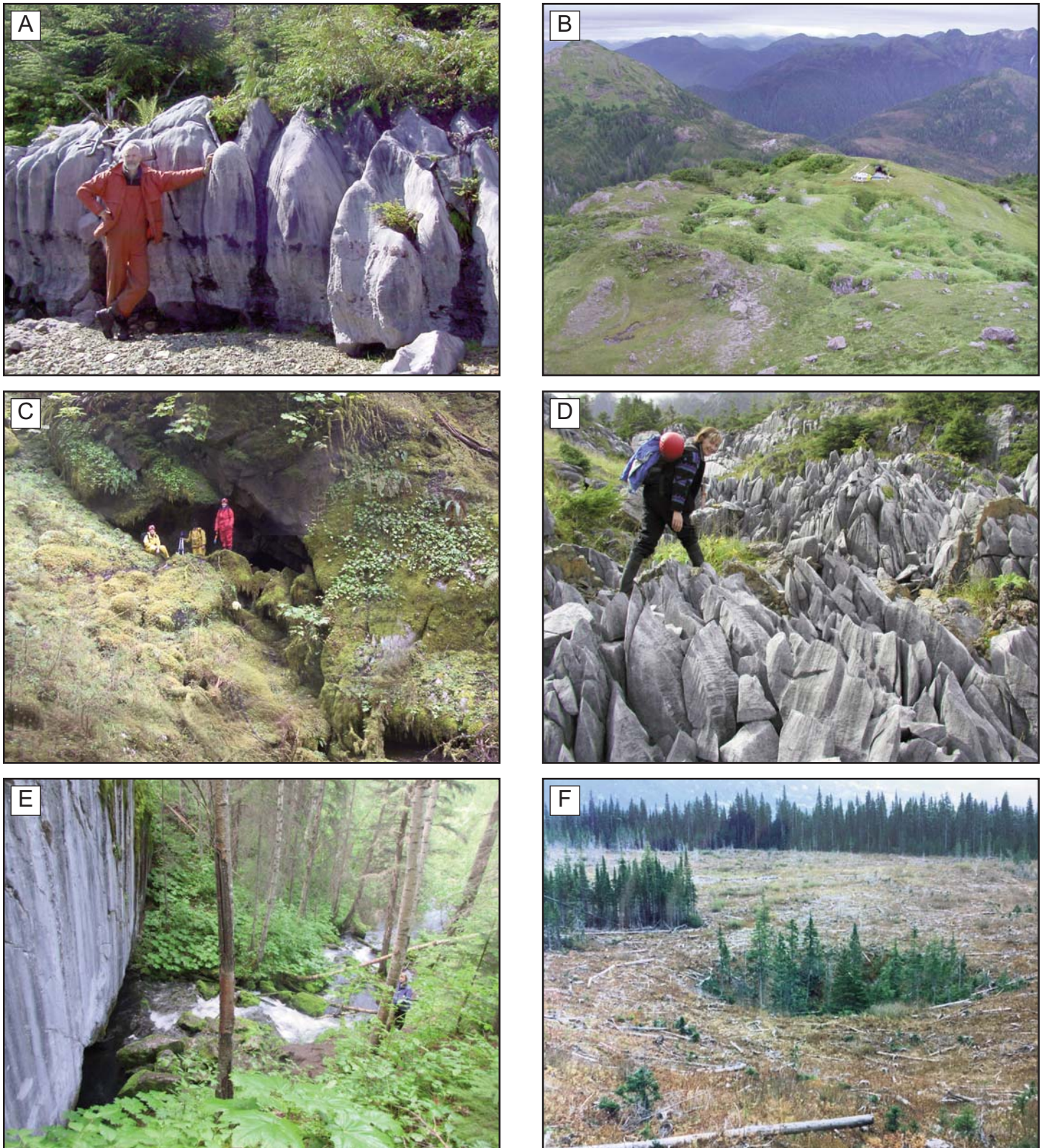
Figure 7. Karst features of Haida Gwaii and Canadian Rocky Mountains, British Columbia. A: Solutionally weathered epikarst exposure with karren features from Moresby Island, Haida Gwaii. Note, apparent narrowing of solutional openings towards base of outcrop. B: Upper elevation karst area with sinkhole cluster, Moresby Island, Haida Gwaii. C: Forested cave entrance, Moresby Island, Haida Gwaii. D: Solutionally weathered and frost shattered epikarst exposure in subalpine karst of Haida Gwaii. E: Karst spring at Hole-in-the-Wall Provincial Park, Chetwynd, BC (Credit: Charles Helm). F: Depression features in thickly mantled limestone of the Club Creek Area. Note, trees left within depressions, while surrounding areas harvested.
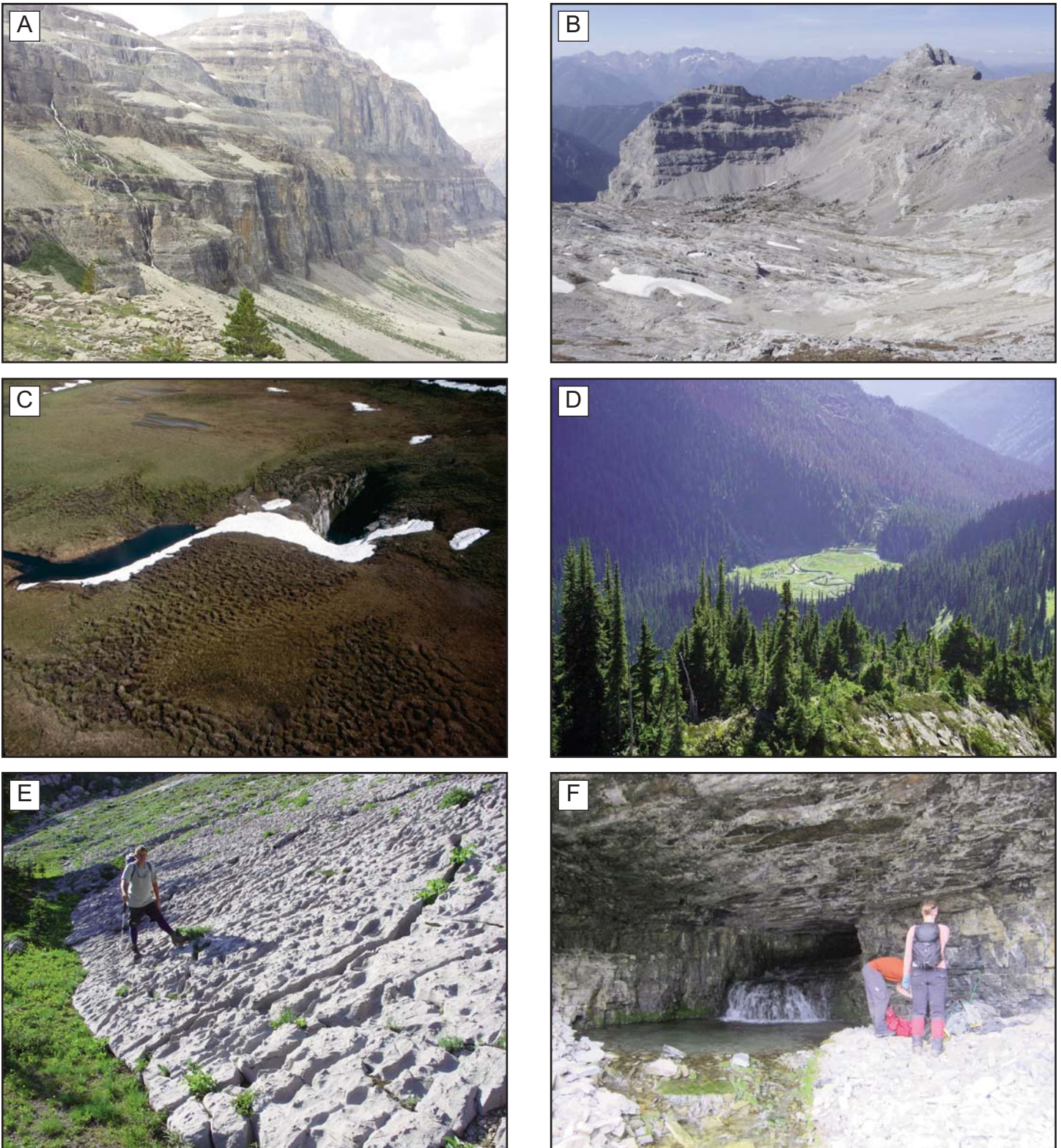
Figure 8. Karst landscape and features of the Columbia Mountains and Southern Canadian Rocky Mountains. A: Series of karst springs hosted in Middle to Upper Cambrian limestone near Mount Stanley, Kootenay National Park (Credit: EmmaYonge). B: Glacially scoured limestone plateau at Mount Bisaro (near Fernie); likely within limestone of Banff, Exshaw and Palliser formations (Credit: Chas Yonge). C: Sinking stream and White Hole sink point in the Bocock Provincial Park; likely hosted in Carboniferous limestone and/or dolomite of the Charlie Lake, Baldonnel, Pardonet and Bocock formations (Credit: Chas Yonge). D: Polje and White Rabbit sink point (located to left of polje); likely hosted in marble pendants within the Monashee Complex/Mountains (Credit: Chas Yonge/Martin Davis). E: Solutional karren on limestone surface near Mount Doupe, Fernie. Features likely hosted within limestone of the Carboniferous Livingston Formation part of the Rundle Group (Credit: Chas Yonge). F: Karst spring and entrance to Her Majesty's Cave, Kootenay National park (Credit: Chas Yonge).
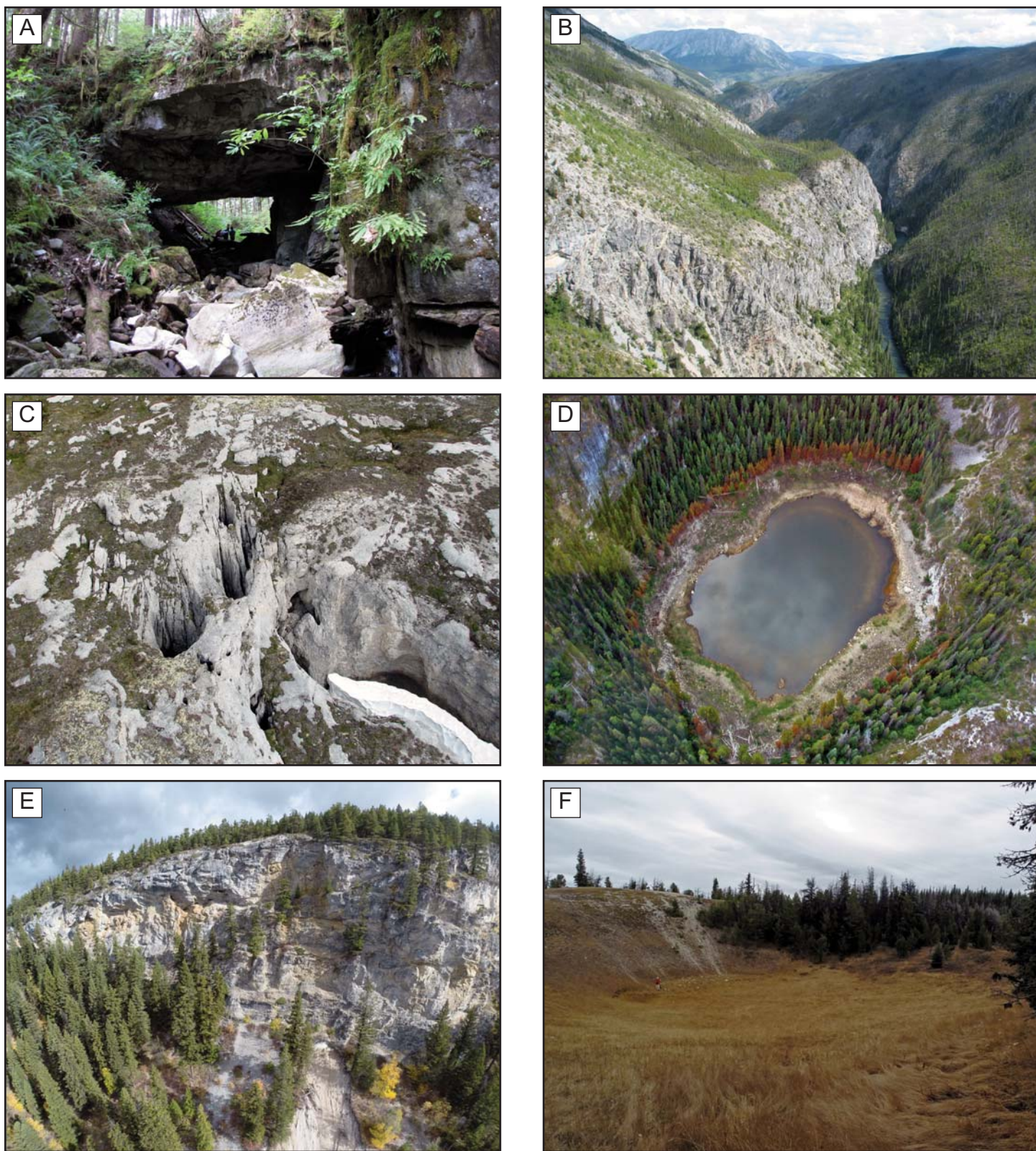
Figure 9. Karst landscapes and features of northern and northwestern British Columbia. A: Karst arch near Bella Bella; probably hosted in limestone/marble pendant of Alexander Terrane within Coast Plutonic Complex. B: Karst canyon along the Nakina River; likely hosted within Horsefeed carbonate unit of Cache Creek Terrane. C: Shafts in karst on Mount Sinwa hosted within limestone of the Sinwa Formation. D: Karst Lake near Atlin Lake; probably hosted within Horsefeed carbonate unit of Cache Creek Terrane. E: Karst ridge and bluffs with solutional openings, north of Fort St James. Karst hosted in massive limestone of the Cache Creek Group. F: Shallow depression/sinkhole near Jesmond. This feature likely occurs with limestone of the Marble Canyon Formation.

and information on postglacial environments, which are important for developing ideas of human coastal migration (Ramsey et al. 2004; Al-Suwaidi et al. 2006).

Isolated areas of karst also occur along the mid- and north-coast of mainland BC. Many of these limestone areas are metamorphosed and occur as isolated roof pendants surrounded by the intrusive granodioritic rocks of the Coast Mountain Belt. These roof pendants are likely metamorphosed remnants of Alexander Terrane rocks and consist of small areas of limestone that are variably transformed to marble. Examples include the area around Chapple Inlet on Princess Royal Island, where numerous grike fields, intensely-developed epikarst exposures, and sinkholes occur (Stokes and Griffiths 2000b), and near Bella Bella (Fig. 9A). Karst areas also occur on the coast of the mainland BC opposite Vancouver Island, such as on the Sechelt Peninsula, where there are limestone zones with known caves. These are likely similar limestone and marble remnants of the Wrangellia Terrane, but knowledge of karst development in these areas is incomplete.

Coast Belt

The Coast Belt of BC and the corresponding Coast Mountains can be subdivided into the northwest Alsek Ranges, the northern Boundary Ranges, the central Kitimat Ranges and the southern Pacific Ranges. The Coast Mountains extend up to elevations of 2500–3000 m and are dissected by several large river systems that drain to the west (e.g. the Fraser, Skeena, Nass, Stikine and Taku rivers). Most of the Coast Mountains are comprised of granitoid rocks with small roof pendants of metamorphic rocks derived from the adjacent terranes.

Extensive areas of soluble bedrock occur in the far northwest of BC within the Alsek Ranges, which form much of the Tatshenshini-Alsek Provincial Park. This area is a northern extension of the karst lands of the Tongass National Forest of Southeast Alaska, which extends from Prince of Wales Island to Chichagof Island (Baichtal and Swanson 1996). The carbonate bedrock units within the Tatshenshini-Alsek Park underlie approximately 40–50% of the region and vary from massive Ordovician and Silurian limestone to mixed Silurian to Permian carbonate, clastic and volcanic sequences. Much of the Alsek Ranges occur in sub-alpine, alpine and glacial settings, with steep sideslopes that lead down to forested valley bottoms and the flood plains and tributaries of the Tatshenshini River system. The nature of the karst in this region is not well documented. However, several small elongate zones of gypsum (Chitistone Formation) are known to occur along a ridge line near O'Connor River, and include numerous large (10–20 m diameter) sinkholes (White 1985).

The northern part of the Coast Belt includes the lower reaches of the Taku, Stikine, Nass and Skeena River systems that are within the Boundary Ranges and abut the border of Southeast Alaska. Large areas of the Paleozoic Stikine Terrane occur along the lower reaches of the Stikine River and include limestone intermixed with other sedimentary and volcanic rocks. Further south along the lower part of the Nass River, limestone is present within the Unuk River Formation, and along the Skeena River, minor limestone and marble areas are present in metasedimentary rocks of the Alexander Terrane. Karst in this region is not well documented. However, several small Permian limestone areas occur near Kitimat and Terrace, within which small caves and other karst features have been investigated by one of the authors.

The southern part of the Coast Belt extends southward from the Skeena River to Chilliwack near the US border (Figs. 3, 4). Small roof pendants of limestone with mixed sedimentary and volcanic rocks, representing parts of the Alexander, Nisling and Stikine terranes, occur within the granodiorite of the Coast Mountain batholith. To the south, numerous limestone zones, which are part of the Permian Chilliwack Formation, occur on the side slopes of the Chilliwack River. Caves and other karst features are known to occur in these limestone zones (Shaw 1997).

Intermontane Belt

The Intermontane Belt is comprised of a series of plateaus (Northern, Interior and Thompson plateaus) and small mountain ranges (e.g. the Skeena Ranges) that extend from the Yukon border southward to the Okanagan Valley. Geologically, the belt is mainly made up of the Stikine, Cache Creek and Quinella terranes, along with several other smaller terranes (Wheeler and McFeely 1991).

In the north, extensive carbonate bedrock units occur in the Atlin region of the Northern Plateau including the Horsefeed Formation, Lower Carboniferous–Triassic limestone with interbedded clastic sedimentary rocks, and black limestone of the Teslin Formation. These are all part of the Cache Creek Terrane. The Stikine Terrane includes the massive limestone of the Sinwa Formation and other Lower Permian limestone units. A karst inventory for the Atlin-Taku Planning Area (Griffiths 2009) identified over 400 karst features in these units and rated the areas for their karst vulnerability potential. The features encountered included numerous karst depressions, shafts, karst canyons, karst lakes, cave entrances, sinkholes and springs; as well as a large spring discharging into the Taku River (Fig. 9B, C and D). This karst inventory provided useful field verification of the karst potential polygons developed during the reconnaissance karst mapping for BC (Stokes 1999).

Areas of carbonate bedrock in the Chilcotin and Cariboo plateau regions include limestone of the Cache Creek Group in areas around Stuart Lake and Fort St James, and karst features and caves near the Mount Pope Provincial Park[1] (Fig. 9E). Much of the carbonate bedrock in this region is overlain by thick glacial deposits that may mask the presence of some karst areas.

Caves, sinkholes and springs have been observed within the limestone areas of the Marble Canyon Formation northwest of Kamloops (Fig. 9F). Examples of these features and limestone cliffs are found within Marble Canyon Provincial Park, which

---

[1] For listings and information of caves and karst in British Columbia's Provincial Parks visit the link: http://www.env.gov.bc.ca/bcparks/explore/

is also known for primary stromatolite features at Pavilion Lake. To the south of Kamloops small limestone zones occur in volcanic and metasedimentary rocks of the Nicola and Harper Ranch Groups.

Omineca Belt

The Omineca Belt is a region of intermediate-elevation mountains located between the intermontane plateaus and the higher mountains of the Rockies, and represents an area of complex deformation underlain by multiple smaller amalgamated terranes (e.g. Cassiar, Slide Mountain and Kootenay terranes). The Omineca Belt is comprised of the Cassiar and Omineca mountains to the north, and the Columbia Mountains to the south. The Rocky Mountain Trench (Fig. 4) bound these three mountain ranges to the east.

In the Cassiar Mountains extensive areas of carbonate bedrock extend from the Yukon border southward along the west side of Williston Lake. These include the limestone of the Rosella and Espee formations (Cassiar Terrane), as well as impure limestone and dolostone that are part of the metamorphosed Ingenika and Kechika groups. A few karst features (e.g. springs) are known to occur in this area. East of Prince George in the northern Columbia Mountains carbonate bedrock units include the limestone and dolostone of the Mural and Cunningham formations, and other unassigned Paleozoic rocks. The Mural Formation is known to host caves in the Rocky Mountains (Rollins 2004).

In the central and southern part of the Columbia Mountains and extending southward from Valemount to Revelstoke and towards Kootenay Lake, discrete and narrow linear units of limestone and marble are present. These include marble of the Horsethief Group and limestone of the Badshot Formation, as well as minor limestone layers within metasedimentary units, such the Index and Broadview formations. This area is climatically different from other interior regions of BC in that it is distinctly wetter, with rainfall amounts and temperature conditions that are similar to the west coast of BC. The Nakimu Caves area and Mount Tupper within Glacier National Park have been classified as examples of steeply dipping 'stripe karst,' where karst develops in narrow and deformed beds of marble that are traceable for kilometres, but are only a few tens of metres wide (Gunn 2003). Ford (1967) connected a major spring in this stripe karst to sink points near the Tupper Glacier, and more recent work of Yonge et al. (2013) has extended the caves in this region. Other examples of stripe karst have been examined in the Monashee Mountains (Yonge 2018). Recently, a large cave entrance and an associated sinking stream were discovered within the Wells Gray Provincial Park and are reported to be in stripe karst (C. Hickson personal communication 2018). Similar limestone and dolostone 'stripes' occur with solutional weathered bedrock surfaces to the east of Argenta and at the north of Kootenay Lake (Stokes and Griffiths 2000b). Cody Caves Provincial Park on the east side of Kootenay Lake also occurs within the narrow limestone layers that are part of the Milford Formation. Sinkholes, springs and sinking streams were identified in this area around the main cave entrance (Stokes and Griffiths 2000b). Dolo-

stone of the Index Formation is present on the west side of Kootenay Lake, near the Pilot Peninsula Provincial Park. In this area, there is evidence for minor surface solutional weathering, shoreline springs with tufa, and a rare limestone-loving orchid (Carver 2000; Stokes and Griffiths 2000b).

Foreland Belt

The Foreland Belt, which encompasses much of the Canadian Rocky Mountains, includes the most extensive areas of carbonate rocks in BC, and straddles the BC-Alberta border (Figs. 3, 4). These carbonate rocks are Cambrian to Mississippian in age and represent uplifted platformal rocks that were originally deposited on ancestral North America, prior to the terrane collisions that occurred in the Mesozoic. The Canadian Rocky Mountains can also be subdivided into four topographic units going from east to west (the Foothills, Front Ranges, Main Ranges and Western Ranges) and can be subdivided from north to south. The Southern (Canadian) Rocky Mountains approximately extend from the US border to Valemount (BC) and Jasper (Alberta), whereas the Northern Rocky Mountains extend from Valemount and Jasper to the Yukon and Northwest Territories borders (Fig. 4).

A detailed review of karst in the Southern Rocky Mountains carried out by Ford (1979) identified the main karst-forming carbonate units as the Cambrian Mural Formation (limestone) and Cathedral Formation (limestone, dolostone), the Upper Ordovician and Silurian Mount Wilson and Beaverfoot formations (limestone, cherty dolostone), the Upper Devonian Palliser Formation (limestone, dolostone), and the Mississipian Rundle Group (Table 2). Ford (1979) also investigated surface karst landform types and their relationships to glacial processes which formed features such as over-deepened cirques with underground drainage, and solutionally-enlarged fractures in frost-shatter zones. One of the major caves in the Foreland Belt is Castleguard Cave, which is partly below the Columbia Icefield, and located just to the east of the BC/Alberta border. The cave system is hosted in limestone of the Cathedral Formation and has more than 21 km of mapped underground passageways. Basal meltwaters from the icefields drain through these passageways, some of which are blocked by ice or till material (Smart 1983; Yonge et al. 2014; Ford and Smart 2017).

Caves in the Southern and Northern Canadian Rocky Mountains are well documented in a book by Rollins (2004) and identified nine cave and karst areas on the BC side of the Southern Rocky Mountains, including Kootenay and Yoho National Parks, the Hamber, Mount Robson, and Small River caves, and Kakwa and Mount Robson Provincial Parks. Karst areas also occur near Golden and at Rogers Pass. Karst plateaus, limestone pavements and springs with associated sinking streams and sinkholes (Fig. 8A, B, E and F) characterize these areas. Many of the caves have entrances that occur at the base of vertical shafts or springs. Some of the caves have considerable depth, such as Arctomys Cave in the Mural Formation within Mount Robson Provincial Park, which has a reported depth of 536 m (Rollins 2004). A cave with a depth of 670 m was recently found near Mount Bisaro north of Fer-

nie, BC, and is currently considered to be the deepest in North America (Genairon 2018).

The Northern Rocky Mountains generally have more dolostone units than the Southern Rocky Mountains. Some of the more extensive carbonate bedrock units include the limestone of the Ketchika, Cache Creek and Rundle groups, as well as the limestone and dolostone of the Mural, Lynx, Dunedin, Stone, Prophet, Nonda, Chushina, Cunningham and Espee formations.

A cave and karst resource evaluation carried out for the Muskwa-Kechika Planning Area (Safford 2000) identified five karst areas including the Liard River (karst springs along river), the Toad River-Racing River area (cliffs with cave entrances), the Through Creek area (cave entrances along Gataga Creek), the Redfern Lake (large sinking streams and depressions) and the Chowade River (a series of large, kilometre-size depressions and sinks). Karst is mostly developed in the Espee, Baldonnel, Pardonnet and Dunedin formations.

Southeast of Chetwynd, a major spring within the Hole-in-the-Wall Provincial Park emerges from the base of limestone bluffs of the Rundle Group (Fig. 7E), but no other surface karst features of note were identified in nearby areas (Stokes and Griffiths 2000b). In the Club Creek - Imperial Creek area, a large sinkhole and other small isolated karst features were encountered (Fig. 7F). This area is masked by thick glacial deposits, but is likely underlain by limestone of the Whitehorse Formation. Further south in the Monkman Provincial Park, karst features include several small caves, a spring and karst sinkholes. This park is underlain by dolostone of the Skoki and Beaverfoot formations, as well as limestone of the Chushina Formation.

Numerous caves occur in the Northern Rocky Mountains, mainly in the McGregor Ranges and the Dezaiko Ranges, as well as in the Kakwa, Bocock and Bowron Lakes Provincial Parks (Lowe 1985; Rollins 2004). Many of these cave and karst areas are difficult to access and occur as higher elevation limestone plateaus with cave entrances, sink points and shafts, along with karst springs at lower elevations.

KARST TYPES AND KARST DEVELOPMENT WITHIN BC

Karst within the various tectonic and physiographic regions of BC is broadly similar having subsurface drainage systems, surface solutional weathering and a range of other karst features. However, there can regionally be significant differences in the intensity of karst development and the distribution and types of karst features encountered, due to variations in carbonate bedrock geology, surficial cover, current climate conditions, types of vegetation and extent of forest cover and the influence of glaciation. These contrasts and differences act in combination to produce the variety of karst types across the province. Figure 10 provides a schematic profile from east to west across the province outlining some of these variations. This figure is, in part, based on a series of models suggested by Ford (2002), who identified three distinct structural settings for BC's karst: 1) the gently tilted limestone and dolostone units associated with thrust faults within the Rocky Mountains, 2) the steeply dipping marble and limestone units immediately west of the Rocky Mountains, and 3) the moderately to steeply dipping limestone units on the west coast.

Coastal BC is dominated by forest-covered islands and mountains. Forest-covered karst or more precisely 'coastal temperate forested karst' is the dominate karst type in this region, where conifers like western hemlock, amabilis fir (balsam) and western red cedar flourish and have a close intimate connection to the underlying karst. The term 'coastal temperate forested karst' is used to differentiate this type of karst from the forested karst that occurs in generally drier climatic zones to the east. Most of the coastal temperate forested karst occurs on slopes or benches within moderately to steeply dipping and faulted limestone units that are interlayered with volcanic sequences. Solutional weathering and karren are apparent on all exposed limestone outcrops that are part of well-developed epikarst exposures. Numerous sinkholes and other surface karst features (e.g. solution holes, shafts, karst canyons) are also common. Active subsurface drainage systems are usually present with associated sinking streams and karst springs. River caves (e.g. Artlish Caves, Little Huson Caves) can also be found. Many of the coastal temperate forested karst areas have significant allogenic recharge, with surface streams from non-karst catchments draining down onto the karst areas. In higher elevation areas (e.g. > 1200 m a.s.l.) subalpine to alpine karst occurs with well-developed surface solutional weathering on exposed ridges (e.g. White Ridge Provincial Park). In these areas, subsurface drainage systems are autogenically recharged by precipitation falling directly onto and vertically infiltrating into the karst. Coastal temperate forested karst and subalpine to alpine karst are likely the main types of karst that occur within the Coast Mountains, but these areas have not been extensively documented.

Forested karst occurs on the plateaus and mountainous regions within the BC interior, where limestone units are mainly interlayered with volcanic units, and in the north where they are associated with both volcanic and sedimentary sequences. Many of the southern regions are drier and mantled by thick glacial deposits. Surface karst development is less evident in these areas. However, isolated sinkholes and other karst features, such as karst springs, indicate the underlying presence of subsurface drainage systems. This type of 'covered karst' is not well documented, but is likely present in several areas based on the mapped distribution of limestone units in the region (e.g. near Kamloops and Prince George). Some uplifted limestone areas, such as the Pavilion Mountain, form highlands that exhibit evidence for karst development, but not of the intensity observed along the coast. Much of these highlands are forest-covered. Forest-covered karst extends into the central and northern parts of the BC interior which are dominated by sub-boreal spruce and pine forests; alpine karst likely occurs in some of the more mountainous areas.

Stripe karst is the principal karst type in the Columbia Mountains of the Omineca Belt, where thin and steeply dipping limestone (marble) layers occur in deformed metamorphic rocks. This karst varies from forest-covered to subalpine and alpine and is well developed, with sinking streams, springs and cave systems. This southwest region of BC has a wetter
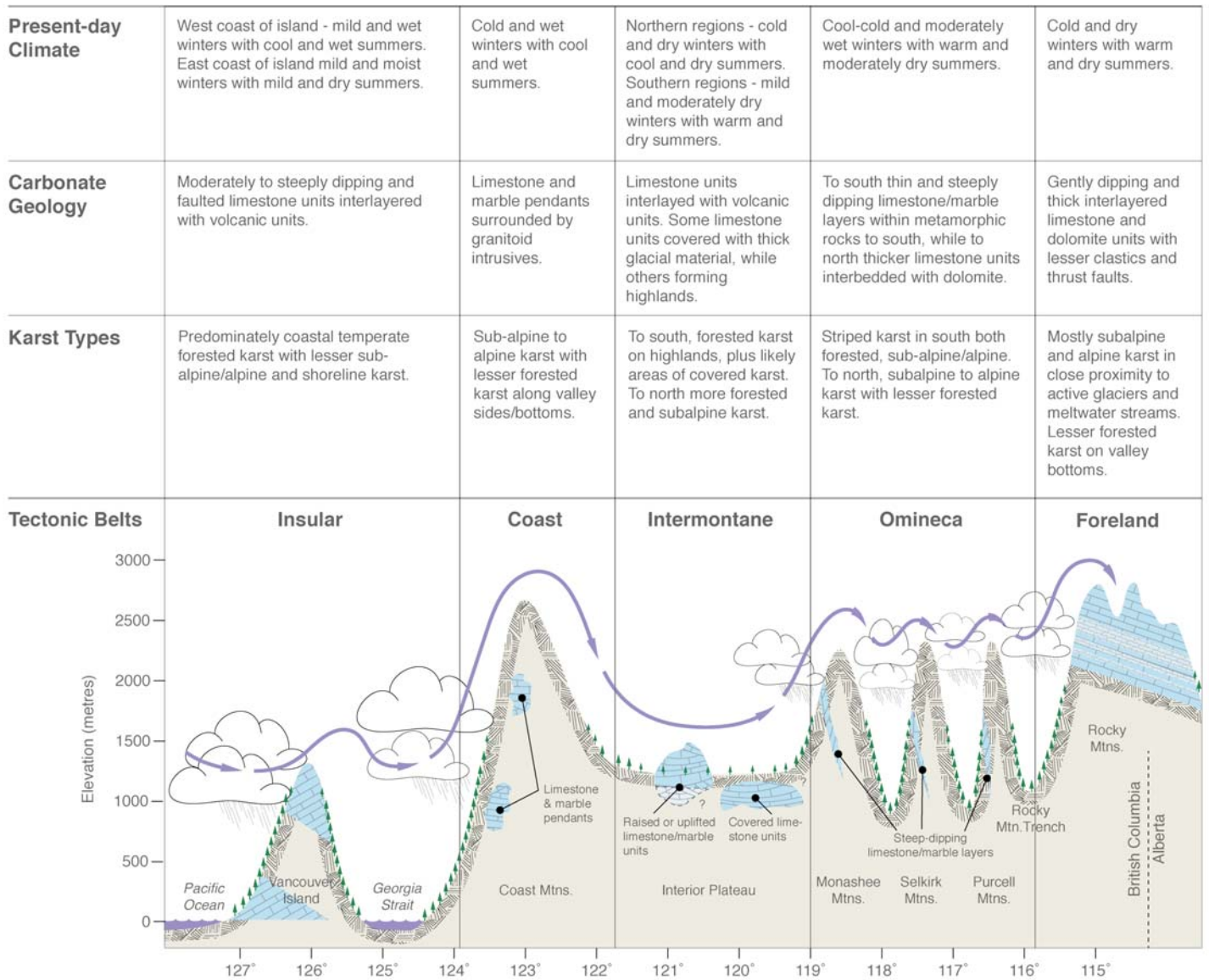
	Insular	Coast	Intermontane	Omineca	Foreland
Present-day Climate	West coast of island - mild and wet winters with cool and wet summers. East coast of island mild and moist winters with mild and dry summers.	Cold and wet winters with cool and wet summers.	Northern regions - cold and dry winters with cool and dry summers. Southern regions - mild and moderately dry winters with warm and dry summers.	Cool-cold and moderately wet winters with warm and moderately dry summers.	Cold and dry winters with warm and dry summers.
Carbonate Geology	Moderately to steeply dipping and faulted limestone units interlayered with volcanic units.	Limestone and marble pendants surrounded by granitoid intrusives.	Limestone units interlayed with volcanic units. Some limestone units covered with thick glacial material, while others forming highlands.	To south thin and steeply dipping limestone/marble layers within metamorphic rocks to south, while to north thicker limestone units interbedded with dolomite.	Gently dipping and thick interlayered limestone and dolomite units with lesser clastics and thrust faults.
Karst Types	Predominately coastal temperate forested karst with lesser sub-alpine/alpine and shoreline karst.	Sub-alpine to alpine karst with lesser forested karst along valley sides/bottoms.	To south, forested karst on highlands, plus likely areas of covered karst. To north more forested and subalpine karst.	Striped karst in south both forested, sub-alpine/alpine. To north, subalpine to alpine karst with lesser forested karst.	Mostly subalpine and alpine karst in close proximity to active glaciers and meltwater streams. Lesser forested karst on valley bottoms.

Figure 10. Schematic profile across southern British Columbia illustrating karst types along with respective climatic conditions and carbonate bedrock geology. Adapted from Chilton (1981) and Moore et al. (2010).

climate than the interior and is similar in part to the coast. Allogenic recharge is dominant, which is typical for stripe karst. To the north, in the Omineca and Cassiar Mountains, thicker limestone units are present and are interbedded with dolostone and fine-grained clastic sequences. Subalpine to alpine karst is likely the main karst type in this region.

Karst in the Rocky Mountains occurs within thrusted and gently dipping limestone and dolostone units that form thick sedimentary sequences, and for the most part subalpine or alpine karst is dominant. In these areas considerable surface solutional weathering has occurred on glacially-scoured limestone pavements, and frost shattering of bedrock has obscured surface karst features such as sinkholes. Most the subsurface karst drainage in this region is recharged autogenically by the diffuse infiltration of melt waters from snow or glaciers. Many

of these caves are accessed through vertical openings and shafts, or through karst springs.

Unravelling the karst development history and associated processes in BC requires not only an understanding of how soluble bedrock types take on the characteristics of karst, but also consideration of landscape erosion rates, present and past climate conditions, tectonic processes and uplift, sea level changes, and glaciation. The initiation of karst development (i.e. when it first formed) and likewise its end (or cessation) remain open to interpretation and discussion (Ford 2002). In general, the initiation of subsurface conduits in karst can take 1000 to 10,000 years before it becomes a fully functioning underground drainage system (Palmer 2007). The timing of cessation is more obvious and tied to erosion and final removal of a karst landscape. Information from cave contents, such as

speleothem and sediment, does not directly provide ages for cave and karst development, but they give some idea on when such materials formed and can thus provide preliminary constraints on cave histories. Castleguard Cave in the Rocky Mountains contains speleothems formed 340,000 to 350,000 years ago, and the oldest speleothem may be as old as 780,000 years, based on uranium series ages (Ford et al. 1981; Gascoyne et al. 1983). More recent uranium-series dating from Rat's Nest Cave in the Rocky Mountains has provided ages of 780,000 years to modern (Yonge 2012). These speleothem ages are thought to match the punctuated glacial record of the Rocky Mountains, suggesting that most speleothem growth occurred during major interglacial periods. The speleothem ages from the Rocky Mountain caves are much older than two groups of uranium-series ages reported from Cascade Cave on Vancouver Island, where speleothems formed at 64,000–45,000 years and later than 15,000 years, respectively (Gascoyne et al. 1981). These speleothem ages can be linked to interglacial Olympia and Fraser events. Age estimates of up to 140,000 years were suggested for Horne Lake Cave based on repeated and overlapping periods of speleothem formation, sediment infilling and cave development (Ford 1975).

The limited geochronological data cited above suggest that some caves in the Rocky Mountains formed speleothems prior to those of Coastal BC. However, without more extensive data, it is difficult to speculate how these ages exactly tie into the ages of cave formation, and when these karst landscapes might have initially developed. The coast, with its greater density of cave and karst features, is a region where karst development is an ongoing process, primarily due to its more temperate maritime climate. The karst features observed at the present-day surface largely result from solutional activity following the end of the last glacial period (12,000 years ago) and are likely superimposed on older 'relict' karst, which is possibly responsible for the deeper cave systems and larger surface features (e.g. Devil's Bath). The influence of the last glacial ice sheet margin along the west coast may also have enhanced surface and subsurface karst development during ice-sheet melting, runoff and isostatic rebound (Ford 1987). More subdued surface karst development in the interior of BC is likely due to lower precipitation rates and the thicker cover by glacial materials. However, this should not preclude earlier development of subsurface hydrological systems, as evident from the presence of large and (sometimes isolated) karst springs. Karst development in the Rocky Mountains is likely the result of multiple episodes of dissolution that alternated with glacial events that eroded and infilled the karst surface, and possibly enhanced subsurface flows during ice-sheet melting (Ford 1983b). Many caves in the Rocky Mountains have passages that may be preglacial, as indicated by conduit size and their glacial truncation on high ridges (Yonge et al. 2014). These caves likely represent the roots of older karst systems that have been uplifted from lower elevations and eroded. In summary, there is still much to discover with respect to the history and processes of cave and karst development in BC.

NEXT STEPS FOR KARST MANAGEMENT AND MAPPING IN BRITISH COLUMBIA

The general approach to karst management in BC has changed in the last 20 years, in that karst resources and values are now better recognized and are being examined in relation to land-use issues beyond forestry (i.e. oil and gas development, alternative energy projects and mining activities; Stokes 2013). Many of these changes reflect recognition of karst as an integrated system with distinctive hydrology and biology, along with a greater appreciation of its scientific, recreation and other values. The potential for karst hazards, such as subsidence and unpredictable subsurface water flows, on development activities has also become more recognized and understood (Zhou and Beck 2011; Parise 2015). However, there is less attention paid to the equally important non-karst catchments and streams that drain onto these karst areas, where they recharge karst aquifers and move groundwater by subsurface conduits to karst springs. Land-use impacts on these non-karst catchments are sometimes overlooked but can have a major impact on downstream karst systems. Careful mapping, assessment and management of non-karst catchments is essential (Gillieson 1996; Watson et al. 1997). Buried or covered karst is also a potential concern, because subsurface openings and associated underground hydrology may occur without any apparent surface manifestation (Veress 2016).

Karst, and its associated aquifers, are globally significant, and require careful consideration in the context of climate change. British Columbia has limited dependence on karst aquifers as a domestic water source, but many river systems are supplied by waters obtained in part from karst regions (e.g. Northern Vancouver Island, Canadian Rocky Mountains). Some rivers and their associated habitats are thus dependent on karst water, which may potentially be important for aquatic productivity and fish populations (e.g. Bryant et al. 1998). In alpine karst regions, the ongoing retreat of glaciers will likely expose more karst areas and increase meltwater flow, changing flow paths within karst aquifers and affecting water that is contributed to streams and lakes down gradient.

Outlining the full extent and nature of karst landscapes in BC is still incomplete. One of the major difficulties with mapping karst in BC is the extensive forest cover that obscures the location of many surface karst features. LiDAR data has successfully been used to better identify karst in forested areas (Langendoen and Baichtal 2004), but are currently not widely available in BC. The 1999 Reconnaissance Karst Potential Mapping for BC attempted to identify all karst and potential karst areas within the region (Stokes 1999); however, it now warrants updating considering the new digital bedrock mapping database available for the province (Cui et al. 2017), the greater accessibility of satellite imagery (e.g. Google Earth) and increased knowledge of karst field sites. Efforts should now be made to better integrate this revised mapping with published and unpublished reports on karst sites within the province. In addition, the map information should be made more easily available and accessible to users (e.g. developed as .kmz files for Google Earth) and in formats suitable for tablet and smart phone use.

ACKNOWLEDGEMENTS

REFERENCES

Al-Suwaidi, M., Ward, B.C., Wilson, M.C., Hebda, R.J., Nagorsen, D.W., Marshall, D., Ghaleb, B., Wigen, R.J., and Enkin, R.J., 2006, Late Wisconsinan Port Eliza cave deposits and their implications for human coastal migration, Vancouver Island, Canada: Geoarchaeology, v. 21, p. 307–332, https://doi.org/10.1002/gea.20106.

Baichtal, J.F., and Swanston, D.N., 1996, Karst landscapes and associated resources: a resource assessment: U.S. Department of Agriculture and Forest Service, Pacific N.W. Research Station, Portland, Oregon. General Technical Report PNW-GTR-383.

BC Ministry of Forests, 1997, A complex landscape sculpted by water (Brochure): British Columbia Ministry of Forests, Forest Practices Branch. Available at: http://www.for.gov.bc.ca/hfp/publications/00192/.

BC Ministry of Forests, 2003, Karst management handbook for British Columbia: British Columbia Ministry of Forests, Research Branch, Victoria, BC, 81 p., Available at: http://www.for.gov.bc.ca/hfp/publications/00189/Karst-Mgmt-Handbook-web.pdf.

Beedle, B., 1997, Management of karst in British Columbia: Proceedings of 1997 Karst and Cave Management Symposium, Bellingham, Washington, p. 13–21.

Bryant, M.D., Swanston, D.N., Wissmar, R.C., and Wright, B.E., 1998, Coho salmon populations in the karst landscapes of North Prince of Wales Island, Southeast Alaska: Transactions of the American Fisheries Society, v. 127, p. 425–433, https://doi.org/10.1577/1548-8659(1998)127<0425:CSPITK>2.0.CO;2.

Carver, M., 2000, Hydrologic assessment, Pilot Peninsula study area: Prepared for British Columbia Parks Kootenay District, 18 p.

Chilton, R.H., 1981, Summary of climate regions of British Columbia: British Columbia Ministry of Environment, Victoria, BC, 46 p.

Church, M., and Ryder, J.M., 2010, Physiography of British Columbia, in Pike, R.G., Redding, T.E., Moore, R.D., Winkler, R.D., and Bladon, K.D., eds., Compendium of Forest Hydrology and Geomorphology in British Columbia: British Columbia Ministry of Forests and Range, Handbook 66, Kamloops, BC, p. 17–46.

Cui, Y., Miller, D., Schiarizza, P., and Diakow, L.J., 2017, British Columbia digital geology: British Columbia Ministry of Energy, Mines and Petroleum Resources, British Columbia Geological Survey Open File 2017-8, 9 p.

Ecock, K., 1984, The hydrology of an alpine karst: White Ridge, Vancouver Island: Unpublished MSc thesis, McMaster University, Hamilton, ON, 138 p.

Fischl, P., 1992, Limestone and dolomite resources in British Columbia: British Columbia Ministry of Energy, Mines and Resources, Mineral Resources Division, Geological Survey Branch, Open File 1992–18, 150 p.

Ford, D., 1987, Effects of glaciations and permafrost upon the development of karst in Canada: Earth Surface Processes and Landforms, v. 12, p. 507–521, https://doi.org/10.1002/esp.3290120508.

Ford, D.C., 1967, The sinking streams of Mt. Tupper - a remarkable karst in Glacier National Park, B.C.: Canadian Geographer, v. XI, p. 49–52.

Ford, D.C., 1975, Report on the Euclatawes-Main Cave System of Horne Lake Caves Provincial Park, Vancouver Island: Unpublished report completed for Parks Branch, Department of Recreation and Conservation, British Columbia, 30 p.

Ford, D.C., 1979, A review of alpine karst in the southern Rocky Mountains of Canada: National Speleological Society Bulletin, v. 41, p. 53–65.

Ford, D.C., 1983a, Effects of glaciation upon karst aquifers in Canada: Journal of Hydrology, v. 61, p. 149–158, https://doi.org/10.1016/0022-1694(83)90240-8.

Ford, D.C., 1983b, The physiography of the Castleguard karst and Columbia Icefields area, Alberta, Canada: Arctic and Alpine Research, v. 15, p. 427–436, https://doi.org/10.1080/00040851.1983.12004371.

Ford, D.C., 1993, Karst in cold environments, in French, H.M., and Slaymaker, O., eds., Canada's Cold Environments: McGill-Queen's University Press, p. 199–222.

Ford, D.C., 2002, From pre-karst to cessation: the complicating effects of differing lithology and geologic structure on karst evolution, in Gabrovšek, F., ed., Evolution of Karst: From prekarst to cessation: Littera picta, Ljubljana, Slovenija, p. 31–42.

Ford, D.C., and Smart, C.C., 2017, Castleguard Cave and Karst, Columbia Icefield, Alberta and British Columbia, in Slaymaker, O., ed., Landscapes and Landforms of Western Canada: Springer, Switzerland, p. 227–239, https://doi.org/10.1007/978-3-319-44595-3_16.

Ford, D.C., Schwarcz, H.P., Drake, J.J., Gascoyne, M., Harmon, R.S., and Latham, A.G., 1981, Estimates of the age of the existing relief within the southern Rocky Mountains of Canada: Arctic and Alpine Research, v. 13, p. 1–10, https://doi.org/10.2307/1550621.

Gascoyne, M., Ford, D.C., and Schwarcz, H.P., 1981, Late Pleistocene chronology and paleoclimate of Vancouver Island determined from cave deposits: Canadian Journal of Earth Sciences, v. 18, p. 1643–1652, https://doi.org/10.1139/e81-152.

Gascoyne, M., Latham, A.G., Harmon, R.S., and Ford, D.C., 1983, The antiquity of Castleguard Cave, Columbia Icefields, Alberta, Canada: Arctic and Alpine Research, v. 15, p. 463–470, https://doi.org/10.2307/1551233.

Genairon, J., 2018, Bisaro Anima: la cavité la plus profonde du Canada: Sous Terre, Société Québécoise de Spéléologie, v. 27, No. 1, p. 12–15.

Gillieson, D., 1996, Caves: Processes, Development, Management: John Wiley & Sons, Ltd., 324 p., https://doi.org/10.1002/9781444313680.

Griffiths, P.A., 2009, Atlin-Taku Planning Area: Report on karst resources: Unpublished report prepared for British Columbia Ministry of Agriculture and Lands, Integrated Land Management Bureau Smithers, BC, 21 p.

Griffiths, P.A., and Ramsey, C.L., 2009, Assessment of Forest Karst Resources of Haida Gwaii: A Strategic Overview: Gwaii Forest Society, Project SFM08-2008, 57 p.

Gunn, J., (editor), 2003, Encyclopedia of Caves and Karst Science: Fitzroy Dearborn, New York, 960 p., https://doi.org/10.4324/9780203483855.

Harding, K.A., and Ford, D.C., 1993, Impacts of primary deforestation upon limestone slopes in northern Vancouver Island, British Columbia: Environmental Geology, v. 21, p. 137–143, https://doi.org/10.1007/BF00775297.

Harmon, R.S., Ford, D.C., and Schwarcz, H.P., 1977, Interglacial chronology of the Rocky and Mackenzie Mountains based upon 230Th–234U dating of calcite speleothems: Canadian Journal of Earth Sciences, v. 14, p. 2543–2552, https://doi.org/10.1139/e77-220.

Langendoen, R.R., and Baichtal, J.F., 2004, Using LIDAR remote sensing to map karst topography in a temperate rain forest – Case study: Tongass National Forest, southeastern Alaska: Geological Society of America Abstracts with Programs, v. 36, p. 385.

Latham, A., Schwarcz, H.P., Ford, D.C., and Pearce, G.W., 1982, The paleomagnetism and U–Th dating of three Canadian speleothems: evidence for the westward drift, 5.4–2.1 ka BP: Canadian Journal of Earth Sciences, v. 19, p. 1985–1995, https://doi.org/10.1139/e82-176.

Lowe, D.J., 1985, Karst development and cave formation in the Bocock Peak karst, Canada: Cave and Karst Science, v. 12, p. 33–44.

Marshall, D., Ghaleb, B., Countess, R., and Gabities, J., 2009, Preliminary paleoclimate reconstruction based on a 12,500 year old speleothem from Vancouver Island, Canada: Stable isotopes and U–Th disequilibrium dating: Quaternary Science Reviews, v. 28, p. 2507–2513, https://doi.org/10.1016/j.quascirev.2009.05.019.

Mills, W., 1981, Karst development and groundwater flow in the Quatsino Formation, Northern Vancouver Island: Unpublished MSc thesis, McMaster University, Hamilton, ON, 183 p.

Moore, R.D., Spittlehouse, D., Whitfield, P., and Stahl, K., 2010, Weather and Climate, in Pike, R.G., Redding, T.E., Moore, R.D., Winkler, R.D., and Bladon, K.D., eds., Compendium of Forest Hydrology and Geomorphology in British Columbia: British Columbia Ministry of Forests and Range, Handbook 66, Kamloops, BC, p. 47–84.

Palmer, A.N., 2007, Cave Geology: Cave Books, Dayton, OH, 454 p.

Parise, M., 2015, Karst geo-hazard: Causal factors and management issues: Acta Carsologica, v. 44, p. 401–414.

Ramsey, C.L., 2015, Morphometry and basic ecological characteristics of dolines in unlogged temperate rainforests karst landscapes of Northern Vancouver Island, British Columbia, Canada: Unpublished PhD thesis, University of Nova Gorica, Slovenia, 316 p.

Ramsey, C.L., Griffiths, P.A., Fedje, D.W., Wigen, R.J., and Mackie, Q., 2004, Preliminary investigation of a late Wisconsinan fauna from K1 cave, Queen Charlotte Islands (Haida Gwaii), Canada: Quaternary Research, v. 62, p. 105–109, https://doi.org/10.1016/j.yqres.2004.05.003.

RISC. Resources Information Standards Committee, 2003, Karst Inventory Standards and Vulnerability Assessment Procedures for British Columbia: British Columbia Ministry of Forests, Victoria, BC, 109 p.

Rollins, J., 2004, Caves of the Canadian Rockies and Columbia Mountains: Rocky Mountain Books, p. 236.

Safford, K., 2000, Cave and karst resources of the Muskwa-Kechika Management Area: Muskwa-Ketchika Advisory Board, Unpublished report, Fort St John, BC, 32 p.

Shaw, P., 1997, Chilliwack Valley Field Trip Guide: Proceedings of 1997 Karst and Cave Management Symposium, Bellingham, Washington, p. 201–207.

Smart, C.C., 1983, The hydrology of the Castleguard Karst, Columbia Icefields, Alberta, Canada: Artic and Alpine Research, v. 15, p. 471–486, https://doi.org/10.2307/1551234.

Smart, C.C., 1997, Hydrogeology of glacial and subglacial karst aquifers: Small River, British Columbia, Canada: Proceedings of the 6th Conference on Limestone Hydrology and Fissured Media, p. 315–318.

Stokes, T.R., 1995, Reconnaissance karst potential mapping for Vancouver Island: British Columbia Ministry of Forests, Nanaimo, BC. Unpublished report and maps.

Stokes, T.R., 1999, Reconnaissance karst potential mapping for British Columbia: British Columbia Ministry of Forests, Research Branch, Victoria, BC. Report and digital maps available from: https://catalogue.data.gov.bc.ca/dataset/reconnaissance-karst-potential-mapping.

Stokes, T.R., 2013, The challenges of identifying, evaluation and managing British Columbia karst lands: Innovation Magazine, Journal of the Association of Professional Engineers and Geoscientists BC, March/April 2013, p. 16–20.

Stokes, T.R., and Griffiths, P.A., 2000a, A preliminary discussion of karst inventory systems and principles (KISP) for British Columbia: British Columbia Ministry of Forests, Research Branch, Victoria, BC, Working Paper 51, 124 p.

Stokes, T.R., and Griffiths, P.A., 2000b, Karst inventory and sensitivity/vulnerability field trials in British Columbia: British Columbia Ministry of Forests, Research Branch, Victoria, BC, Unpublished Report, 68 p.

Stokes, T.R., Griffiths, P.A., and Ramsey, C., 2010, Geomorphology, hydrology and management of karst landscapes in British Columbia, in Pike, R.G., Redding, T.E., Moore, R.D., Winkler, R.D., and Bladon, K.D., eds., Compendium of Forest Hydrology and Geomorphology in British Columbia: British Columbia Ministry of Forests and Range, Handbook 66, Kamloops, BC, p. 373–400.

Stokes, T.R., Ramsey, C.L., and Griffiths, P.A., 2013, Constraints for karst landscape evolution on Vancouver Island, British Columbia, Canada: Concepts, research plans and outcomes: Proceedings for the 20th Australasian Cave and Karst Management Association Conference, Waitomo, New Zealand, p. 124–140.

Watson, J., Hamilton-Smith, E., Gillieson, D., and Kiernan, K., 1997, Guidelines for cave and karst protection: IUCN –The World Conservation Union, Cambridge, UK, 53 p.

Weary, D.J., and Doctor, D.H., 2014, Karst in the United States: A digital map compilation and database: USGS Open-File Report 2014-1156, 23 p.

Wheeler, J.O., and McFeely, P., 1991, Tectonic assemblage map of the Canadian Cordillera and adjacent parts of the United States of America: Geological Survey of Canada, "A" Series Map 1712A, (2 sheets), https://doi.org/10.4095/133549.

White, G.V., 1985, Preliminary report, O'Connor River Gypsum Deposit (114P/10E): British Columbia Geological Survey Fieldwork 1985, p. 279–282.

Wigley, T.M.L., Drake, J.J., Quinlan, J.F., and Ford, D.C., 1973, Geomorphology and geochemistry of a gypsum karst near Canal Flats, British Columbia: Canadian Journal of Earth Science, v. 10, p. 113–129, https://doi.org/10.1139/e73-014.

Worthington, S.R., 1991, Karst hydrology of the Canadian Rocky Mountains: Unpublished PhD thesis, McMaster University, Hamilton, ON, 406 p.

Worthington, S.R., and Ford, D.C., 1995, High sulfate concentrations in limestone springs: An important factor in conduit initiation?: Environmental Geology, v. 25, p. 9–15, https://doi.org/10.1007/BF01061825.

van Beynen, P.E., (editor), 2011, Karst Management: Springer Science, Dordrecht, NL, 489 p., https://doi.org/10.1007/978-94-007-1207-2.

Veress, M., 2016, Covered Karsts: Springer Science, Dordrecht, NL, 536 p., https://doi.org/10.1007/978-94-017-7518-2.

Yonge, C.J., 2012, Under Grotto Mountain: Rat's Nest Cave (2nd Edition): Rocky Mountain Books, Surrey, BC, 152 p.

Yonge, C.J., 2018, The White Rabbit Marble Cave, Monashee Mountains, BC, Canada: A Cave System in Stripe Karst: 28th BCRA Cave & Karst Symposium, P. 17–18.

Yonge, C.J., Vieira, N., and Walker, A., 2013, The Tupper – Raspberry Rising Cave System: A remarkable example in Stripe Karst: 16th International Congress of Speleology, 2013 ICS Proceedings, BRNO Czech Republic, p. 158–163.

Yonge, C.J., Bruns, H., Corlett, A., Graham, K., Horne, G., Lavigne. J., Lowe, D.J., McKenzie, I., Pollack, J., and Safford, K., 2014, Mountainous karst of the Canadian Rockies and Columbia Mountains: Abstract in Proceedings of Geological Society of America, Vancouver, BC, p. 392.

Zhang, R., Schwarcz, H.P., Ford, D.C., Schroeder, F.S., and Beddows, P.A., 2008, An absolute paleotemperature record from 10 to 6 Ka inferred from fluid inclusion D/H ratios of a stalagmite from Vancouver Island, British Columbia, Canada: Geochemica et Cosmochimica Acta, v. 72, p. 1014–1026, https://doi.org/10.1016/j.gca.2007.12.002.

Zhou, W., and Beck B., 2011, Engineering issues on karst, in van Beynen, P., ed., Karst Management: Springer Science, Dordrecht, NL, p. 9–45, https://doi.org/10.1007/978-94-007-1207-2_2.

In Appreciation

SECTION EDITORS

Oliver Bonham   David Lentz   J. Brendan Murphy   Andrea Waldie
Jaroslav Dostal   Robert Linnen   David Rudkin   Graham Young

REVIEWERS

Kevin Ansdell   Hendrik Falck   David Lentz   Neil Rogers
Sarah-Jane Barnes   Jana Fedortchouk   Michele Lustrino   Theresa Rushton
Hugh Barron   Jim Gehling   Ken Lyon   Kelly Russell
Trevor Bell   Charles Gower   Ian Macdonald   Dany Savard
Anthony Berger   Tassos Grammatikopoulos   Katherine MacLachlan   Andrew Schaeffer
R. Frank Blackwood   John Greenough   Alison Malcom   Julie Selway
John Calder   John Haid   William Mercer   John Spray
Andrew Calvert   Kristin Hanson   Gema Olivo   Mehmet Taner
Dante Canil   Chris Harris   Dave Pattison   Phillips Thurston
David Carter   Friedrich Horz   Joe Petrus   Craig Waldie
Tony Chong   Scott Jobin-Bevans   Brian Pratt   J. Kim Welford
Tim Corkery   Andrew Kerr   Paul Rennick   Phil Wilby
John England   Dan Kontak   Toby Rivers   Derek Wilton
George Eynon   Marc Laflamme

AGC-AMC-AIH
QUÉBEC 2019
Où les géosciences convergent
12-15 mai 2019
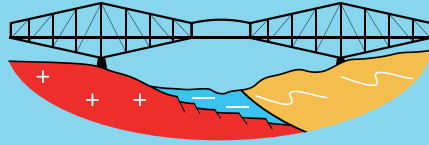
GAC-MAC-IAH
QUÉBEC 2019
Where geosciences converge
May 12-15 2019

www.gacmac-quebec2019.ca

GEOLOGICAL ASSOCIATION OF CANADA
ASSOCIATION GÉOLOGIQUE DU CANADA

MINERALOGICAL ASSOCIATION OF CANADA
ASSOCIATION MINÉRALOGIQUE DU CANADA

CNC - SNC
International Association of Hydrogeologists
Association internationale des hydrogéologues

L'Association géologique du Canada (AGC), l'Association minéralogique du Canada (AMC) et la section nationale Canadienne de l'Association internationale des hydrogéologues (AIH/SNC) vous invitent cordialement à vous joindre à eux pendant la conférence AGC-AMC-AIH/SNC, qui se tiendra du 12 au 15 mai 2019 dans la ville historique de Québec, site du patrimoine mondial de l'UNESCO. Les participants auront l'opportunité de visiter et vivre le charme et l'hospitalité de cette merveilleuse ville ainsi que d'explorer ses nombreux sites naturels avoisinants.

Sous la bannière "Où les géosciences convergent", le comité organisateur tient à promouvoir la collaboration et les échanges stimulants entre géologues, minéralogistes, pétrologues, hydrogéologues, géophysiciens et géochimistes. La conférence mettra l'emphase sur les thèmes suivants:
• Géosystèmes et hydrogéosystèmes;
• Ressources minérales, énergie et environnement;
• Science des données en géoscience;
• Géosciences et société

Sessions générales incluant:
• Minéralogie et cristallographie;
• Pétrologie ignée et métamorphique;
• Sédimentologie, stratigraphie et paléontologie;
• Géophysique;
• Géologie structurale et tectonique;
• Hydrogéologie générale;
• Géologie glaciaire et géomorphologie au Canada.

The Geological Association of Canada (GAC®), the Mineralogical Association of Canada (MAC) and the Canadian National Chapter of the International Association of Hydrogeologists (IAH/CNC) invite you to join them at the joint GAC–MAC–IAH/CNC meeting from May 12th to 15th 2019 in historic Québec City, a UNESCO World Heritage site. Participants will have the opportunity to visit and discover the warmth and charm of this beautiful city and to explore its many attractive nearby natural sites.

Under the theme "Where Geosciences Converge", the organizing committee wishes to promote collaboration and stimulating discussions among geologists, mineralogists, petrologists, hydrogeologists, geophysicists and geochemists. The conference will highlight the following themes:
• Geosystems and hydro-geosystems;
• Resources, energy and environment;
• Data science for geosciences;
• Geosciences and society

General Sessions including:
• Mineralogy and crystallography;
• Igneous and metamorphic petrology;
• Sedimentology, stratigraphy and paleontology;
• Geophysics;
• Structural geology and tectonics;
• General hydrogeology;
• Glacial geology and geomorphology in Canada.

gacmac-quebec2019.ca

SÉANCES PLÉNIÈRES/PLENARY SESSIONS

Dr. Barbara Sherwood Lollar	**"Subsurface Habitability in the Earth's Deep Hydrosphere: Implications for Planetary Science and Astrobiology"**
Mr. Darrell Beaulieu	**"A Dene perspective on resource development in Canada for, by and among First Nations"**
Dr. Guy Desharnais	**"How BIG Data is changing Mining"**

Dr. Barbara Lollar   Darrell Beaulieu   Dr. Guy Desharnais

JE VEUX PARTICIPER!
Ouverture des inscriptions : 1er mars 2019

I WANT TO ATTEND!
Registration opens: March 1st, 2019

Au plaisir de vous voir!
Looking forward to seeing you!

GEOSCIENCE CANADA